QUANTUM MECHANICAL ASPECTS OF FREE ELECTRON LASERS

By

SELCUK SARITEPE

Bachelor of Science
Bogazici University
Istanbul, Turkey
1981

Master of Science
Oklahoma State University
Stillwater, Oklahoma
1985

Submitted to the Faculty of the
Graduate College of the
Oklahoma State University
in partial fulfillment of
the requirements for
the Degree of
DOCTOR OF PHILOSOPHY
July, 1988

QUANTUM MECHANICAL ASPECTS OF

FREE ELECTRON LASERS

Thesis Approved:

N. V. V. J. Swamy

Thesis Advisor

Mark Samuel

J P Chandler

R. C. Bozell

Norman N. Durham

Dean of the Graduate College

TO MY TEACHER

SHRII SHRII ANANDAMURTI

ACKNOWLEDGMENTS

I would like to express my deepest respect and thanks to my major advisor, N. V. V. J. Swamy for his guidance and invaluable help in completing this thesis. I am especially grateful for his concern in conducting his administrative duties as my Ph.D. committee Chairman while he was away. He showed his great sense of responsibility by coming here from India to administer my Ph.D. Final Examination.

I also thank Dr.R. C. Powell, Dr M. A. Samuel and Dr.J. P. Chandler for serving on my committee.

I owe special thanks to my parents Hasan and Yuksel Saritepe and parents in law Nakip and Nuran Anlar for their love and moral support. I thank Fikret Yıldırım for partially typing my thesis and most of all I thank my wife Nilüfer for typing most of the thesis and for her love and understanding.

TABLE OF CONTENTS

LIST OF TABLES

LIST OF FIGURES

CHAPTER I

INTRODUCTION TO FREE ELECTRON LASERS

Introduction

After the discovery [1] of Synchrotron Radiation, many devices based on the concept of "stimulated synchrotron emission" have been proposed and successfuly operated during the period between 1950 and 1960. Free Electron Lasers (refered to henceforward by its acronym, FEL) belong to this large family of "free electron" devices which include Klystrons[2], Magnetron [3], traveling wave tubes [4], Orotron [5], Ubitron [6], and Gyrotron [7]. These other devices generated coherent radiation in cm and mm wavelengths. The generation of short wavelength coherent radiation via stimulated synchrotron emission at infrared, visible and ultraviolet regions of the electromagnetic spectrum have eluded researchers for some time until the first successful operation of Stanford FEL in 1976 [8].

FEL was proposed in its present form by Madey [9] in 1971 but the history of FEL goes back to Pierce [10] who derived the gain expression for traveling wave tubes in 1950 and to Motz [11] who proposed the magnetic undulator and successfuly generated spontaneous emission using this undulator in 1951. Coherence could not be achieved due to the lack of a bunching mechanism. This shows the critical dependence of FEL operation on the characteristics of the accelerator being used.
A separate chapter (Chapter II) will be devoted to the physics of

accelerators used in FEL experiments.

Components

The basic components of an FEL are an accelerator, an undulator (wiggler) and a set of mirrors . Figure 1 depicts the FEL set-up at Bell Laboratories. In other FEL facilities different accelerators are used. The original Stanford FEL was inserted to the end of the superconducting rf-linac (SCA). A diagram of the original Stanford oscillator along with other parameters is given in Figure 2 . While a more detailed description of these accelerators will be given in Chapter II, here we will simply assume that an accelerator produces relativistic electrons (pulsed or continous beam) which are injected into a wiggler where the electrons radiate due to the wiggling motion. This is basically a synchrotron radiation even though some researchers prefer the term "magnetic bremstrahlung" refering to the fact that electrons slow down as they radiate. But there is a subtle difference between the concepts of "synchrotron radiation" and "magnetic bremstrahlung". In the synchrotron radiation the transverse momentum of the electron need not be conserved (it can be absorbed by the bending magnets) whereas in a bremstrahlung process momentum in every direction must be strictly conserved. Therefore wiggler (undulator) radiation should be labeled as a synchrotron radiation.

The theory of synchrotron radiation can be found in Schwinger's original paper [1] . Spectral and directional properties of synchrotron radiation in relation to FEL radiation will be discussed in Chapter VIII Here it will suffice to say that the synchrotron radiation from circular accelerators exhibit a very broad spectrum and as a consequence

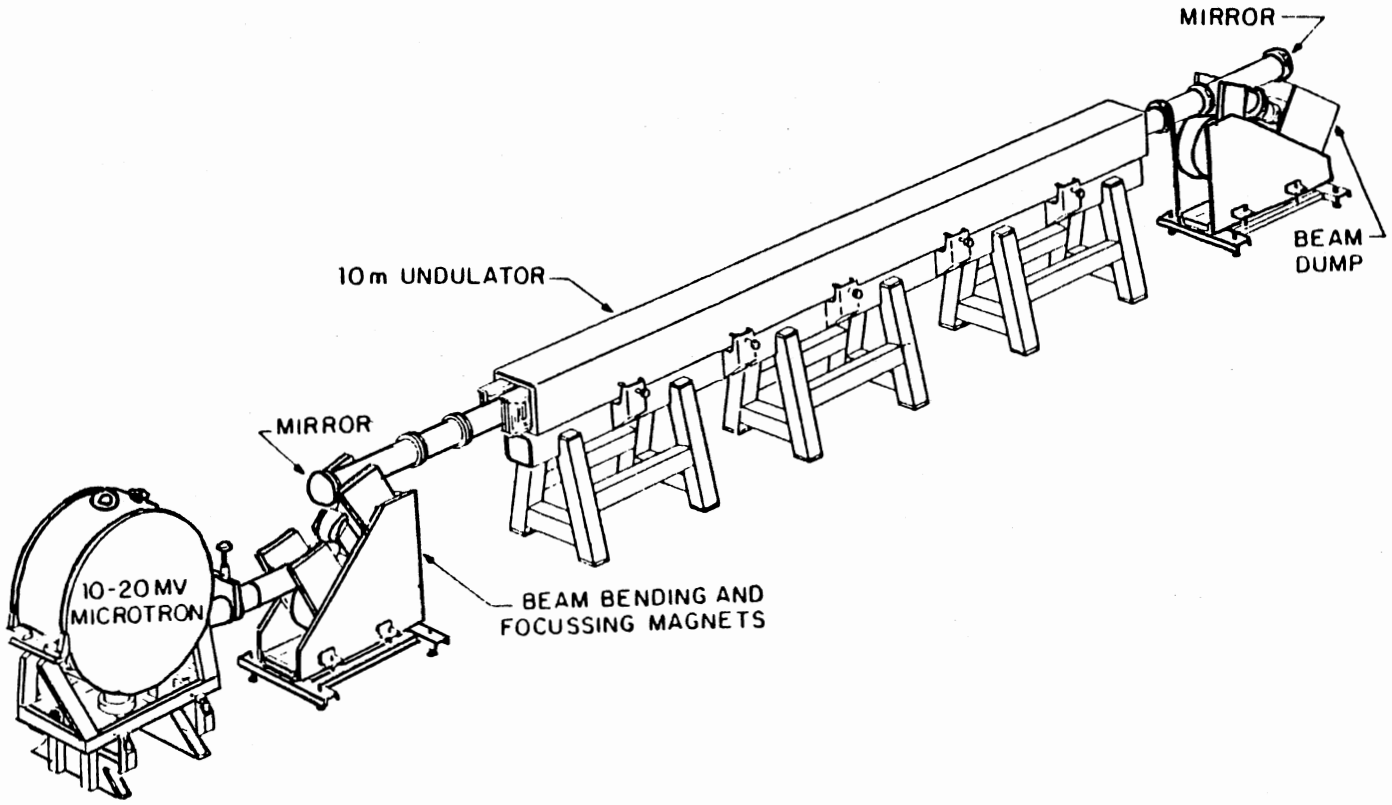

Figure 1. The FEL at Bell Laboratories

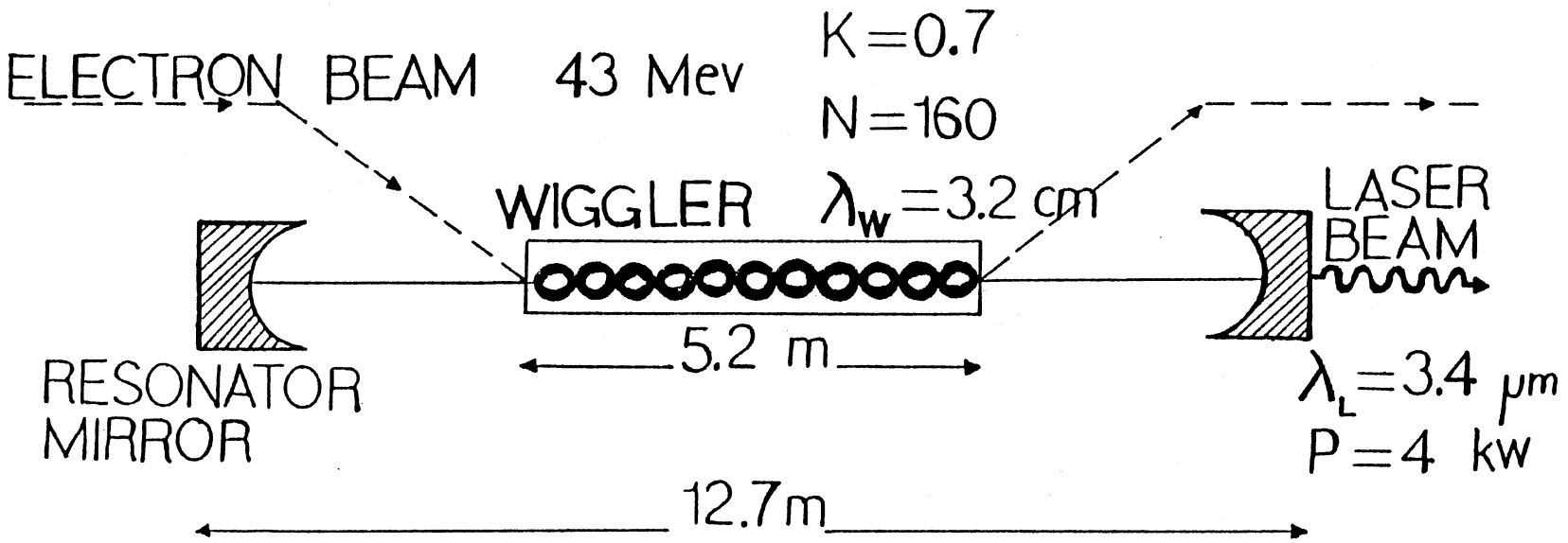

Figure 2. A schematic diagram of the original Stanford FEL oscillator

power-per-frequency is low. A light source with a broad spectrum has its advantages but generaly is not suitable for spectroscopic studies.

Motz [11] proposed the undulator [Figure 3] to improve the power-per-frequency. Figure 4 compares the spectra of circular machine synchrotron radiation and undulator radiation. The sharpness of the undulator radiation spectrum is due to the fact that in the undulator the average angle of deviation of the trajectory from the axis is lower than the aperture of emission cone (Hence the necessity for relativistic electrons which emit photons in a very narrow cone, approximately $1/\gamma$ radians, where γ is the Lorentz factor). Therefore the pulse duration observed by an observer on the axis will be much longer than that of circular-machine radiation. For the undulator δt will be approximately

$$\delta t \cong \frac{L}{2c} \gamma^{-2} (1+K^2) \tag{1.1}$$

where L is the length of the undulator and K is the strength parameter given by

$$K = \frac{eB_{rms}\lambda_w}{2\pi m_0 c^2} \tag{1.2}$$

B_{rms} is the magnetic field on the axis. The uncertainty relation $\Delta\omega\ \delta t \sim \pi$ leads us to

$$\Delta\omega \simeq \frac{\pi}{\delta t} \simeq \frac{2\pi c}{L} \gamma^2 \frac{1}{1+K^2} \tag{1.3}$$

This bandwith is γ times smaller than the circular-machine radiation bandwith which is given by

$$\Delta\omega \simeq \frac{3\pi c}{4\rho} \gamma^3 \qquad \rho : \text{radius of curvature} \tag{1.4}$$

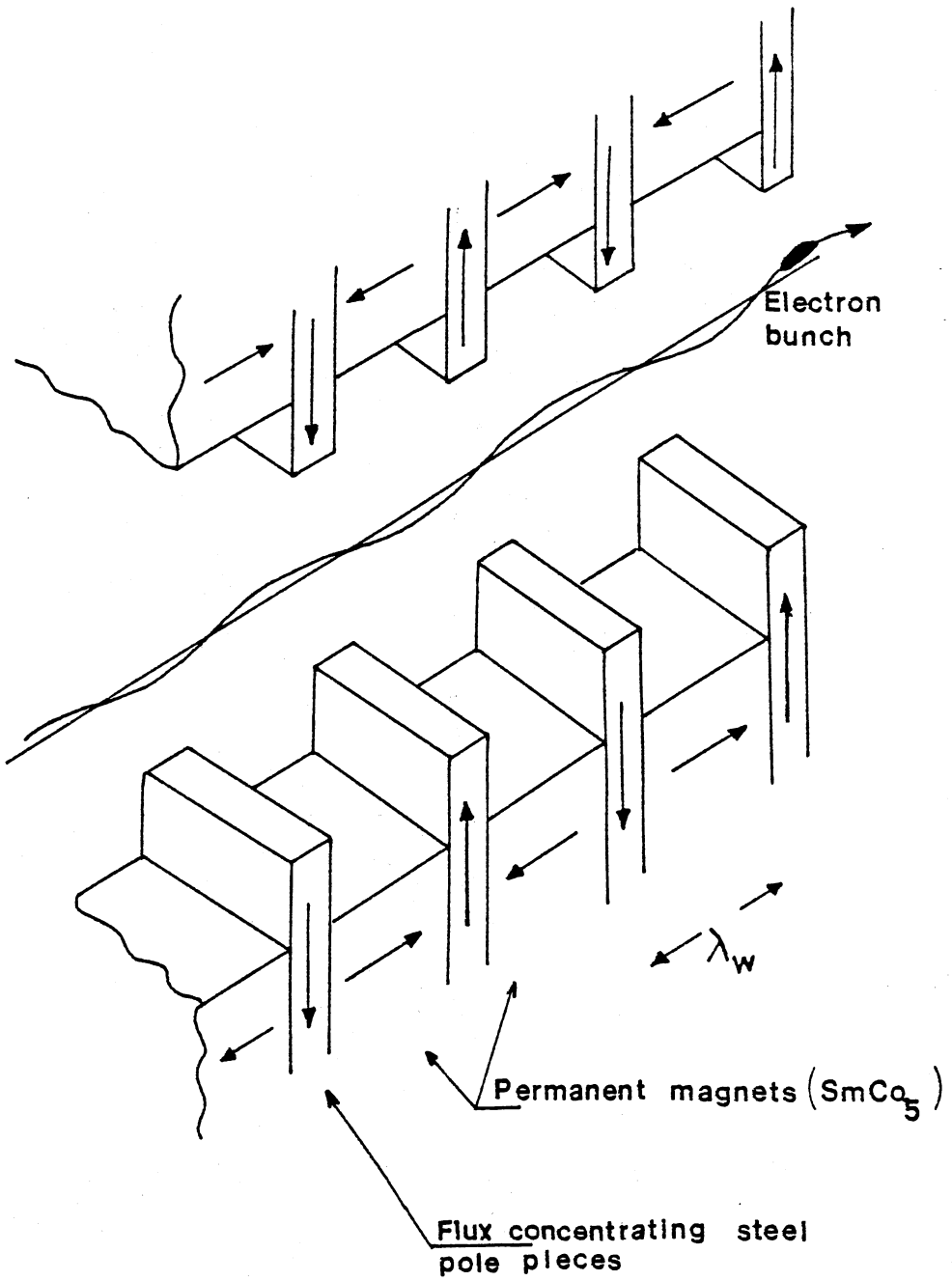

Figure 3. Undulator

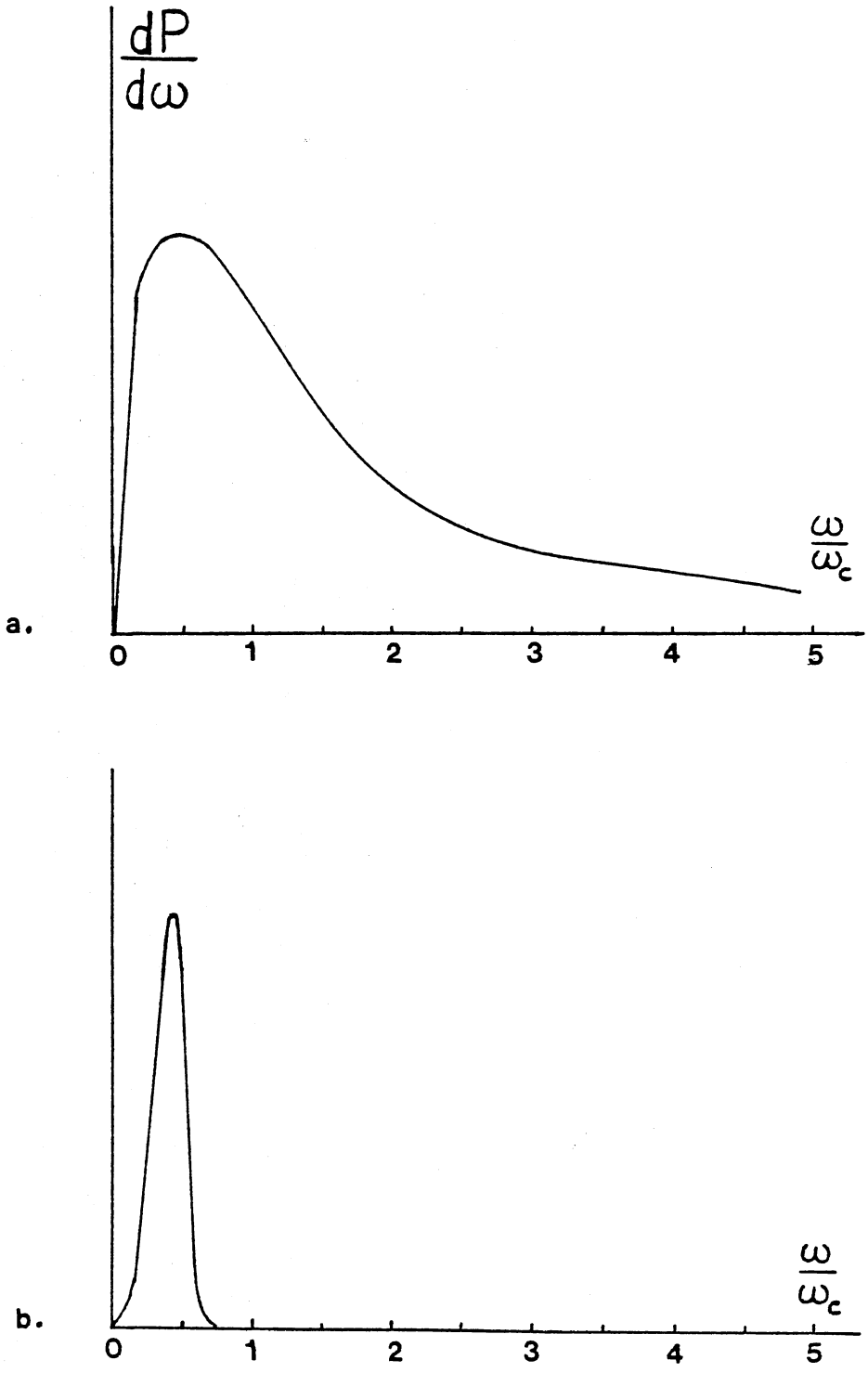

Figure 4. Comparison of spectra, a. Circular machine
b. Undulator

The fundemental frequency of the undulator radiation will be formally calculated in later chapters, here we simply report the result.

$$\omega_0 = 2ck_w\gamma^2/(1+K^2) \qquad \text{where} \qquad k_w \equiv 2\pi/\lambda_w \tag{1.5}$$

There are also harmonics but only odd harmonics are emitted in the axis direction. The harmonics can be utilized for the purpose of higher frequency generation of coherent radiation but in general they are detrimental to the operation of FEL since they steal power from the fundemental. This situation motivated the development of the helical wigglers. Figure 5 shows various helical wiggler magnets. The synchrotron radiation from a helical wiggler does contain harmonics but only the fundemental is emitted on the axis. Since it is the most widely used magnet geometry we shall concentrate on the helical wigglers from this point on. For a theoretical quantum mechanical treatment, the vector potential of the helical wiggler can be represented as (on the axis)

$$\vec{A} = a\cos k_w z\,\hat{x} + a\sin k_w z\,\hat{y} \tag{1.6}$$

We conclude this section by mentioning the significance of the strength parameter K. As we shall see in Chapter VIII, when $K > 1$ most of the radiation is emitted in an off-axis direction which is not desirable in a laser device. In most experiments K is chosen to be approximately $K \simeq 1$ and this corresponds to a magnetic field strength of 1 KG.

FEL Interaction

A quantitative description of the interaction between the electron beam (pulsed or continuous) and the radiation field (single mode or multi-mode) inside a wiggler and the growth of radiation (gain) along

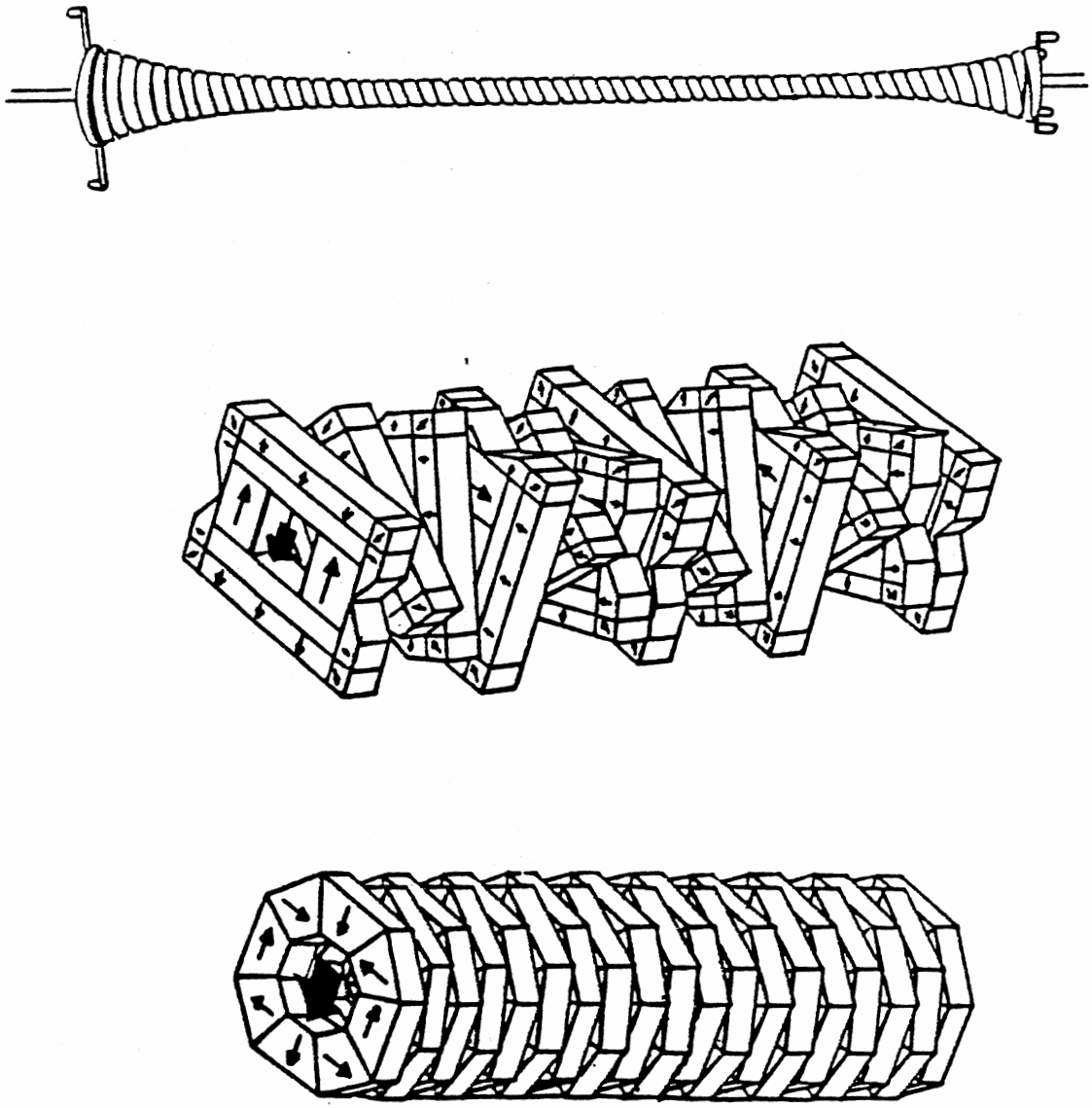

Figure 5. Various helical wiggler magnets, a. Bifilar helical, b. and c. Permanent magnet wigglers

with the growth of coherence, have been approached by many physicists from very different angles. The literature on the subject is voluminuous. Historicaly the first analysis was quantum mechanical [9] but here we shall present the simplest classical analysis given by Colson [12]. The easiest way to calculate photon gain is by calculating the energy loss of the electrons. It is assumed that the energy lost by the electrons is the energy gained by the radiation field. The electron energy variation can be written as

$$\dot{\gamma} = \frac{eE_s v_\perp}{m_0 c^2} \tag{1.7}$$

where $v_\perp$ is the transverse electron velocity and E_s is the electric field of the copropagating wave.

$$v_\perp = \frac{p_x}{m_0 \gamma} = - \frac{cK\sqrt{2}}{\gamma} \sin k_w z \tag{1.8}$$

$$E_s = E_0 \cos(\omega t - kz + \phi) \tag{1.9}$$

where ϕ is the field phase and $k = \omega / c$ is the laser phase wavenumber. The laser energy gain is related to the electron energy loss as follows.

$$\Delta W_s = - m_0 c^2 \Delta\gamma \tag{1.10}$$

The gain is defined as

$$G = \frac{\Delta W_s}{W_{0s}} = - m_0 c^2 \frac{\Delta\gamma}{W_{0s}} \tag{1.11}$$

where W_{0s} is the initial energy of the laser field. For a linearly polarized electromagnetic wave

$$W_{0s} = (1/8\pi) E_0^2 V \tag{1.12}$$

V is the volume. Inserting (1.8) and (1.9) in (1.7) we obtain

$$\dot{\gamma} = - \frac{eE_0K_0}{m_0c^2\gamma\sqrt{2}} \left(\sin\Psi_- - \sin\Psi_+ \right) \tag{1.13}$$

where we define

$$\Psi_{\pm} = (k \mp k_w)z - \omega t - \phi \tag{1.14}$$

Assuming weakly perturbed electron motion (small-signal regime)

$$z \simeq \beta ct \tag{1.15}$$

then we can neglect $\sin\Psi_+$ since it is the rapidly oscillating part. (1.13) becomes (by taking $\Psi \equiv \Psi_-$)

$$\dot{\gamma} = - \frac{E_0eK}{m_0c^2\gamma\sqrt{2}} \sin\Psi \tag{1.16}$$

and (1.14) can be differentiated with respect to time

$$\dot{\Psi} \equiv \dot{\Psi}_- = - \omega + (k+k_w)\dot{z} \tag{1.17}$$

The square of the instantaneous velocity can be written as

$$\dot{z}^2 + \langle v_\perp^2 \rangle = c^2(1- \gamma^{-2}) \tag{1.18}$$

Substituting this in (1.17)

$$\dot{z} \cong c \left[1 - \frac{1}{2\gamma^2}(1+K^2)\right] \tag{1.19}$$

taking the derivative with respect to time, we obtain

$$\ddot{z} = c \frac{\dot{\gamma}}{\gamma^3} (1+K^2) \tag{1.20}$$

which can be written , by using (1.16), as

$$\ddot{z} = - \frac{e^2E_0B_0\lambda_w}{4\pi\gamma^4(m_0c^2)^2} (1+K^2) \sin\Psi \tag{1.21}$$

This is the well-known equation of FEL dynamics. It states that the

dynamics of an FEL obeys a pendulum equation. This allows us to write the gain in terms of the variation in $\dot{\Psi}$. By integrating (1.21) we obtain (assuming $\Delta\gamma << \gamma$)

$$\Delta\gamma = \frac{\gamma}{2k_w c}\,\Delta\dot{\Psi} \qquad , \quad \ddot{\Psi} = -\Omega^2 \sin\Psi \tag{1.22}$$

Combining equations (1.11), (1.17) and (1.22) we obtain

$$G = -\frac{8\pi k_w r_0 c^3 K^2}{\gamma^3 V}\,\frac{\Delta\dot{\Psi}}{\Omega^4} \tag{1.23}$$

where $$\Omega \equiv \frac{e^2 E_0 B_0}{(m_0 c\gamma)^2} \qquad , \qquad r_0 \equiv \frac{e^2}{m_0 c^2} \tag{1.24}$$

For n electrons the gain expression becomes

$$G = -\frac{8\pi k_w r_0 c^3 K^2 n}{\gamma^3 V}\,\frac{<\Delta\dot{\Psi}>}{\Omega^4} \tag{1.25}$$

where $$<\Delta\dot{\Psi}> = \frac{1}{n}\sum_{i=1}^{n} (\Delta\dot{\Psi})_i \tag{1.26}$$

Integration of (1.21) yields

$$\dot{\Psi}^2 - \dot{\Psi}(0) = 2\Omega^2(\cos\Psi - \cos\Psi(0)) \tag{1.27}$$

where $\Psi(0)$ and $\dot{\Psi}(0)$ contain all the initial conditions

$$\Psi(0) = -(\omega\, t_0 + \phi) \tag{1.28}$$

$$\dot{\Psi}(0) = -\frac{(\omega - \omega_0)}{\omega_0}\, ck_w \tag{1.29}$$

where t_0 is the starting time and ω_0 is the central frequency of the wiggler spontaneous emission. The small-signal regime which we have assumed all along is characterized by $\Omega << (c/L)$, also note that (1.29) can be written in terms of a dimensionless detuning parameter ν.

$$\nu \equiv 2\pi N \frac{\omega_0 - \omega}{\omega_0} \qquad , \text{ N : Number of magnet elements in the wiggler} \tag{1.30}$$

$$\dot{\Psi}(0) = (c/L)\nu \tag{1.31}$$

This leads us to

$$\Delta\dot{\Psi} \cong -\left(\frac{\Omega L}{c}\right)^2 \frac{c}{L}\left[\frac{\sin(\nu/2)}{(\nu/2)}\right]\sin\left[\nu/2 + \Psi(0)\right] + \left(\frac{\Omega L}{c}\right)^4 \frac{c}{4L}\frac{d}{d\nu}\left[\frac{\sin(\nu/2)}{(\nu/2)}\right]^2\left\{\sin\left[\nu/2 + \Psi(0)\right]\right\}^2 \tag{1.32}$$

The average of the quantity $\Delta\dot{\Psi}$ is the physically relevant parameter so we take the average of $\Delta\dot{\Psi}$ over all the initial phases.

$$\langle\Delta\dot{\Psi}\rangle = \left(\frac{\Omega L}{c}\right)^4 \frac{c}{4L}\frac{d}{d\nu}\left[\frac{\sin(\nu/2)}{(\nu/2)}\right]^2 \tag{1.33}$$

The average of the first term in (1.32) vanishes. The gain expression becomes

$$G = -\frac{4\pi^2 r_0 K^2 L^3 n}{\lambda_w \gamma^3 V}\frac{d}{d\nu}\left[\frac{\sin(\nu/2)}{(\nu/2)}\right]^2 \tag{1.34}$$

This is an important and unique result in FEL theory. It is known as Madey's theorem [13]. Madey has shown that the gain is proportional to the derivative of the spontaneous emission line-shape and this holds true for all the undulators and the wigglers. This conclusion has since been experimentally verified [14].

The expression for gain can be written in terms of the parameters which are more relevant to the experiments.

$$G = -g\pi \frac{d}{d\nu}\left[\frac{\sin(\nu/2)}{(\nu/2)}\right]^2 \tag{1.35}$$

where $$g \equiv \frac{4\pi}{\gamma}\frac{\lambda_0 L}{\Sigma_E}\frac{I}{I_0} F\xi\, 4N^2 \tag{1.36}$$

λ_0 is the central wavelength of the spontaneous radiation, Σ_E is the e-beam cross-section, I is the beam current and F is a filling factor which takes into account the fact that only the electrons in the intersection of the e-beam and the laser beam count. That is

$$F = \begin{cases} 1 & \text{if} \quad \Sigma_E > \Sigma_L \\ \dfrac{\Sigma_E}{\Sigma_L} & \text{if} \quad \Sigma_E < \Sigma_L \end{cases} \tag{1.37}$$

$$\xi \equiv \frac{1}{2} \frac{K^2}{1+K^2} \qquad I_0 \equiv \frac{ec}{r_0} \tag{1.38}$$

Bunching, gain and the coherence

Having discussed the gain mechanism, let us now consider the relationship between the gain and the bunching mechanism. The electron beam from rf-accelerators come in pulses which may sometimes exhibit a micro-structure. Each pulse consists of many bunches of electrons. These bunches are typically 1 mm - 1 cm long spatially. The FEL bunching is conceptually very similar to the rf-cavity bunching. Inside the wiggler each electron bunch is further bunched at the optical wavelengths (the spatial dimension of these bunches is approximately equal to the wavelength of the FEL radiation) and this is the mechanism responsible for the coherence of FEL radiation since the radiation emitted from each electron in the bunch will interfere constructively. FEL bunching is independent of the size of the rf-electron pulse, therefore FEL bunching will occur even when a continous electron beam is used. The growth of coherence and the coherence properties of FEL radiation will be examined in much more detail in later chapters here we

would like to describe the bunching mechanism from the viewpoint of classical physics.

For the purpose of this section we will express the helical wiggler vector potential in the following form.

$$\vec{A}_w = \frac{\hat{e}_- a}{\sqrt{2}} e^{-\frac{i}{2}(k_w z + ck_w t)} + c.c \qquad (1.39)$$

where $\hat{e}_\mp = \frac{(\hat{e}_x \mp i\hat{e}_y)}{\sqrt{2}}$ are unit vectors representing left and right circular polarization. This is one of the possible ways of representing the static wiggler field as a traveling wave propogating in a direction opposite to the incident electrons. The laser field may be expanded as a sum over all the spatial modes of the cavity. If we assume that only one lasing mode is supported, then the laser field vector potential will be

$$\vec{A}_L = \frac{\hat{e}_- a_s}{\sqrt{2}} e^{-i(\omega t - kz)} + c.c \qquad (1.40)$$

Now consider the Lorentz force on the electrons,

$\vec{F} = e(\vec{E} + \vec{v} \times \vec{B})$, we are interested in the longitudinal force $\vec{F}_L$ given by $\vec{F}_L = e\,\vec{v}_\perp \times \vec{B}$

since $v_\perp = \frac{p_x}{m_0\gamma} = -\frac{cK\sqrt{2}}{\gamma} \sin k_w z \propto \vec{A}_w$

$v_\perp$ is proportional to $\vec{A} = \vec{A}_w + \vec{A}_L$, therefore

$$\vec{F}_L \propto \vec{A} \times \text{curl}\, \vec{A} \propto \frac{\partial}{\partial z}(A^2) \qquad (1.41)$$

where A^2 is the square of the total field and given by

$$A^2 = a^2 + a_s^2 + \left\{ aa_s \, e^{-[(\omega - ck_w/2)t - (k_w/2 + k)z]} + c.c \right\} \qquad (1.42)$$

a_s^2 and a^2 do not contribute to the derivative, only the cross terms (beating of the wiggler and the laser fields) give rise to $\vec{F}_L$. This force creates a "bunching potential" which is sinusoidal in nature and propogates with the velocity

$$v_r = \frac{\omega - ck_w/2}{k + k_w/2} \qquad (1.43)$$

Figure 6 illustrates how the bunching process works. The electrons are either accelerated or decelerated depending on their relative phase with respect to the phase of the bunching potential. In either case they tend to fall into the potential wells and become bunched at the bottom which determines the size of the bunch (approximately equal to $2\pi/k$) . If the electron enters the wiggler with the velocity v_r it will neither be accelerated nor decelerated hence no gain. Therefore it is necessary to bias the average electron velocity v_z of the rf-bunch so that $v_z \geq v_r$. This makes sure that there is some net deceleration of the electrons, and their excess energy is radiated into the laser field.

The relationship between the gain and the bunching is an indirect one. For the most part, gain can be derived from single particle dynamics (assuming no space-charge effects). There is however a subtle relationship which can only be explained by noting the fact that when the electrons are not bunched at the optical wavelengths, the fields produced by different electrons tend to interfere destructively, resulting in a low operating efficiency.

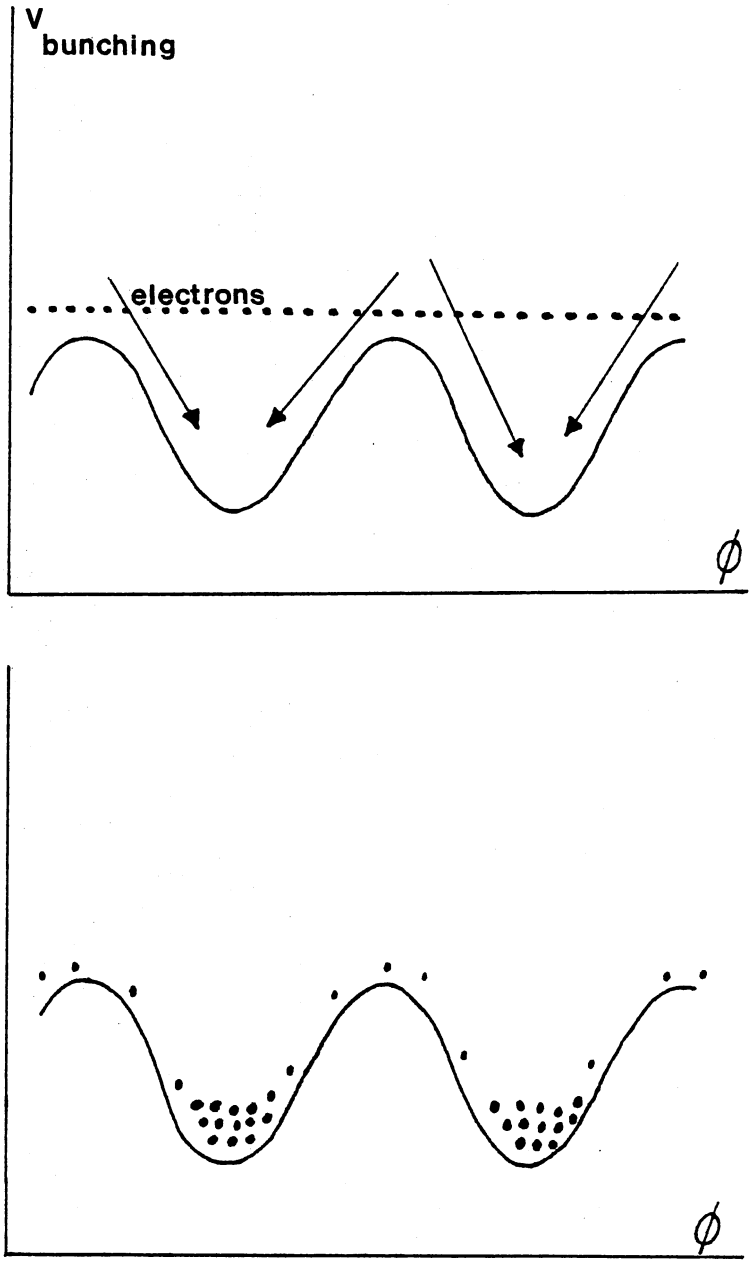

Figure 6. FEL bunching. Here the incident electrons are shown stationary with respect to bunching potential.

REFERENCES

[1] J. Schwinger, Phys.Rev., 75, 1912 (1949).

[2] J.C. Slater, "Microwave Electronics", page 222, van Nostrand, Princeton, NJ (1963)
The design is due to W.W. Hansen of Stanford University.

[3] J.C. Slater, ibid, page 302 .

[4] J.C. Slater, ibid, page 280 .

[5] F.S.Rusin and G.D. Bogomolov, JETP Lett., 4 , 160 (1966) .

K.Mizuno, S. Ono and Y. Shibata, IEEE Trans.Electron.Devices, ED-20,749 (1973).

[6] R.M. Phillips, IRE Trans.Electron.Devices, ED-7, 231 (1960) .

[7] K.K. Chow and R.H. Pantell, IRE Trans.Electron.Devices, ED-9, 351 (1962) .

V.L. Granatstein et al, J.Appl.Phys., 46 , 2021 (1975) .

[8] L.R. Elias, W.M. Fairbank, J.M.J. Madey, H.A. Schwettman and T.I. Smith, Phys.Rev.Lett., 36 , 717 (1976).

[9] J.M.J. Madey, J.Appl.Phys., 42 , 1906 (1971) .

[10] J. Pierce, "Traveling Wave Tubes", van Nostrand, NY (1950) .

[11] H. Motz, J.Appl.Phys., 22 , 527 (1951).

[12] W.B. Colson, Phys.Lett., 64A , 190 (1977) .

[13] J.M.J. Madey, Nuovo Cimento, 50B , 64 (1979).

[14] D.A.G. Deacon et al , Opt.Comm., 40 , 373 (1982).

CHAPTER II

FREE ELECTRON LASERS FROM ACCELERATOR PHYSICS PERSPECTIVE

Introduction

The relationship between the particle accelerator and the FEL goes beyond the component-device connection. Obviously the accelerator is a component of the FEL and it will have effects on the operation of FEL as such. But as mentioned by Morton [1], the equations of FEL dynamics are analogous to the equations of electron dynamics in an accelerator. This analogy made it possible for accelerator physicists to formulate the FEL dynamics in their own language and make significant contributions in the practical realizations of the FEL devices. From this formulation emerged the conclusion that not any accelerator can be used as an FEL component and that it has to be optimized for the FEL operation. In some cases a totally new design was needed. The most recent trend in FEL development is to build accelerators specifically tuned to FEL operation since the beam quality requirements for an FEL operation exceeds the up-grading capabilities of the existing accelerators which were designed and built for high-energy physics and synchrotron-radiation research experiments originally.

It is beyond the scope of this thesis to give a complete treatment of the electron dynamics in an accelerator. We will briefly review the

properties of accelerators relevant to the FEL operation. Even though Linac type accelerators are commonly used for FEL experiments, we shall concentrate on storage-ring type accelerators in this chapter. This is due to our emphasis on quantum mechanical aspects of FELs throughout the thesis and the fact that those FELs which exhibit quantum mechanical properties are designed to be inserted in storage-rings.

Single Particle Dynamics

In circular accelerators there is an orbit called "design orbit" or "equilibrium orbit" which is a function of particle energy, such that if a particle is launched on this orbit in the ring it will return to the same point traveling with the same initial direction.

Obviously, not all the particles in the beam follow this design orbit since they enter the ring at slightly different positions and times. The seperation of equilibrium-orbits for different energies is given by

$$\delta x = \eta \frac{\delta\gamma}{\gamma} \tag{2.1}$$

where η , a function of azimuth in the accelerator, is called the "Dispersion". The difference between the total path length of two different energy equilibrium orbits is given by

$$\frac{\delta L}{L} = \frac{\alpha_c}{\beta^2}\left(\frac{\delta\gamma}{\gamma}\right) \tag{2.2}$$

where α_c is an integral around the azimuth called the "momentum compaction factor". This integral involves the dispersion function η and the local bending radius R . $\beta = v/c$

Let us investigate the particle motion in the transverse plane (x,y). The path length s along the ring is used as the independent variable instead of time t, since for relativistic particles the velocity is practically independent of the energy (ds/dt ≅ c). Linearized and decoupled equations of motion for a particle with the design energy are [2]

$$\frac{d^2x}{ds^2} = - K_x(s)\, x \tag{2.3}$$

$$\frac{d^2y}{ds^2} = - K_y(s)\, y \tag{2.4}$$

The coefficients $K_{x,y}(s)$ ("Focusing functions") are periodic functions of the magnetic configuration of the guide field. In Table I, we have listed $K_{x,y}$ for various elements. The periodicity of $K_{x,y}$ is the same as that of the machine

$$K_{x,y}(s+L) = K_{x,y}(s) \tag{2.5}$$

where L is the orbit length. The general solutions of equations (2.3)-(2.4) can be written as

$$x(s) = a\xi(s)\cos[\phi(s)-\phi_0] \tag{2.6}$$

where $\xi(s)$ and $\phi(s)$ are specially defined functions of s with certain convenient properties and "a", "ϕ_0" are constants (initial conditions) which determine a particular trajectory. It is customary to define

$$\phi(s) = \int_0^s \frac{ds'}{\xi^2(s')} \tag{2.7}$$

so that

$$\phi'(s) \equiv \frac{d\phi}{ds} = \frac{1}{\xi^2} \equiv \frac{1}{\beta(s)} \tag{2.8}$$

therefore the solution looks like

$$x(s) = a\sqrt{\beta(s)}\,\cos(\phi(s)-\phi_0) \tag{2.9}$$

with $$\phi(s) = \int_0^s \frac{ds'}{\beta(s')} \tag{2.10}$$

and $$\beta(s) \equiv \xi^2(s) \tag{2.11}$$

The "Beta function" $\beta(s)$ can be interpreted as the "instantaneous wavelength" of the betatron oscillations (oscillations of the particle with respect to design orbit) and is uniquely determined once the "focusing function" $K_{x,y}(s)$ for the ring is given. Therefore $\beta(s)$ can serve as an alternate representation of the focusing characteristics of the ring. Usually a plot of the desired $\beta(s)$ is the first step in the design of a circular (cyclic) accelerator. Accelerator designers try to come up with a magnet configuration ("Lattice") which has the desired Beta-function. This process of design is an art-form and involves intricate engineering considerations.

Once the Beta-function is known, one can also define the frequency of "Betatron oscillations" per revolution which is commonly called the "Betatron tune".

$$\nu = \frac{1}{2\pi}\int_0^L \frac{ds'}{\beta(s')} \tag{2.12}$$

Until now, we have assumed that the particle's energy is equal to the design-orbit energy. Particles with different energies see different $K_{x,y}$ which leads to a change in the betatron tune $\nu_{x,y}$. At this point we have to define a new parameter called the "Chromaticity" of the machine.

$$C_{x,y} = \frac{E_0 \, \Delta\nu_{x,y}}{\nu_{x,y} \, \Delta E} \tag{2.13}$$

In a well designed machine this parameter must be kept as small as possible to avoid a large frequency spread in the beam. Chromaticity is controlled by sextupole magnets.

If we follow the evolution of x(s) and (dx/ds), turn after turn, at a particular s_0, we see that x, $x' \equiv (dx/ds)$ describe an ellipse whose area is given by

$$\varepsilon_x = \pi W \tag{2.14}$$

where ε_x is called the beam-emittance. W is an invariant given by

$$W = \gamma(s)x^2 + 2\alpha(s)xx' + \beta(s)x'^2 = \text{constant} \tag{2.15}$$

where $\alpha(s)$ and $\gamma(s)$ are functions dependent on $\beta(s)$

$$\alpha(s) \equiv -\frac{1}{2}\frac{d\beta(s)}{ds} \tag{2.16}$$

$$\gamma(s) \equiv \frac{1+\alpha^2(s)}{\beta(s)} \tag{2.17}$$

$\alpha(s)$, $\beta(s)$, $\gamma(s)$ are generally called "Twiss coefficients" and W is called the "Courant-Snyder" invariant [4]. The ellipse described by (2.15) changes throughout the machine but the area (emittance) is constant which is a consequence of the Liouville theorem.

From (2.14) and (2.15) one can derive the beam envelope (transverse dimension of the beam) σ_x and its divergence σ'_x, defined as the rms values of x and x' over many betatron-oscillations (at a fixed s)

$$\sigma_x(s) = \sqrt{\langle x^2 \rangle} = \left(\frac{\varepsilon_x \, \beta(s)}{2\pi} \right)^{1/2} \tag{2.18}$$

$$\sigma_{x'}(s) = \sqrt{\langle x'^2 \rangle} = \left(\frac{\varepsilon_x \beta(s)}{2\pi} \right)^{1/2} \tag{2.19}$$

TABLE I

FOCUSING FUNCTIONS FOR VARIOUS MAGNET ELEMENTS

Element	K_x	K_y
Free Space	0	0
Bending magnet	$\left(\frac{eB_y}{E}\right)^2$	0
Quadrupole magnet	$\frac{e}{E}\frac{\partial B_y}{\partial x}$	$-\frac{e}{E}\frac{\partial B_y}{\partial x}$
Helical wiggler magnet	$\frac{1}{2}\left(\frac{eB_y}{E}\right)^2$	$\frac{1}{2}\left(\frac{eB_x}{E}\right)^2$

E : Energy of the particle

e : Electrical charge of the particle

$B_{x,y}$: Magnetic field components

same reasonings apply to y and y' and one can similarly derive σ_y and $\sigma_{y'}$.

Now, let us investigate the longitudinal motion. This refers to the interaction of charged particles with the accelerating cavities. During acceleration, a radio-frequency voltage is generated across the gap of an accelerating cavity. There is one particle arriving at the gap at a proper time to receive a predetermined energy gain to stay at the design orbit governed by the guide field (Lattice). Such a particle is called "synchronous particle" (s.p). Other particles in the vicinity of s.p. will execute "Synchrotron Oscillation" around the s.p. in both energy deviation and phase coordinates. Since the phase deviation is manifested as coordinate deviation in the longitudinal direction this oscillatory motion is called longitudinal motion. The voltage accross the gap of the accelerating cavity can be written as

$$V(t) = V_0 \sin \Psi(t) \tag{2.20}$$

The rf-frequency ω is an integral multiple h ("harmonic number") of the revolution frequency Ω_0 of the synchronus particle

$$\omega = h\Omega_0 \tag{2.21}$$

The energy gain of the s.p. in one revolution will be

$$\delta E_0 = eV_0 \sin \Psi_0 \tag{2.22}$$

For a non-synchronous particle (n.s.p.) in the vicinity of s.p. the parameters will be

$$\begin{aligned} E &= E_0 + \delta E & \Omega &= \Omega_0 + \delta\Omega \\ p &= p_0 + \delta p & \gamma &= \gamma_0 + \delta\gamma \\ \Psi &= \Psi_0 + \delta\Psi \end{aligned} \tag{2.23}$$

where p is the momentum of the particle. Now we can define the "dispersion" η which was briefly mentioned in (2.1)

$$\eta(s) \equiv - \frac{d\Omega}{\Omega} / \frac{dp}{p} = \frac{1}{\gamma_{tr}^2} - \frac{1}{\gamma^2} \tag{2.24}$$

where γ is the relativistic factor and γ_{tr} is the γ which defines the "transition energy". It can be seen from (2.24) that at a particular energy γ_{tr} the increase in in particle speed with energy is exactly compensated by the increase in path length with energy. Above γ_{tr}($\gamma > \gamma_{tr}$) η becomes negative meaning that the revolution frequency Ω (which is equal to v/L) decreases with increasing energy. This is a relativistic effect and somewhat surprising to common sense.

The change in path-length with increasing energy was given in (2.2) where the "momentum compaction factor" α_c was introduced. Now we give the full definition of α_c .

$$\alpha_c \equiv \frac{1}{L} \oint \frac{\eta(s)}{\rho(s)} \tag{2.25}$$

where $\rho(s)$ is the "radius of curvature" of the particle. Using (2.24), (2.25) and (2.2) we derive the change in the angular revolution frequency

$$\frac{d\Omega}{\Omega} \equiv \left(\frac{dv}{v} - \frac{\delta L}{L} \right) = \frac{1}{\beta^2} \left(\frac{1}{\gamma^2} - \frac{1}{\gamma_{tr}^2} \right) \frac{\delta\gamma}{\gamma} \tag{2.26}$$

Since $\omega = h\Omega$ the average change in the phase Ψ of the electric field in the cavity between the time of successive passages of the particle through the cavity is given by

$$\frac{d\Psi}{dz} = \frac{\delta\Psi}{2\pi R} = - \frac{h}{\beta^2 R} \left(\frac{1}{\gamma^2} - \frac{1}{\gamma_{tr}^2} \right) \frac{\delta\gamma}{\gamma} \tag{2.27}$$

where R is the average ring radius equal to the circumference divided by

2π , and z is the coordinate measured along the design-orbit ($s \rightarrow z$).

The rate of change of the particle energy can easily be derived from (2.22) for the n.s.p.

$$\frac{d\gamma}{dz} = \frac{eV_0}{m_0c^2} \sin\Psi \tag{2.28}$$

and for the s.p.

$$\frac{d\gamma_0}{dz} = \frac{eV_0}{m_0c^2} \sin\Psi_0 \tag{2.29}$$

subtracting we obtain

$$\frac{d(\delta\gamma)}{dz} = \frac{eV_0}{m_0c^2} [\, \sin\Psi - \sin\Psi_0 \,] \tag{2.30}$$

The equations (2.30) and (2.27) are the standard rf-equations of accelerator physics. Compare (2.30) to (1.13) of Chapter I. Equation (2.30) of accelerator dynamics and Eq.(1.13) of FEL dynamics are very similar. This similarity becomes more obvious when we write K in (1.13) in terms of magnetic field strength and also by making the transformation

$\frac{d}{dt} \rightarrow \frac{c}{dz}$, the Eq.(1.13) becomes

$$\frac{d}{dz}(\delta\gamma) = -\frac{(eE_0)(eB_{0w}c)}{\sqrt{2}\, k_w \gamma (m_0c^2)\sqrt{2}\, m_0c^2} [\sin\Psi_- - \sin\Psi_+] \tag{2.31}$$

$$\equiv -\frac{k_s a_s a_w}{\gamma} [\sin\Psi_- - \sin\Psi_+]$$

since the vector potential of the laser (signal) field is

$$a_s = \frac{eE_0}{\sqrt{2}\, k_s m_0c^2} \tag{2.32}$$

and

$$a_w = \frac{eB_0 c}{\sqrt{2}\, k_w m_0 c^2} \tag{2.33}$$

Now (2.31) and (2.30) are analogous. The transition from accelerator to FEL dynamics is made by the replacement

$$\frac{eV_0}{m_0 c^2} \rightarrow -\frac{k_s a_s a_w}{\gamma} \tag{2.34}$$

This similarity makes it possible to describe the entrapment of electrons in the ponderomotive potential of the FEL in terms of the "phase stability" concepts of accelerator physics. In other words the ponderomotive potential (a moving beat-wave) of the FEL acts just like the acceleration cavity of the accelerator.

Having established this analogy we now introduce the "phase stability" of an accelerator. Changing back to "time" t as the independent variable and combining (2.27) and (2.30) and linearizing we obtain the following differential equation for the relative phase $\Delta\Psi = \Psi - \Psi_0$

$$\frac{d^2(\Delta\Psi)}{dt^2} - \Omega_s^2(\Delta\Psi) = 0 \tag{2.35}$$

where

$$\Omega_s^2 \equiv \frac{eV_0 h\eta\Omega_0 \cos\Psi_0}{2\pi p_0 R}$$

Equation (2.35) has stable oscillatory solutions if

$$\eta \cos\Psi_0 < 0 \tag{2.36}$$

which is realizable in a synchrotron in two situations

$$\begin{aligned} &\text{a)} \quad \gamma < \gamma_t \qquad \text{and} \qquad 0 < \Psi_0 < \pi/2 \\ &\text{b)} \quad \gamma > \gamma_t \qquad \text{and} \qquad \pi/2 < \Psi < \pi \end{aligned} \tag{2.37}$$

(assuming that particles are being accelerated) Ω_s is called the "synchrotron oscillation frequency" and the physical interpretation of this phase oscillation is as follows. A lagging particle B will gain energy when it passes through the cavity and will speed up. At a certain point it overtakes the synchronous particle and leads it. This will make it to arrive at the cavity earlier than the s.p. therefore obtaining less energy from the rf-cavity than the s.p. Then the reverse process will start. This oscillation in phase (hence in longitudinal position) is the machanism of "phase stability". The ratio of "synchrotron oscillation" frequency Ω_s to revolution frequency Ω_0 is often called the "tune of the synchrotron oscillation"

$$\nu_s = \frac{\Omega_s}{\Omega_0} \tag{2.38}$$

This number is usually in the order of 10^{-2}-10^{-3} for proton synchrotrons and 10^{-1} for the electron storage-rings. As a comparison, $\nu_{x,y}$ of the betatron oscillations is in the order of 10, usually less than 10 but greater than 1. The concept of "phase stability" and "synchrotron oscillations" is illustrated in Figures 7 and 8.

It is instructive to see the trajectories of stable solutions in the $\delta\gamma$-Ψ plane (Figure 9). The closed trajectories correspond to particles trapped in "buckets". The maximum stable phase curve of a single bucket is shown in Figure 10. The maximum value of $\delta\gamma$ for which a particle may be trapped in a bucket is given by

$$\delta\gamma_{max} = \frac{2\beta^2 ReV_0\gamma}{h\left(\frac{1}{\gamma^2} - \frac{1}{\gamma_{tr}^2}\right)} \Gamma(\Psi_0) \tag{2.39}$$

where

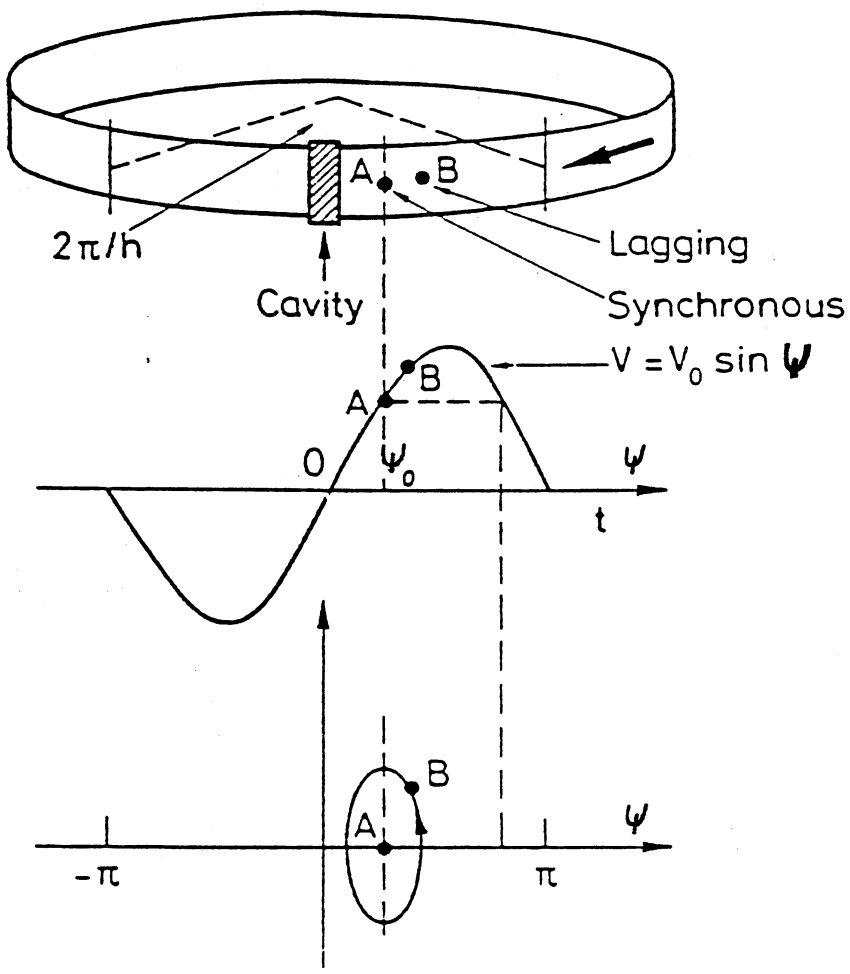

Figure 7. RF phase angle in longitudinal phase space

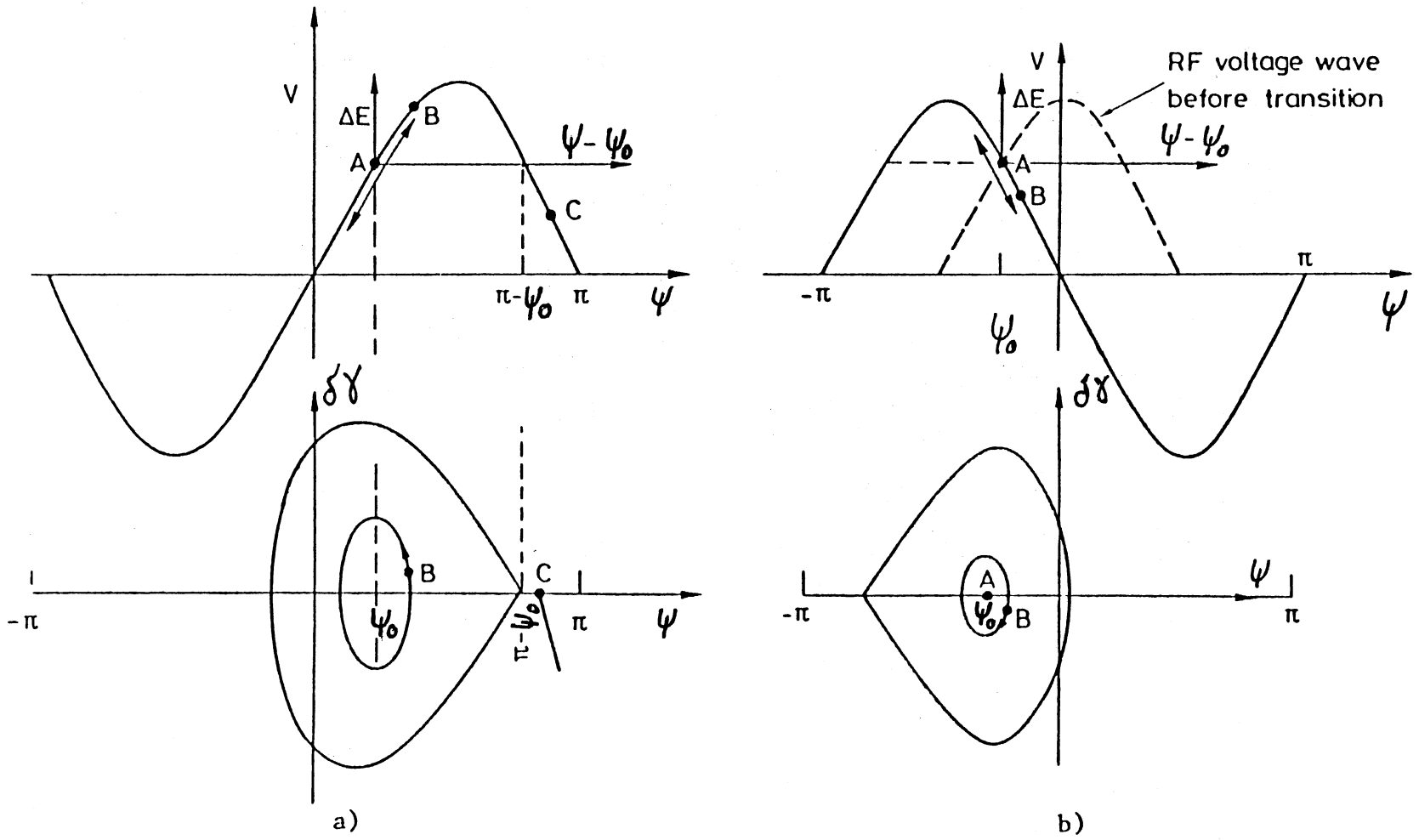

Figure 8. Phase stability of synchrotron motion (a) below and (b) above transition

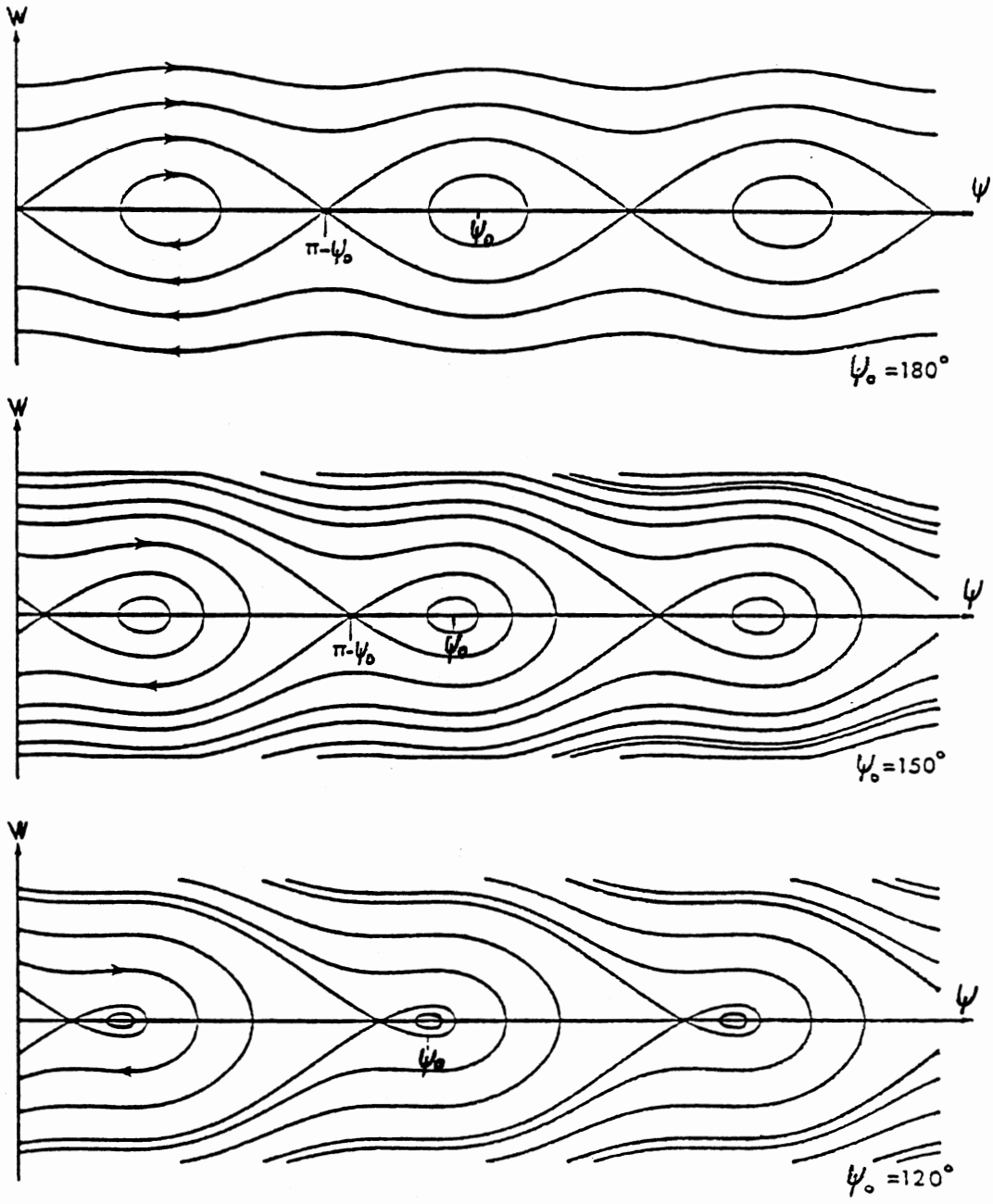

Figure 9. Trajectories of constant Hamiltonian

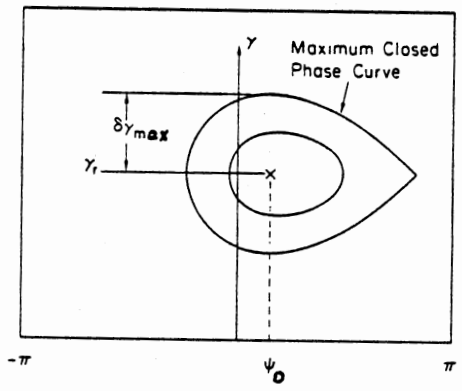

Figure 10. Stable phase plane trajectories

$$\Gamma(\Psi_0) = [\cos\Psi_0 - (\frac{\pi}{2}\sin\Psi_0 - \Psi_0)\sin\Psi_0]^{1/2}$$

The analogous expression in the FEL dynamics is

$$\left(\frac{\delta\gamma_{max}}{\gamma}\right) = 2\left(\frac{a_s a_w}{1+a_w^2}\right)^{1/2}\Gamma(\Psi_0) \tag{2.40}$$

To complete the analogy we list here the other transformations from accelerator physics to FEL dynamics

$$-\frac{h}{\beta^2 R}\left(\frac{1}{\gamma_0^2} - \frac{1}{\gamma_{tr}^2}\right) \Rightarrow k_s\left(\frac{1}{\gamma_0^2} + \frac{a_w^2}{\gamma_0^2}\right) \tag{2.41}$$

$$\Omega_s \Rightarrow \Omega_{s_{FEL}} = 2k_w\left(\frac{a_s a_w \cos\Psi_0}{1+a_w^2}\right)^{1/2} \tag{2.42}$$

In the light of (2.42) we now have the understanding that the fundamental frequency emitted in the FEL is a result of the "synchrotron-oscillations" of the electrons trapped in the optical-bucket (opposed to the rf-bucket of the acceleration cavity). This formulation has been developed in great detail in references [5], [6] so here we only mentioned the basics of accelerator physics, FEL dynamics analogy. We shall now move on to other aspects of FEL-Accelerator complex.

FEL Interaction and Electron Energy Spread

In addition to the energy spread introduced by the rf cavities of the accelerator (natural-energy spread), the FEL interaction also introduces an energy-spread. This spread depends on the gain of the FEL and for the small signal regime there is a theorem derived by Madey [7] which relates the net energy loss of the electrons $\langle\gamma_f - \gamma_i\rangle$ averaged over the entry phases relative to the phase of ponderomotive potential, to

the phase-averaged energy spread $\langle(\gamma_f-\gamma_i)^2\rangle$

$$\langle \gamma_f-\gamma_i\rangle = \frac{1}{2}\frac{\partial}{\partial\gamma_i}\langle(\gamma_f-\gamma_i)^2\rangle \tag{2.43}$$

The theorem connects the mechanism of FEL gain with the broadening of the electron energy distribution. This connection will be examined in some detail again in Chapter VII. From the accelerator physics perspective this FEL introduced energy spread means trouble if the accelerator being used is not a Linac. In the Linac a fresh bunch enters the wiggler and when it exits the wiggler it is dumped. But in a cyclic accelerator such as storage-ring the same electron bunch is re-injected into the wiggler over and over again. Therefore the beam must be cooled down before it is re-injected into the wiggler. In a storage-ring accelerator (electron or positron machine) one does not have to devise extra measures of cooling, the beam cools down rather automatically due to "Radiation damping". Radiation damping due to the effect of the radiation loss on the motion of the charged particle is a well known consequence in Synchrotron Radiation [8]. This damping process can be slow for the high-gain FELs, in that case the wiggler is not inserted into the ring but set-up on a by-pass. This way the electron beam is diverted into the by-pass only when it is cool enough to satisfy the FEL requirements.

Other FEL Issues in a Storage-Ring Operation

As can be seen from (1.35) and (1.36), the most important requirements for an FEL to work, ie., to have sufficient gain and to reach saturation at a reasonable power level, are as follows:

a) The current density of the beam must be sufficiently high.

b) The energy (or momentum) spread of the beam must be sufficiently small.

The first requirement is especially strong for the short-wavelength (λ <1000 A^0) FELs since no good mirrors are available at these wavelengths and the only way to achieve coherent radiation from free electrons is to have a very high gain (hence very bright electron beam) and a long wiggler.

When we look at these requirements from the accelerator physics perspective we see that they are conflicting. A high current density in a storage-ring accelerator is only achieved at the expense of a large energy-spread. It is difficult to achieve a high electron density in a storage-ring because of the "quantum-excitation" process. If it were not for the "quantum-excitation process" (which is a consequence of the fact that synchrotron radiation is emitted in photons of discrete energy) the "radiation damping" would cause the beam to collapse into a very dense and singular electron bunch. The transverse size $\sigma_{x,y}$ of the beam is finalized when a balance is reached between the "radiation damping" and the "quantum excitations".

As the current density increases the collective effects become important. The most important of these are

a) Touschek-effect (Intra-beam scattering): Two electrons oscillating within a bunch may Coulomb scatter, transferring some of the oscillation energy of each electron from one coordinate to another. When such a scatter occurs in a dispersive region of the Lattice, a radial betatron oscillation is excited. As a result, beam grows both radially and longitudinally, thereby increasing the emittance and decreasing the electron density.

Formal treatment of the intrabeam-scattering is very complicated but an approximate expression for the radial diffusion rate was found [9].

$$\frac{1}{\tau_x} \propto \frac{\hat{I}}{\varepsilon_x^2} < \frac{\sqrt{H}}{\sigma_p \gamma^3 \sqrt{\beta_y}} > \tag{2.44}$$

where

$$H \equiv \gamma_x \eta^2 + 2\alpha_x \eta\eta' + \beta_x \eta'^2$$

with α_x , β_x , γ_x being the Twiss parameters, η the dispersion function and η' its derivative with respect to s. σ_p is the natural momentum spread.

The stored beam in a storage-ring accelerator has a finite life time. The Touschek lifetime is proportional to γ^3 , to the square of the momentum acceptance and inversely to the beam density. So aside from the limitation that Touschek-effect prevents the achivement of a dense beam, supposing that we have such a beam, then the lifetime of the beam would be shortened, an undesirable feature.

b) Coherent Instabilities: The circulating electron beam produces electromagnetic fields on the vacuum chamber walls which influence the motion of the other stored electrons. Such collective interactions can cause "unstable coherent oscillations" which lead to a growth of the bunch size $\sigma_{x,y}$ or to the loss of electrons from the bunch thereby decreasing current density.

It is now clear that in a storage-ring accelerator one cannot achieve very dense electron beam (compared to other type of accelerators storage-ring still has the best beam quality, i.e. highest current density and lowest energy spread) without increasing the energy spread or without causing some collective effects to arise.

REFERENCES

[1] P.L. Morton, in "Physics of Quant. Elec.", vol 8, p:1 (1982) eds: S.F. Jacobs, G.T. Moore, H.S. Pilloff, M. Sargent III M.O. Scully, R. Spitzer (Addison Wesley).

[2] D. Edwards, in "1987 Fermilab US. Particle Acce. School Proceedings" to be published.

[3] G. Dattoli et al, in "Free Electron Lasers", p:343 (1983) eds: S. Martellucci and A.N. Chester (Plenum Press).

[4] E.D. Courant and H.S. Snyder, Ann.Phys. 3, 1 (1958).

[5] N.M. Kroll et al, J.Quant.Electr. QE-17, 1496 (1981).

[6] A. Szoke et al, in "Phys.Quant.Electr.", 7, 175 (1980).

[7] J.M.J. Madey, Nuovo Cim. 50B, 64, (1979).

[8] J.D. Jackson, "Classical Electrodynamics",pp:783, Wiley (1975)

[9] A. Jackson et al, Proc. SPIE, 582, 131 (1985).

CHAPTER III

QUANTUM THEORY OF THE FREE ELECTRON LASER : INTRODUCTION TO LATER CHAPTERS

Introduction

Classical theories of the FEL have been largely successful in explaining the experimentally relevant features of the existing FEL devices as we described in Chapters I and II. The first analysis and the proposal of the FEL mechanism was based on a quantum mechanical calculation by Madey [1]. It was however realized later that the expression for gain did not contain h and the quantum theory of the FEL was abandoned so that subsequent research efforts were concentrated on the classical aspects of the FEL.

From a theoretical point of view, classical theory of the FEL is not satisfactory. At the most fundamental level the gain mechanism of the classical theory ignores the recoil momentum of the electron due to the emission or absorption of a photon and thus becomes only a rough approximation.

Even though the quantum theory was neglected in the early development of FEL, everyone agrees on the fact that a quantum theory is essential for a proper treatment of the start-up of the FEL from the initial noise and for an explanation of the evolution of coherence. This is due to the fact that in the early stages of FEL start-up the number of photons in the cavity is small and the relative magnitude of

the fluctuations is large. The frequency and the phase of the signal are not very well defined and the gain is much lower than the value predicted by the classical theory.

The questions involving photon statistics and the quantum coherence are far from being purely academic questions, on the contrary, photon statistics has observable, macroscopic consequences in the operation of an FEL. Unfortunately we do not have a satisfactory fully quantum mechanical many photon theory of the FEL at hand to treat the start-up problem properly. The problem of photon statistics cannot be treated separately from the electron dynamics. Until now all the efforts for the formulation of the photon statistics of an FEL relied on approximate solutions of either Klein-Gordon or Dirac equation (in the case of moving frame formulation the solutions of Schrodinger equation) for the motion of electrons. In this thesis, we shall derive the solutions of Dirac equation for the motion of an electron in a uniform helical wiggler, a tapered helical wiggler and a wiggler with axial guide field respectively. These solutions are 2-D solutions, i.e., transverse momentum components have been included right from the beginning in the Dirac Hamiltonian. Once the transverse momentum effects have been included in the electron dynamics, it is our hope that a complete theory of the photon statistics of the FEL will be developed based on our 2-D solutions.

In addition to derivations of 2-D solutions of Dirac Equation for the motion of an electron in various helical wiggler geometries we also carried out perturbational calculations to obtain the small-signal gain expressions in these configurations. We especially demonstrated

the effects of quantum mechanical transverse momentum corrections on the spontaneous-emission linewidth and gain. Quantum mechanics sheds some further light on the "instability region" when there is an axial-guide field, this will be discussed in Chapter VI. In Chapter VII we carry out numerical calculations to investigate the effects of quantum mechanics on saturation mechanism. In Chapter VII we also develop a classical model for the FEL and incorporate the quantum mechanical effects into it.

Finally, we would like to point out that quantum theory, especially the electron dynamics aspects of it, significantly alters the classical theory of the FELs operating in the x-ray region. Therefore the quantum theory of the FEL becomes absolutely essential for the short-wavelength FELs.

Formulation: Preliminaries

In our formulation we chose the Relativistic-Quantum Mechanical approach since in general the transverse motion is nontrivial and there is no frame in which the electron is completely nonrelativistic. Also multimode fields, pulse propagation problems and nonuniform wigglers cannot be handled by a nonrelativistic approach. Above all, we want to avoid approximations as much as possible. A moving-frame formulation involves many approximations. Before we discuss the laboratory-frame formulation in detail let us briefly summarize the moving-frame formulation.

The moving-frame approach is based on the basic idea that the wiggler field is seen by the electron as a radiation field moving towards it. This is the inherent approximation of this formulation

(akin to Weisacker-Williams approximation) which is problematic from a theoretical point of view since the transverse motion complicates this picture. Once this is accepted then the FEL interaction reduces to a scattering problem. In other words the laser and wiggler photons hit the electron from opposite directions and the electron scatters the "wiggler-photons" into "Laser-photons" and vice versa. Gain is possible because the stimulated forward scattering of wiggler photons into laser photons is larger than that of backward scattering. This process is illustrated in Figure 11.

In the formulation one has the freedom of choosing any moving frame in which the motion of the electron is nonrelativistic. There is one choice which is particularly useful for the clarification of the ideas, namely the so called Bambini-Renieri frame [2], in which the laser photons and the wiggler photons have the same frequency. Let us assume only two modes and hence a quantized radiation field

$$A = \vec{A}_L + \vec{A}_w \tag{3.1}$$

L and w label the laser and wiggler fields.

$$\vec{A}_L = i\left(\frac{2\pi c\hbar}{\omega V}\right)^{1/2}(a_L\, e^{ikz}\,\hat{e} + a_L^+\, e^{-ikz}\,\hat{e}^*) \tag{3.2}$$

$$\vec{A}_w = i\left(\frac{2\pi c\hbar}{\omega V}\right)^{1/2}(a_w\, e^{-ikz}\,\hat{e} + a_w^+\, e^{ikz}\,\hat{e}^*) \tag{3.3}$$

where a and a^+ are the annihilation and creation operators respectively. Both Laser and Wigglar photons are assumed to be circularly polarized

$$\hat{e} = \frac{1}{\sqrt{2}}(\hat{x} + i\hat{y}) \tag{3.4}$$

V is the interaction volume, ω is the common frequency of photons in

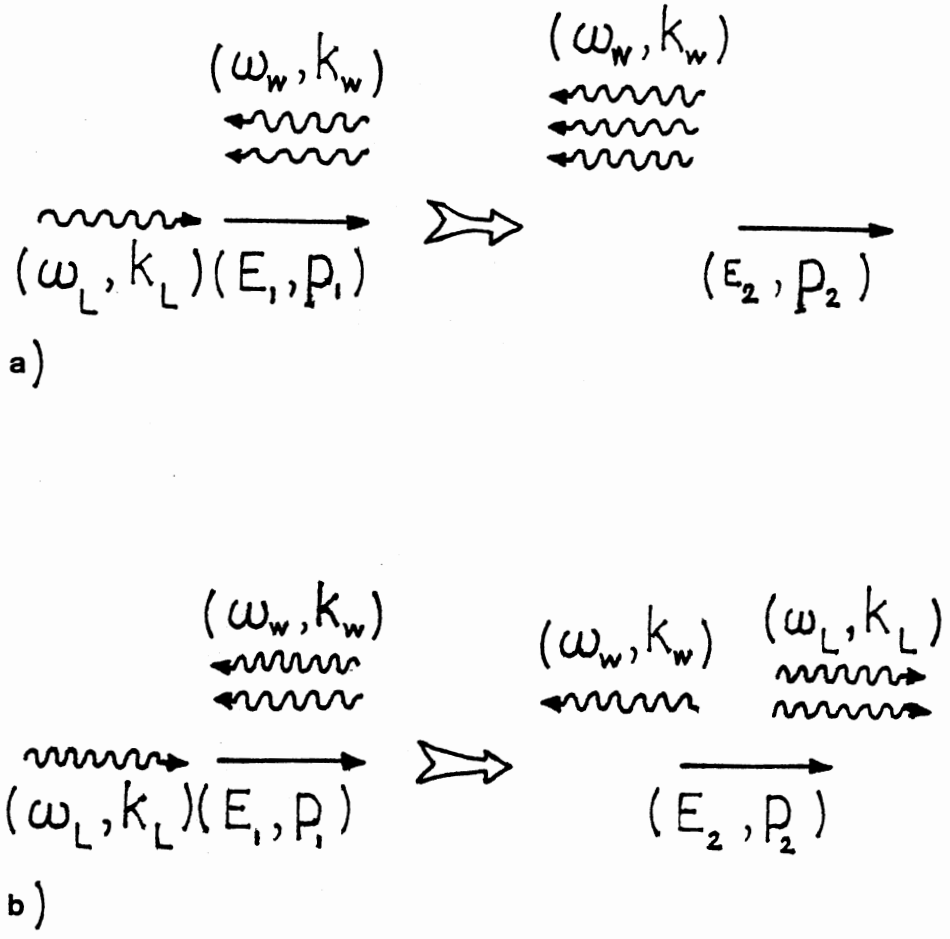

Figure 11. FEL process in non-relativistic formulation (a) stimulated backward scattering (negative gain) (b) stimulated forward scattering (positive gain)

Bambini-Renieri frame. The Hamiltonian can be written as

$$H = \frac{1}{2m_0}\left(\vec{p} - \frac{e}{c}\vec{A}\right) + \hbar\omega\left(a_L^+ a_L + \frac{1}{2}\right) + \hbar\omega\left(a_w^+ a_w + \frac{1}{2}\right) \tag{3.5}$$

more explicitly

$$H = \frac{p_z^2}{2m_0} + \hbar C\left[a_L^+ a_w\, e^{-2ikz} + a_w^+ a_L\, e^{2ikz}\right] + \hbar(\omega + C)\left(a_L^+ a_L + \frac{1}{2}\right) + \hbar(\omega + C)\left(a_w^+ a_w + \frac{1}{2}\right) \tag{3.6}$$

where p_z is the longitudinal momentum and

$$C \equiv \frac{2\pi c^2 r_0}{\omega V} \quad , \quad r_0 \equiv \frac{e^2}{m_0 c^2}$$

the interaction term of the above Hamiltonian is the second term

$$H_I = \hbar C\left[a_L^+ a_w\, e^{-2ikz} + a_w^+ a_L\, e^{2ikz}\right] \tag{3.7}$$

which can be understood as follows

1st term in (3.7): a Laser photon is created, a wiggler photon is annihilated, the electron loses $2\hbar k$ of its momentum.

2nd term in (3.7): a Laser photon is annihilated, a Wiggler photon created, the electron gains $2\hbar k$ of momentum.

In order to derive gain it is simpler to use a Schrodinger wave function. The Hilbert space is taken as [3]

$$H = |\, n_L\rangle \otimes |\, n_w\rangle \otimes |p\rangle \tag{3.8}$$

namely the direct product of fields and electron Fock spaces. The quantum state can be written as [4]

$$|\Psi\rangle = e^{-i(p_z/2\hbar k)^2 \omega t} \sum_l C_l \left|n_L^0 + l,\ n_w^0 - l,\ \frac{p_{z0}}{2\hbar k} - l\right\rangle \tag{3.9}$$

where p_{z0} is the initial electron momentum, $n_{L,w}^0$ is the initial number of laser (wiggler) photons and l is the number of exchanged photons.

Number of wigler photons is practically unchanged ($n_w^0 >> |l|$). Using this information, Schrodinger equation yields the following differential equation for the time-dependent C_l coefficient.

$$iC_l' = -(\nu-\varepsilon l)lC_l + \rho(\sqrt{n_L^0+l+1}\ C_{l+1} + \sqrt{n_L^0+l}\ C_{l-1}) \tag{3.10}$$

with initial condition

$$C_l(0) = \delta_{l,0} \tag{3.11}$$

where the prime means derivative with respect to $\tau = (t/\Delta t)$, Δt being the interaction time and

$$\nu \equiv 2\omega\ \Delta t\ \frac{p_{z0}}{m_0 c} \quad , \quad \varepsilon \equiv \omega\ \Delta t \quad , \quad \rho \equiv C\sqrt{n_w^0}\ \Delta t \tag{3.12}$$

we now use the small-signal approximation

$$\rho\sqrt{n_L^0} \ll 1 \tag{3.13}$$

which allows a perturbative solution of (3.10). Expanding up to the first order in ρ, it was found

$$C_l \simeq C_l^0 + \rho\ C_l^1 \tag{3.14}$$

with initial conditions

$$C_l^0(0) = \delta_{l,0} \quad , \quad C_l^1(0) = 0 \tag{3.15}$$

inserting (3.14) into (3.10) and using (3.15), it was obtained

$$\begin{aligned} C_0^0(\tau) &= 1 \\ C_1^1(\tau) &= \rho\sqrt{n_L^0+1}\left(\frac{1-e^{i(\nu-\varepsilon)\tau}}{\nu-\varepsilon}\right) \\ C_{-1}^{-1}(\tau) &= -\rho\sqrt{n_l^0}\left(\frac{1-e^{i(\nu+\varepsilon)\tau}}{\nu+\varepsilon}\right) \end{aligned} \tag{3.16}$$

The difference between the probabilities of absorbing and emitting a photon will be

$$\Delta n_L = |C_1^1|^2 - |C_{-1}^1|^2 = \rho^2\left[-n_L^0\left(\frac{\sin(\nu+\epsilon)/2}{(\nu+\epsilon)/2}\right)^2+(n_L^0+1)\left(\frac{\sin(\nu-\epsilon)/2}{(\nu-\epsilon)/2}\right)^2\right] \tag{3.17}$$

since ϵ a small quantity (for the Stanford experiment $\epsilon \simeq 10^{-7}$) we can use the relation

$$\left(\frac{\sin(\nu\mp\epsilon)/2}{(\nu\mp\epsilon)/2}\right) = e^{\mp\epsilon\frac{\partial}{\partial\nu}}\left(\frac{\sin\nu/2}{\nu/2}\right)^2 \simeq (1\mp\epsilon\frac{\partial}{\partial\nu})\left(\frac{\sin\nu/2}{\nu/2}\right) \tag{3.18}$$

(3.17) can be rewritten as

$$\Delta n_L \simeq \rho^2\ [1-(2n_L^0+1)\epsilon\frac{\partial}{\partial\nu}\ ]\left(\frac{\sin\nu/2}{\nu/2}\right)^2 \tag{3.19}$$

From (3.19) it can be concluded that there are two contributions to Δn_L, i.e., those from the stimulated and those from the spontaneous emission

$$(\Delta n_L)_{stimulated} = -2n_L^0\rho^2\epsilon\frac{\partial}{\partial\nu}\left(\frac{\sin(\nu/2)}{(\nu/2)}\right)^2 \tag{3.20}$$

$$(\Delta n_L)_{spon} = (\Delta n_L)_{spon}^{QM} + (\Delta n_L)_{spon}^{CM} \tag{3.21}$$

where

$$(\Delta n_L)_{spon}^{QM} = -\rho^2\epsilon\frac{\partial}{\partial\nu}\left(\frac{\sin(\nu/2)}{(\nu/2)}\right)^2 \tag{3.22}$$

$$(\Delta n_L)_{spon}^{CM} = \rho^2\left(\frac{\sin(\nu/2)}{(\nu/2)}\right) \tag{3.23}$$

Therefore the spontaneous emission consists of a quantum part $(\Delta n_L)_{spon}^{QM}$ and a classical part $(\Delta n_L)_{spon}^{CM}$. The quantum contribution is the "stimulated emission" due to the vacuum field fluctuations and cannot be derived in any way from a classical theory. If one compares the expression for gain $G = (\Delta n_L)/n_L^0$ to (1.35) of Chapter I, it can easily be verified that (1.35) is equivalent to G .

Relativistic Quantum Mechanical Formulation of the FEL

The question of Dirac equation versus Klein-Gordon equation is resolved clearly and easily in the favor of Dirac equation for the following reasons. By using Klein-Gordon equation we ignore the spin effects, important to this thesis, which are nonnegligable for the x-ray FELs. Not only are the spin-effects important in FEL gain and frequency calculations but they are also very important to investigate the polarization of the emitted radiation. We also believe that our solutions of Dirac equation for the motion of an electron in a helical wiggler field will find applications in accelerator physics in general, especially in high energy experiments at SLC type linear colliders where there is no reliable method of polarizing the electron-beam. Helical wigglers modified under the guidance of our 2-D solutions of Dirac equation can be used to polarize electrons in linear colliders (storage-ring machines automatically polarize the electron beam, given enough time).

We have to include the wiggler field as an external potential because it is too strong to be treated as a perturbation to the free-particle Dirac-spinors. Therefore the solutions of the Dirac equation for the motion of an electron in a helical wiggler field is the starting point of a correct quantum theory of the FEL. We shall derive these solutions for various wiggler geometries in the following chapters, here we assume that such solutions exist and proceed with the methods of the formulation.

The QED interaction Hamiltonian for a charged particle and a photon is given by

$$H_I = e\, J_\mu A^\mu \tag{3.24}$$

where the current density J_μ for a single particle is

$$J_\mu = \bar{\Psi}\, \gamma^\mu\, \Psi \tag{3.25}$$

Here γ^μ are the Dirac-γ matrices, the bar means the Dirac conjugate and the spinors Ψ are the solutions of the Dirac equation for the electron moving in the presence of an external wiggler potential. And A^μ is the wavefunction of a photon. This interaction Hamiltonian can be illustrated by Feynman diagrams as in Figure 12. By looking at the Feynman diagram in Figure 12 one can argue that the stimulated emission is not included in this picture since it shows only the spontaneous emission and absorption. This argument is a valid one since in a real FEL interaction an electron can emit or absorb more than one photon during its flight through the wiggler due to stimulated emission process. Therefore we have to include the multiphoton processes (2nd, 3rd, ... order graphs in the Feynman diagram) in the interaction Hamiltonian.

But due to a remarkable process unique to the FEL interaction this will not be necessary if we want to calculate the small-signal gain. We shall discuss this point shortly, but first, we need to lay-out the plan for the calculation of small-signal gain.

First, we have to calculate the matrix elements for various transitions. There are four possible transitions

$$\uparrow p \Rightarrow \uparrow p'$$
$$\downarrow p \Rightarrow \downarrow p'$$
$$\uparrow p \Rightarrow \downarrow p'$$
$$\downarrow p \Rightarrow \uparrow p'$$

Here the arrows refer to up-spin and down-spin. A relativistic electron

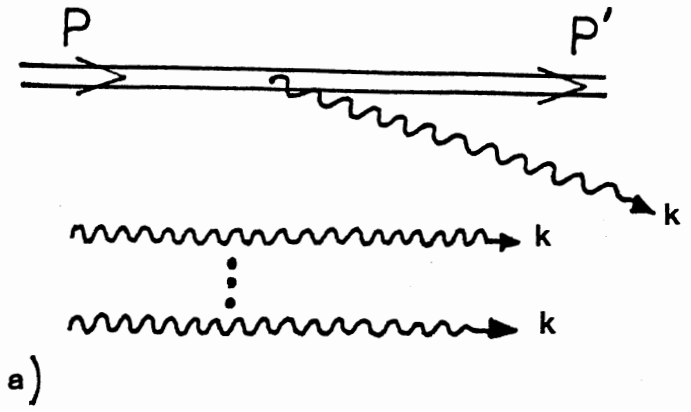

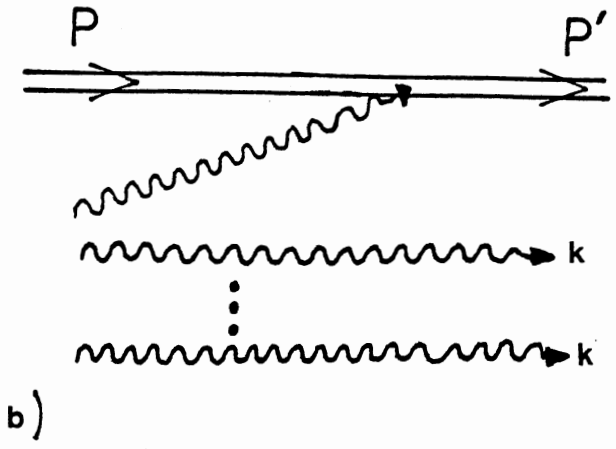

Figure 12. Feynman diagrams for (a) the emission (b) absorption of a photon by an electron

of momentum p emits or absorbs a photon and makes a transition to p' and during this transition its spin may or may not flip. All of these four transitions can produce a backward emission of a photon as well as a forward emission and same is true for absorption. The emitted or the absorbed photon can be left-circularly or right-circularly polarized, so altogether there are 32 matrix elements that need to be calculated. But fortunately the backward emission and absorption probabilities are very small and almost equal to each other and thus there is no gain in the backward direction. But formally one has to calculate these matrix elements and probabilities.

The matrix element for the emission or absorption of one photon is then given by

$$M = -\frac{i}{\hbar} < \text{final} | \int d^4x \, H_I | \text{initial} > \tag{3.26}$$

where

$$\begin{aligned} |\text{initial} > &= |p> \, |n_L> \\ |\text{final} > &= |p'> \, |n_L \mp 1> \end{aligned} \tag{3.27}$$

n_L stands for the number of photons. The integration in (3.26) is extended either over all space and a finite interaction time Δt or, equivalently, over the wiggler Length L_w and an unrestricted interaction time (from $-\infty$ to $+\infty$).

Once we have the knowledge of $|p>$ and $|p'>$ we can easily calculate the matrix elements. The gain is then defined as the difference between the rates for emission and absorption, integrated over the phase-space of the final electron state, divided by the number of initial photons and multiplied by the number of electrons.

$$G = \frac{N_e}{V} \int \frac{d^3p'}{(2\pi)^3} \left(|M_{emiss}|^2 - |M_{absorp}|^2 \right) \tag{3.28}$$

From the quantum mechanics of atoms one would think that $|M_{emiss}|^2$ and $|M_{absorp}|^2$ are the same but in the case of FEL interaction this is not true. $|M_{emiss}|^2$ is slightly greater than $|M_{absorp}|^2$ due to the recoil. Therefore a gain is possible.

Now in (3.28) it was assumed that all the electrons initially had the same energy and momentum, but in a real electron beam there is always an energy spread. In that case (3.28) will be modified as

$$G = \frac{N_e}{V} \int d^3p\ f(p) \int \frac{d^3p'}{(2\pi)^3} \left(|M_{emiss}|^2 - |M_{absorp}|^2 \right) \tag{3.29}$$

where f(p) is the initial electron momentum distribution with the following normalization

$$\int d^3p\ f(p) = 1 \tag{3.30}$$

The approach outlined above calculates the small-signal gain. We have considered the probabilities of emission and absorption of a single photon, although we know that in the FEL interaction one electron can emit or absorb about 1- 10^5 photons during one pass through the wiggler. But if we examine (3.29), it can be seen that G involves a subtraction operation, in other words even though we did not include the higher order terms in the perturbational calculation we still get the correct answer since the higher order contributions tend to cancel out each other. Indeed it has been shown [4] that if a proper account is taken of all the multiphoton (higher order graphs) processes the meaning of the first order quantity $|M_{emiss}|^2$ changes. It does no longer give the probability of one photon emission, but specifies instead the mean number of emitted photons. This makes it plausible the fact that we

obtained the correct small-signal gain by merely considering the 1st order (single-photon) processes [5].

REFERENCES

[1] J.M.J. Madey, J.Appl.Phys. 42, 1906 (1971).

[2] A. Bambini and A. Renieri, Lett.Nuovo Cim. 21, 399 (1978).

[3] G. Dattoli and A. Renieri, in "Laser Handbook Vol 4", p:1. eds: M. L. Stitch and M. Bass (North Holland) (1985).

[4] R.J.Glauber, Phys.Rev. 84, 395 (1951).

[5] W. Becker and J.K. McIver, J.de Physique, Supp 2, 44, C1-289 (1983).

CHAPTER IV

TWO-DIMENSIONAL SOLUTIONS OF THE DIRAC EQUATION FOR THE MOTION OF AN ELECTRON IN A HELICAL WIGGLER FIELD

Introduction

In the classical analyses of the FEL interaction, the equations of motion for the relativistic electrons in a helical wiggler play an essential role and they have been studied exhaustively in the literature [1]. In the quantum theory of the FEL, one needs a wavefunction in place of the classical equation of motion. When the amplitude of the radiation field is small (small-signal regime) the radiation field can be treated as a perturbation. Therefore one needs the eigenfunctions of a relativistic quantum mechanical Hamiltonian which includes the helical wiggler field as an external potential since it can not be treated as a perturbation. Therefore, the solutions of the Dirac equation for the motion of an electron in a helical wiggler field is the starting point of a correct quantum theory of the FEL.

The Form of the Solutions

We write the Dirac equation (time-independent) in the direct product notation $\vec{\alpha} = \vec{\rho}_1 \otimes \vec{\sigma}$

$$\underset{\sim}{H}\,\Psi \equiv (c\rho_1 \vec{\sigma} \underset{\sim}{\vec{P}} + \rho_3 m_0 c^2 - E)\Psi = 0 \qquad (4.1)$$

Here $\vec{P}$ is the kinetic momentum $\vec{P} = \vec{p} - \frac{e}{c}\vec{A}$ where

$$\vec{A} = a\cos(k_w^* z)\hat{x} + a\sin(k_w^* z)\hat{y} \tag{4.2}$$

is the vector potential of the wiggler field on the axis and k_w^* is the wavenumber of the wiggler. Here the star * refers to a tapered wiggler where k_w^* is a smoothly increasing function of the form

$$k_w^*(z) = k_{w0} - \frac{b_t}{z} \tag{4.3}$$

This function is plotted in Figure 13 to show that it is possible to obtain a smoothly increasing curve by choosing the initial and final values of the z-parameter. In our matrix elements calculations, only the length of the wiggler L_w is important and z_{final}, $z_{initial}$ do not affect the results, therefore one is free to choose z_{init} and z_{final} to make k_w as smooth as desired. Ultimately this form of tapering, i.e., the decrement of the distance in between magnet poles (λ_w) of a wiggler along the axis so that the radiating and slowing electrons would stay in resonance, approaches a linear function which is the most commonly used tapering form in the experiments. The form of tapering that we adopted (4.3), was illustrated and explained in more detail in reference [3].

Since we derived the 2-D solutions for both a uniform wiggler and a tapered one, we shall present the derivation for the tapered one so that the derivation for the uniform wiggler basically runs along the same lines and one can obtain the solutions for the uniform wiggler by simply taking the limit $b_t \to 0$ in the solutions for the tapered wiggler.

The Dirac Hamiltonian in equation (4.1) can be written in the 4x4 form

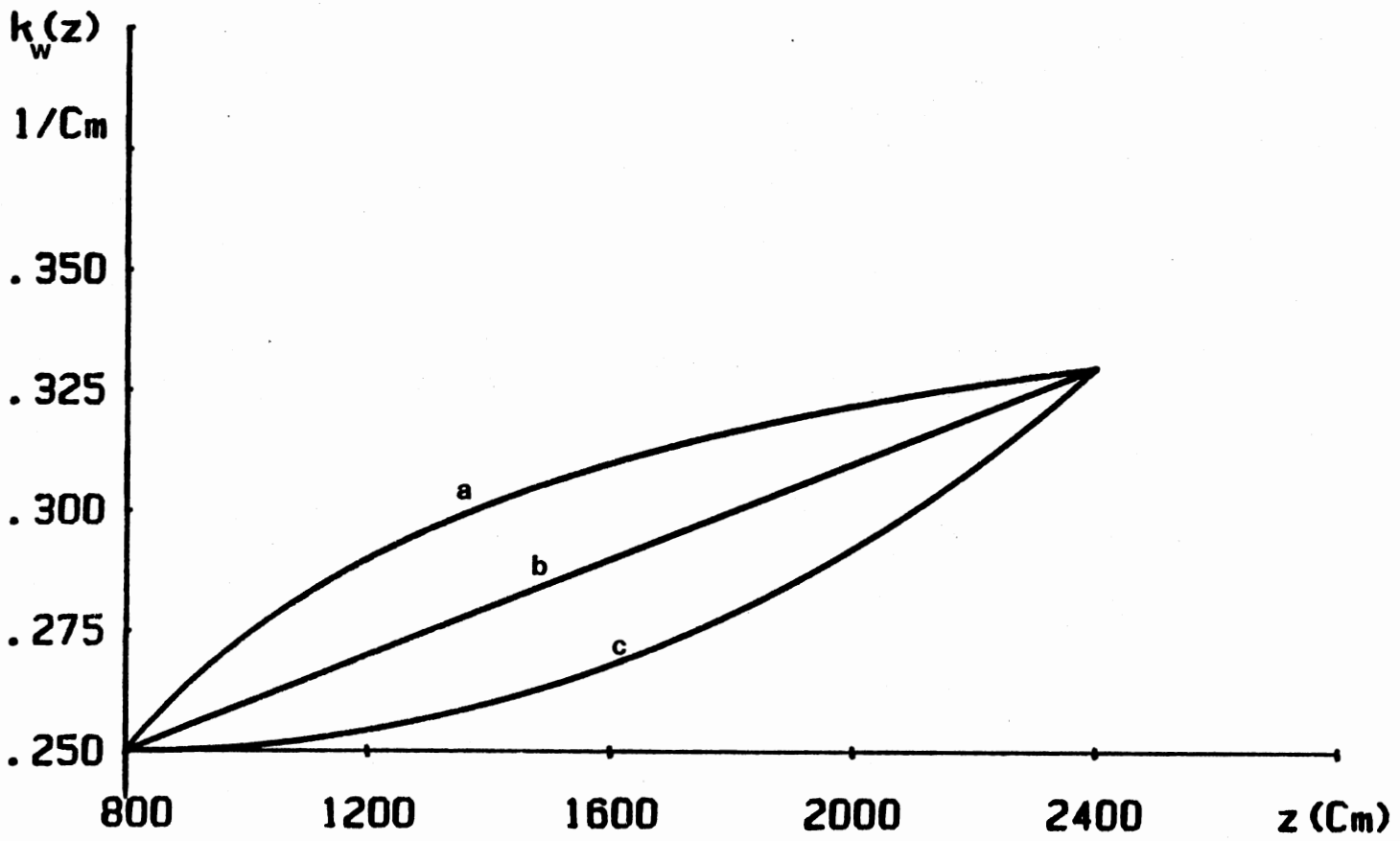

Figure 13. (a) Proposed tapering (b) Linear tapering (c) Exponential tapering

$$\begin{bmatrix} A & B \\ B & C \end{bmatrix} \begin{bmatrix} \phi_1 \\ \phi_2 \end{bmatrix} = \begin{bmatrix} 0 \\ 0 \end{bmatrix} \tag{4.4}$$

where

$$A \equiv \begin{bmatrix} (m_0c^2-E) & 0 \\ 0 & (m_0c^2-E) \end{bmatrix}$$

$$C \equiv \begin{bmatrix} -(m_0c^2+E) & 0 \\ 0 & -(m_0c^2+E) \end{bmatrix}$$

$$B \equiv \begin{bmatrix} cp_z & cp_- - ea\, e^{-ik_w^* z} \\ cp_+ - ea\, e^{ik_w^* z} & -cp_z \end{bmatrix}$$

Here

$$p_+ = p_x + ip_y \quad , \quad p_- = p_x - ip_y$$

and the tilde ~ indicates a quantum mechanical operator.

In earlier quantum mechanical treatments of the FEL, the transverse momentum components p_x ,p_y were ignored. Becker and Mitter [2] gave the exact 1-D solutions ($p_x=0$, $p_y=0$) for the case of a uniform helical wiggler. Later, 1-D exact solutions for the case of a tapered wiggler were derived [3]. In this thesis we shall derive the 2-D [4] solutions using the Hamiltonian which includes one of the transverse momentum operators ($p_x \neq 0$, $p_y=0$). In principle one can also derive 3-D solutions but these unnecessarily complicate the gain and frequency calculations. 2-D solutions on the other hand are tractable and also fully account for the effects of transverse momentum. Experimentally, 2-D solutions are meaningful because the electron beam stays very close to the axis.

The Hamiltonian (4.4) commutes with the p_x and p_y operators. The solutions have therefore to be simultaneous eigenfunctions of p_x , p_y

and $\underset{\sim}{H}$. Therefore we try the ansatz

$$\begin{bmatrix} f_1(z) \\ f_2(z) \\ f_3(z) \\ f_4(z) \end{bmatrix} e^{i/\hbar\,(p_{1x}x + p_{1y}y)} \tag{4.5}$$

$$\begin{bmatrix} g_1(z) \\ g_2(z) \\ g_3(z) \\ g_4(z) \end{bmatrix} e^{i/\hbar\,(p_{2x}x + p_{2y}y)} \tag{4.6}$$

for the up-spin and down-spin electron respectively, although this nomenclature is not that meaningful when a particle is in a field. Here $p_{1x}, p_{1y}, p_{2x}, p_{2y}$ are c-numbers. This way the spinors are already the eigenfunctions of $\underset{\sim}{p}_x$, and $\underset{\sim}{p}_y$.

Derivation: Equations

Operation on (4.5) and (4.6) with the (4.4) we obtain two sets of equations.

$$\begin{aligned}
&(m_0c^2-E)f_1 + c\underset{\sim}{p}_z f_3 + cp_{1-}f_4\, e^{ik_w^* z} - eaf_4 = 0 \\
&(m_0c^2-E)f_2 + cp_{1+}f_3\, e^{-ik_w^* z} - eaf_3 - c\underset{\sim}{p}_z f_4 - \hbar ck_w f_4 = 0 \\
&c\underset{\sim}{p}_z f_1 + cp_{1-}f_2\, e^{ik_w^* z} - eaf_2 - (m_0c^2+E)f_3 = 0 \\
&cp_{1+}f_1 e^{-ik_w^* z} - eaf_1 - c\underset{\sim}{p}_z f_2 - \hbar ck_w f_2 - (m_0c^2+E)f_4
\end{aligned} \tag{4.7}$$

$$\begin{aligned}
&(m_0c^2-E)g_1 + cp_z g_3 - \hbar ck_w g_3 + cp_{2-}g_4\, e^{ik_w^* z} - eag_4 = 0 \\
&(m_0c^2-E)g_2 + cp_{2+}g_3\, e^{-ik_w^* z} - eag_3 - c\underset{\sim}{p}_z g_4 = 0
\end{aligned}$$

$$cp_{\sim z}g_1 - \hbar ck_w g_1 + cp_{2-}g_2\, e^{ik_w^* z} - eag_2 - (m_0c^2+E)g_3 = 0$$

$$cp_{2+}g_1 e^{-ik_w^* z} - eag_1 - cp_{\sim z}g_2 - (m_0c^2+E)g_4 = 0 \qquad (4.8)$$

here

$$p_{1+} = p_{1x} + ip_{1y} \qquad p_{1-} = p_{1x} - ip_{1y}$$

$$p_{2+} = p_{2x} + ip_{2y} \qquad p_{2-} = p_{2x} - ip_{2y} \qquad (4.9)$$

are c-numbers not operators.

From the last two equations of (4.7) we have

$$f_3 = \frac{1}{(E+m_0c^2)}\left(cp_{\sim z}f_1 + cp_{1-}f_2 e^{ik_w^* z} - eaf_2 \right) \qquad (4.10)$$

$$f_4 = \frac{1}{(E+m_0c^2)}\left(- cp_{\sim z}f_2 - \hbar ck_w f_2 + cp_{1+}f_1 e^{-ik_w^* z} - eaf_1 \right) \qquad (4.11)$$

substituting these in the first two equations of (4.7) we obtain

$$\left(c^2 p_{\sim z}^2 - eac(p_{1-}e^{ik_w^* z} + p_{1+}e^{-ik_w^* z}) + \eta_1^2 \right) f_1 + (ea\hbar ck_w) f_2 = 0 \qquad (4.12)$$

$$\left(c^2 p_{\sim z}^2 - eac(p_{1-}e^{ik_w^* z} + p_{1+}e^{-ik_w^* z}) - 2(\hbar ck_w)cp_{\sim z} + \eta_1^2 + (\hbar ck_w)^2 \right) f_2 + (ea\hbar ck_w) f_1 = 0 \qquad (4.13)$$

where $$\eta_1^2 \equiv m_0^2c^4 - E^2 + e^2a^2 + c^2(p_{1x}^2 + p_{1y}^2) \qquad (4.14)$$

is the effective energy parameter (or mass parameter).

Combining (4.12) and (4.13) we obtain

$$\left(c^2 p_{\sim z}^2 - ea(p_{1-}e^{ik_w^* z} + p_{1+}e^{-ik_w^* z}) - 2(\hbar ck_w)cp_{\sim z} + \eta_1^2 + (\hbar ck_w)^2 \right)$$

$$x \left(c^2 p_{\sim z}^2 - eac(p_{1-}e^{ik_w^* z} + p_{1+}e^{-ik_w^* z}) + \eta_1^2 \right) f_1(z) = (ea\hbar ck_w)^2 f_1(z) \qquad (4.15)$$

Similarly another equation exist for $g_2(z)$ of the down-spin electron.

$$\left(c^2 p_z^2 - eac(p_{2-}e^{ik_w^* z} + p_{2+}e^{-ik_w^* z}) - 2(\hbar ck_w)cp_z + \eta_2^2 + (\hbar ck_w)^2\right)$$

$$x\left(c^2 p_z^2 - eac(p_{2-}e^{ik_w^* z} + p_{2+}e^{-ik_w^* z}) + \eta_2^2\right) g_2(z) = (ea\hbar ck_w)^2 g_2(z) \qquad (4.16)$$

where $$\eta_2^2 \equiv m_0^2 c^4 - E^2 + e^2 a^2 + c^2(p_{2x}^2 + p_{2y}^2) \qquad (4.17)$$

at this stage we change the variable

$$k_w^* z \rightarrow 2\xi \qquad (4.18)$$

then (4.15) becomes ($p_{1x} \neq 0$, $p_{1y} = 0$)

$$\left([\frac{d^2}{d\xi^2} - 4i\frac{d}{d\xi} - 2q\cos 2\xi - (\lambda_2+4)][\frac{d^2}{d\xi^2} - 2q\cos 2\xi - \lambda_2] - \lambda_3\right) f_1(\xi) = 0 \qquad (4.19)$$

where

$$q \equiv \frac{4|e|acp_{1x}}{(\hbar ck_w)^2} \qquad (4.20)$$

$$\lambda_2 \equiv \frac{4\eta_1^2}{(\hbar ck_w)^2} \quad , \quad \lambda_3 \equiv \left(\frac{4ea}{\hbar ck_w}\right) \qquad (4.21)$$

and ξ is a dimensionless variable. Let

$$f_1(\xi) = ce_\nu(\xi, q) + r\, se_\nu(\xi, q)$$

where ce_ν and se_ν are the Mathieu functions [5] (even and odd respectively) of fractional order. r is an unknown constant to be determined and ν is the fractional order parameter. Later we will see that ν is related to p_1 , the effective longitudinal momentum of the electron moving in a helical wiggler.

The differential equation (4.19) is a 4th order equation, therefore there must be four independent solutions in general. In (4.22) we considered two of these solutions ce_ν and se_ν. Both ce_ν and se_ν individually satisfy (4.19) and they are independent since ν is not an

integer [5]. We claim that (4.22) is the most general solution because (4.22) satisfies, with a change of multiplicative constant, the 2nd order differential equations that constitute equation (4.19). This can be seen from

$$\left(\frac{d^2}{d\xi^2} - 2q\cos 2\xi - \lambda_2\right)(ce_\nu + r\, se_\nu) = -(a_q+\lambda_2)(ce_\nu+rse_\nu) \tag{4.23}$$

where a_q is a constant which is related to q and ν . In other words a_q is the constant which is involved in the definition of Mathieu functions.

$$\left(\frac{d^2}{d\xi^2} - 2q\cos 2\xi + a_q\right)\begin{matrix} ce_\nu(\xi,q) \\ se_\nu(\xi,q) \end{matrix} = 0 \tag{4.24}$$

with the expansion

$$a_q = \nu^2 + \frac{1}{2(\nu^2-1)}\, q^2 + \frac{5\nu^2+7}{32(\nu^2-1)^3(\nu^2-4)}\, q^4 + \ldots \tag{4.25}$$

subject to the condition

$$\frac{q^2}{2(\nu^2-1)} \ll \nu^2 \tag{4.26}$$

For more details of the Mathieu functions see reference [5].

Thus, the 4th order differential equation is reduced to a 2nd order differential equation by employing the defining differential equation for Mathieu functions of the fractional order. Then (4.22), involving two independent solutions that satisfy (4.19), becomes the most general solution. A more physical way of saying the same thing is that the other two solutions that do not show up belong to the charge conjugate states (positrons when there is no field) whereas (4.22) is the solution for "positive energy" electron states of the Dirac equation.

The method of solution we are employing here can be described as the "ansatz" method. We are assuming that the final solution will come out

to be in the form of (4.22) with no undetermined constants and r will be a constant not a function of z. If r or any other assumed constant turns out to be a function of z then (4.22) would no longer be a solution. A similar assumption was made in the beginning for p_{1x}, p_{1y} p_{2x} and p_{2y}. If these turn out to be functions of z then again solutions will fail. But as we shall see at the end, the ansatz of (4.22), (4.5) and (4.6) work very well and the final solution does not contradict the assumptions.

Using (4.23), (4.19) reduces to

$$[\lambda\ (\lambda+4)\ -\ \lambda_3](ce_\nu+\ r\ se_\nu)\ +\ 4i\lambda\ \left(r\ \frac{dse_\nu}{d\xi}\ -\ \frac{dce_\nu}{d\xi}\right)\ =\ 0 \qquad (4.27)$$

where $\lambda = a_q+\lambda_2$. For (4.27) to be equal to zero, considering the evenness and the oddness of the Mathieu functions, we must have

$$[\lambda\ (\lambda+4)\ -\ \lambda_3]ce_\nu\ -\ 4i\lambda rF\ =\ 0 \qquad (4.28)$$

$$[\lambda\ (\lambda+4)\ -\ \lambda_3]r\ se_\nu\ -\ 4i\lambda G\ =\ 0 \qquad (4.29)$$

Here we denoted

$$F \equiv \frac{dse_\nu}{d\xi} \quad , \quad G \equiv \frac{dce_\nu}{d\xi} \qquad (4.30)$$

We obtain the same conditions (4.28), (4.29) from the second set of equations (4.8) by letting $g_2(\xi) = ce_\nu + r\ se_\nu$. The next step is to solve these equations (4.28) and (4.29) simultaneously for λ and r . We obtain

$$r\ =\ \frac{X}{4i\lambda(F/ce_\nu)} \qquad (4.31)$$

where

$$X \equiv \lambda(\lambda+4)\ -\ \lambda_3 \qquad (4.32)$$

$$X^2+16\lambda^2(F/ce_\nu)(G/se_\nu)\ =\ 0 \qquad (4.33)$$

Equation (4.33) is the most crucial step towards the solution of the Dirac equation. This is a determining equation for ν since X , λ ,F G, se_ν and ce_ν are all functions of ν . If we could determine ν exactly from this equation we would have exact solutions of the Dirac equation. But the Mathieu functions ce_ν , se_ν and their derivatives F and G are only known as power series [5] therefore explicit exact solutions do not exist in closed form. Exact solutions exist only in the sense that ν can be expressed in terms of Mathieu functions algebraicly.

Mathieu functions of fractional order can be expanded as

$$ce_\nu(\xi,q) = \cos\nu\xi - \frac{q}{4}\left(\frac{\cos(\nu+2)\xi}{(\nu+1)} - \frac{\cos(\nu-2)\xi}{(\nu-1)}\right) + \frac{q^2}{32}\left(\frac{\cos(\nu+4)\xi}{(\nu+1)(\nu+2)} + \frac{\cos(\nu-4)\xi}{(\nu-1)(\nu-2)}\right) + \ldots \tag{4.34}$$

$$se_\nu(\xi,q) = \sin\nu\xi - \frac{q}{4}\left(\frac{\sin(\nu+2)\xi}{(\nu+1)} - \frac{\sin(\nu-2)\xi}{(\nu-1)}\right) + \frac{q^2}{32}\left(\frac{\sin(\nu+4)\xi}{(\nu+1)(\nu+2)} + \frac{\sin(\nu-4)\xi}{(\nu-1)(\nu-2)}\right) + \ldots \tag{4.35}$$

Therefore the derivatives will be

$$G = -\nu\sin\nu\xi + \frac{q}{4}\left(\frac{(\nu+2)}{(\nu+1)}\sin(\nu+2)\xi - \frac{(\nu-2)}{(\nu-1)}\sin(\nu-2)\xi\right) - \frac{q^2}{32}\left(\frac{(\nu+4)}{(\nu+1)(\nu+2)}\sin(\nu+4)\xi + \frac{(\nu-4)}{(\nu-1)(\nu-2)}\sin(\nu-4)\xi\right) + \ldots \tag{4.36}$$

$$F = \nu\cos\nu\xi - \frac{q}{4}\left(\frac{(\nu+2)}{(\nu+1)}\cos(\nu+2)\xi - \frac{(\nu-2)}{(\nu-1)}\cos(\nu-2)\xi\right) + \frac{q^2}{32}\left(\frac{(\nu+4)}{(\nu+1)(\nu+2)}\cos(\nu+4)\xi + \frac{(\nu-4)}{(\nu-1)(\nu-2)}\cos(\nu-4)\xi\right) + \ldots \tag{4.37}$$

recalling the condition (4.26) we can easily observe that

$$(F/ce_\nu) \cong \nu \tag{4.38}$$

$$(G/se_\nu) \cong -\nu \tag{4.39}$$

We shall shortly prove that condition (4.26) is always satisfied for the FELs in particular and for all the relativistic electron beams in general.

Using (4.38) and (4.39), after some tedious algebra we obtain

$$r \cong i$$

which is a constant (imaginary numbers are allowed) and thus our original assumption is not contradicted.

The 2-D solutions are required to be consistent with the 1-D solutions derived in references [2] and [3], i.e., when q = 0 the 2-D solutions must go over into the 1-D solutions. Mathieu functions reduce to

$$ce_\nu(\xi, q=0) = \cos\xi\nu \tag{4.41}$$

$$se_\nu(\xi, q=0) = \sin\xi\nu \tag{4.42}$$

and $f_1(\xi)$ becomes

$$f_1(\xi)\big|_{q=0} = ce_\nu + r\, se_\nu\big|_{q=0} = \cos\xi\nu + i\sin\xi\nu = e^{i\xi\nu} \tag{4.43}$$

This must be equal to the exponential in the 1-D solution [3]

$$e^{i\xi\nu} \equiv e^{i\nu(k_w^* z/2)} \Rightarrow e^{i/\hbar\, p_1 z} \tag{4.44}$$

This leads us to the identity

$$\nu \equiv \frac{2p_1}{\hbar k_w} \tag{4.45}$$

Here p_1 is the effective longitudinal momentum of the up-spin electron moving in a helical wiggler field. Since p_1 is very large compared to the momentum imparted by $\hbar k_w$, ν is a very large number. That is why condition (4.26) is always satisfied for relativistic electron beams

(recall that q is proportional to the transverse momentum and $p_\perp/p_z$ ratio for a relativistic electron in an accelerator is always a small fraction).

Using (4.38) and (4.39), (4.33) becomes

$$[\lambda(\lambda+4)-\lambda_3]^2 - 16\lambda^2\nu^2 = 0 \tag{4.46}$$

Further expanding we obtain

$$\lambda^2 + 4\lambda - \lambda_3 \mp 4\lambda\nu = 0 \tag{4.47}$$

The solution of this equation leads us to

$$p_1 \cong -\frac{1}{2}\hbar k_w + \left[\left(p_{0z}+\frac{1}{2}\hbar k_w\right)^2 - \frac{e^2a^2}{c^2} + p_{0\perp}^2 - p_{1x}^2\right]^{1/2} \tag{4.48}$$

This is the determining equation for the effective longitudinal momentum in terms of the "design" parameters "a", k_w , the initial momentum components p_{0z} , $p_{0\perp}$ and the quantum mechanical correction p_{1x} which is going to be determined from a condition given by the normalization procedure.

Derivation: Solutions

The determination of p_1 and p_{1x} in terms of the given quantities completes the solution of the Dirac equation. Once we know $f_1(z)$ then $f_2(z)$, $f_3(z)$ and $f_4(z)$ can be determined from (4.7). The 2-D solution for an up-spin electron moving in a helical wiggler, satisfying all the conditions (commutes with $\underset{\sim}{p}_x$, reduces to 1-D solution when $p_{1x}= 0$) and within the range of the approximations discussed before, will be

$$\Psi^{\uparrow} = N_1 \begin{bmatrix} \phi_{11} \\ \phi_{12} \\ \phi_{21} \\ \phi_{22} \end{bmatrix} \left(ce_{\nu}(z,p_{1x}) + ise_{\nu}(z,p_{1x}) \right) e^{i/\hbar\, p_{1x} x} \tag{4.49}$$

where

$$\begin{aligned} \phi_{11} &\equiv 1 \\ \phi_{12} &\equiv K_1 e^{ik_w^* z} \\ \phi_{21} &\equiv \frac{[cp_{1x} e^{ik_w^* z} - ea\,]K_1 + cp_1}{E + m_0 c^2} \\ \phi_{22} &\equiv \frac{[cp_{1x} e^{-ik_w^* z} - ea\,] - c(p_1 + \hbar k_w)K_1}{E + m_0 c^2}\, e^{ik_w^* z} \end{aligned} \tag{4.50}$$

with

$$K_1 \equiv -\frac{c^2 p_1^2 + \eta_1^2 + \frac{1}{2} e^2 a^2 (p_{1x}/p_1)^2}{eahck_w} \tag{4.51}$$

and p_1 as given in (4.48).

The normalization constant N_1 and p_{1x} are determined from the normalization condition

$$\bar{\Psi}\,\Psi = 1 \tag{4.52}$$

where $\bar{\Psi}$ is the Dirac conjugate

$$\bar{\Psi} = \Psi^* \gamma^0 \tag{4.53}$$

after some algebra and the same approximations that were used in the derivation of (4.49) we obtain

$$N_1 \cong (1/2\gamma)^{-1/2} \tag{4.54}$$

$$c^2 p_{1x}^2 \cong \gamma\, (m_0 c^2)(\hbar c k_w)\left(\frac{\gamma}{K} + 1 \right) \tag{4.55}$$

where γ is the relativistic Lorentz factor of the electron and K is the wiggler strength parameter.

A similar solution is obtained for the down-spin electron along the same lines.

$$\Psi^{\downarrow} = N_2 \begin{bmatrix} \phi_{11} \\ \phi_{12} \\ \phi_{21} \\ \phi_{22} \end{bmatrix} \left(ce_{\nu}(z,p_{2x}) + ise_{\nu}(z,p_{2x}) \right) e^{i/\hbar\, p_{2x} x} \tag{4.56}$$

where

$$\phi_{11} \equiv K_2 e^{-ik_w^* z}$$

$$\phi_{12} \equiv 1$$

$$\phi_{21} \equiv \frac{[cp_{2x} e^{ik_w^* z} - ea\,] + c(p_2 - \hbar k_w) K_2}{E + m_0 c^2}\, e^{-ik_w^* z}$$

$$\phi_{22} \equiv \frac{[cp_{2x} e^{-ik_w^* z} - ea\,] K_2 - cp_2}{E + m_0 c^2} \tag{4.57}$$

with

$$K_2 \equiv - \frac{c^2 p_2^2 + \eta_2^2 + \frac{1}{2} e^2 a^2 (p_{2x}/p_2)^2}{eahck_w} \tag{4.58}$$

$$\eta_2^2 \equiv m_0^2 c^4 - E^2 + e^2 a^2 + c^2 p_{2x}^2 \tag{4.59}$$

$$cp_2 \cong \frac{1}{2}\hbar c k_w + \left(c^2 (p_{0z} - \frac{1}{2}\hbar k_w)^2 - e^2 a^2 + c^2 p_{0\perp} - c^2 p_{2x}^2 \right)^{1/2} \tag{4.60}$$

$$N_2 \cong (1/2\gamma)^{-1/2} \tag{4.61}$$

$$c^2 p_{2x}^2 \cong \gamma\, (m_0 c^2)(\hbar c k_w) \left(\frac{\gamma}{K} - 1 \right) \tag{4.62}$$

These 2-d solutions (4.56) and (4.49) can easily be converted to the solutions of Dirac equation for the motion of an electron moving in a uniform wiggler (k_w =constant) by simply setting $b_t = 0$ then $k_w^* \rightarrow k_w$= constant , and all the expressions retain their form.

It is a simple matter to see that (4.56) and (4.49) reduce to 1-D

solutions of reference [3], by letting $p_{1,2x} = 0$.

Further, note that these go over into free-particle spinors of Dirac theory when we switch-off the wiggler field, i.e., $a \to 0$, $k_w \to 0$.

Now we would like to comment on the physical interpretation of $p_{1,2x}$ Obviously $p_{1,2x}$ are the eigenvalues of p_x operator. Physically it is the quantum mechanical correction to (ea/c) which is the classical counterpart of the transverse momentum introduced by the wiggling motion. (ea/c) should not be confused with the initial transverse momentum of the electron $p_{0\perp}$ which is a constant of the motion. The term $p_{1,2x}$ has a purely quantum mechanical origin and is a consequence of the Dirac equation. It could not be predicted by any other equation such as Klein-Gordon or Schrodinger equations. Also note that p_{1x} and p_{2x} for up-spin and down-spin electrons respectively are slightly different therefore the effects of spin on the electron dynamics is naturally included. Finally $p_{1,2x}$ is proportional to γ therefore this quantum mechanical correction to (ea/c) should become more significant when the electrons are highly relativistic ($\gamma > 10^3$). We will develop this idea fully in the next chapter.

To conclude this chapter we can say that the solutions presented in this chapter can form the basis for a perturbation theory of the FEL operating in the small-signal regime. More importantly, the 2-D Dirac solutions derived here could provide guidance in the development of a Dirac Theory of the FEL in a helical wiggler including transverse momentum based on a Hamiltonian which includes the radiation field ab inito. Such a formulation could rigorously treat the strong-signal regime of the FEL. We concentrate in this thesis on the perturbative

Dirac Theory of the FEL and do not attempt the difficult task of finding an exact solution of the Hamiltonian including the radiation field. An approximate way of treating the strong-signal regime in the context of Quantum Theory of the FEL is available however developed by Fedorov, McIver and Becker [6]. This treatment of strong-signal regime relies on the Klein-Gordon equation thereby ignoring the spin effects. It is possible to extend these calculations by using the solutions of the Dirac equation for the motion of an electron in the field of a strong plane wave given by Volkov[7]. Swamy gave an elegant rederivation of these Volkov solutions [8] which are more suitable for matrix element calculations that are involved in the FEL quantum theory. Swamy's solutions are presented in Appendix A.

REFERENCES

[1] B.M. Kincaid, J.Appl.Phys. 48, 2684 (1977).
J.P. Blewet and R. Chasman, J.Apll.Phys. 48, 2692 (1977).

[2] W. Becker and H. Mitter, Z.Physik, B35, 399 (1979).

[3] S. Saritepe and N.V.V.J. Swamy, Phys.Lett. 113A, 69 (1985).

[4] S. Saritepe and N.V.V.J. Swamy, Phys.Lett. 126A, 28 (1987).

[5] N.W. McLachlan, "Theory and Application of Mathieu Functions", Dover (1964).

[6] M.V. Fedorov and J.K. McIver, Phys.Lett.72A, 83 (1979).
W. Becker and J.K. McIver, J.de Physique,44, C1-289 (1983).

[7] D.M. Volkov , Comptes Rendus de l'Acad. des Sciences,U.S.S.R March 21, pp:605-610 (1935).

[8] N.V.V.J. Swamy , private communication.

CHAPTER V

QUANTUM THEORY OF THE FEL : TRANSVERSE MOMENTUM EFFECTS

Introduction

In this chapter we will develop the perturbative Dirac Theory of the FEL based on the 2-D solutions derived in Chapter IV. Perturbative theory treats the radiation field as a perturbation on the wiggler potential and utilizes the 2-D solutions as basis functions for calculation of gain and frequencies. We shall proceed exactly the way it was laid out in Chapter III. Before we take up the calculation of matrix elements we would like to present the derivation of frequencies emitted by an FEL. We shall see that quantum theory predicts four different frequencies in contrast to the single (fundamental) frequency predicted by the classical theory for the helical wiggler FELs (frequencies emitted on the axis).

Frequencies

Frequencies are calculated by applying the conservation of four-momentum requirement [1]. In this method one introduces the effective four-momentum for the up-spin and the down-spin electrons respectively.

$$p^{\mu}_{1eff} = (\frac{E_1}{c}, p_{1x}, p_{1y}, p_1) \tag{5.1}$$

$$p^{\mu}_{2eff} = (\frac{E_2}{c}, p_{2x}, p_{2y}, p_2) \tag{5.2}$$

The squares of these four-vectors will be

$$\left(p^{\mu}_{1eff}\right)^2 = \frac{E_1^2}{c^2} - (p_{1x}^2 + p_{1y}^2 + p_1^2) \tag{5.3}$$

$$\left(p^{\mu}_{2eff}\right)^2 = \frac{E_2^2}{c^2} - (p_{2x}^2 + p_{2y}^2 + p_2^2) \tag{5.4}$$

For the emission of a photon the conservation of our-momentum condition can be written as

$$p'^{\mu}_{1,2eff} = p^{\mu}_{1,2eff} - \hbar k^{\mu} - n\hbar k^{\mu}_{w} \quad , \quad n = 0,1,2 \tag{5.5}$$

where

$$k^{\mu}_{w} = (0,0,0,k_w) \tag{5.6}$$

$$k^{\mu} = (\frac{\omega}{c}, \mp k_x, \mp k_y, k_z) \tag{5.7}$$

Here $\hbar k_w$ is the magnetic quantum of the wiggler field and $\hbar\sqrt{k_x^2+k_y^2+k_z^2}$ is the quantum of the radiation field. The reason for $n = 0, 1, 2$ will be clear when we discuss the matrix elements in the next section. By squaring both sides of (5.5) we obtain

$$\left(\frac{E_1'^2}{c^2} - p_1'^2\right) = \left(\frac{E_1}{c} - \frac{\hbar\omega_1}{c}\right)^2 - (p_1 \mp \hbar k_z + n\hbar k_w)^2 - (p_{1x} \mp \hbar k_x)^2 - (p_{1y} \mp \hbar k_y)^2 \tag{5.8}$$

From (5.8) we can obtain the frequency ω_1

$$\uparrow\uparrow \hbar\omega_1 = - \frac{c^2p_1^2 - c^2p_1'^2 + 2ncp_1\hbar ck_w + E_1'^2 - E_1^2 + (n\hbar k_w)^2 + (p_{1x} \mp \hbar k_x)^2 + (p_{1y} \mp \hbar k_y)^2}{2(E_1 - cp_1 - n\hbar ck_w)}$$

$$\text{where} \quad n = \begin{cases} -1 & \text{emission} \\ +1 & \text{absorption} \end{cases} \tag{5.9}$$

ω_1 refers to the angular frequency of the photon emitted or absorbed by an up-spin electron making a transition from the momentum state p_1 to p_1' without a spin-flip. Arrows indicate the spin of the electron before and after the transition respectively. Similarly for the other processes we obtain the following frequencies

$$\downarrow\downarrow\ \hbar\omega_2 = -\frac{c^2p_2^2 - c^2p_2'^2 + 2ncp_2\hbar ck_w + E_2'^2 - E_2^2 + (n\hbar ck_w)^2 + (p_{2x} \mp \hbar k_x)^2 + (p_{2y} \mp \hbar k_y)^2}{2(E_2 - cp_2 - n\hbar ck_w)}$$

$$\text{where}\quad n = \begin{cases} -1 & \text{emission} \\ +1 & \text{absorption} \end{cases} \tag{5.10}$$

$$\downarrow\uparrow\ \hbar\omega_3 = -\frac{c^2p_2^2 - c^2p_1'^2 + 2ncp_1\hbar ck_w + E_1^2 - E_2'^2 + (n\hbar ck_w)^2 + (p_{2x} \mp \hbar k_x)^2 + (p_{2y} \mp \hbar k_y)^2}{2(E_2 - cp_2 - n\hbar ck_w)}$$

$$\text{where}\quad n = \begin{cases} -2 & \text{emission} \\ +2 & \text{absorption} \end{cases} \tag{5.11}$$

$$\uparrow\downarrow\ \hbar\omega_4 = -\frac{c^2p_1^2 - c^2p_2'^2 + E_2'^2 - E_1^2 + (p_{1x} \mp \hbar k_x)^2 + (p_{1y} \mp \hbar k_y)^2}{2(E_1 - cp_1)} \tag{5.12}$$

emission only

In the ultrarelativistic the frequencies will be (for emission)

$$\uparrow\uparrow\ \hbar\omega_1 = \frac{2\gamma^2\hbar ck_w}{[1 + K^2 + K_{0\perp}^2 + 2\gamma K_0 + \gamma K_0(\frac{\gamma}{K} + 1)]} \quad \text{left-circularly polarized} \tag{5.13}$$

$$\downarrow\downarrow\ \hbar\omega_2 = \frac{2\gamma^2\hbar ck_w}{[1 + K^2 + K_{0\perp}^2 + 2\gamma K_0 + \gamma K_0(\frac{\gamma}{K} - 1)]} \quad \text{left-circularly polarized} \tag{5.14}$$

$$\downarrow\uparrow\ \hbar\omega_3 = \frac{4\gamma^2\hbar ck_w}{[1 + K^2 + K_{0\perp}^2 + 4\gamma K_0 + 2\gamma K_0(\frac{\gamma}{K} - 1)]} \quad \text{left-circularly polarized} \tag{5.15}$$

$$\uparrow\downarrow \quad \hbar\omega_4 = \frac{4\gamma^2 \hbar c k_w}{[1 + K^2 + K_{0\perp}^2 + 2\gamma K_0(\frac{\gamma}{K} + 1)]} \qquad \text{right-circularly polarized} \qquad (5.16)$$

where

$$K_{0\perp} \equiv \frac{cp_{0\perp}}{m_0 c^2} \qquad (5.17)$$

$$K_0 \equiv \frac{\hbar c k_w}{m_0 c^2} \qquad (5.18)$$

The information about the polarizations of the emitted photon is gained from the matrix elements. This will be discussed in the next section.

As can be seen above, the quantum theory predicts four different frequencies for the photons emitted within the cone of synchrotron radiation emission. There are of course a few photons having the harmonics of the above mentioned frequencies emitted in the directions beyond the synchrotron radiation cone, but we are not interested in those photons since their number is very small. The classical theory [2] in contrast to the quantum theory, predicts the following frequency for the photons emitted in the same cone if the wiggler geometry is helical

$$h\omega_{\text{fundemental}} = \frac{2\gamma^2 \hbar c k_w}{[1 + K^2 + K_{0\perp}^2]}$$

where $K_{0\perp}$ can also be written as $\gamma\theta$, θ being the angle between the average trajectory and the wiggler axis. When we compare (5.19) to (5.13)-(5.16) we see that quantum mechanics yields the same result plus two correction terms. The 4th term in the denominator of (5.13)-(5.15) is the correction term due to recoil which is ignored in classical calculations. The 5th term in the same denominator is the correction

term which arises as a consequence of 2-D Dirac solutions and is missing in the frequency expressions given by the 1-D theory [3], [4]. Therefore the 5th term is the new contribution to the Quantum Theory of the FEL.

Also note that the 5th term is different for ω_1 and ω_2 . Even in the 1-D quantum theory $\omega_1 - \omega_2$ difference is noticable, with the discovery of 5th term this difference becomes even more significant and it may very well be observable in the short-wavelength FELs. We conclude this section by noting the fact that the 5th term is proportional to γ^2 whereas the 4th term is only proportional to γ . Therefore we conclude that the transverse momentum effect, hitherto ignored, is greater than the previously noted recoil effect as far as the frequencies are concerned. As γ gets larger so does the quantum mechanical correction to frequencies.

Matrix Elements and Transition Rates

Matrix elements for various transitions are given by the integral

$$M^{\mp} = \frac{\sqrt{4\pi}}{\sqrt{2\omega}} e \int_{-\infty}^{\infty} dt \int_{-L/2}^{L/2} dz \; 2\pi R \int_{-R}^{R} dx \left(\bar{\Psi}(p') \gamma_{\mp} \Psi(p) \right) e^{i(\omega t - \vec{k}.\vec{r})} \qquad (5.20)$$

Here + and - refer to the right-circular and left-circular polarizations respectively. L is the length and R is the radius of the cylindrical interaction region, ω and k are the angular frequency and the wavenumber of the emitted photon. The interaction time is assumed to be infinite to conserve energy. $\gamma_{\mp}$ are the Dirac-γ matrices combined with the polarization vectors.

$$\gamma_{\mp} \equiv \gamma^1 \mp i\gamma^2 \tag{5.21}$$

$\frac{e\sqrt{4\pi}}{\sqrt{2\omega}}$ is the normalization constant of the photon wavefunction. Using the 2-D solutions given in (4.56) and (4.49) we obtain the following matrix elements

$$M^{-}_{\uparrow\uparrow} = \frac{2e\sqrt{\pi}}{\sqrt{\omega}} \frac{\frac{1}{s_1}\sin Rs_1}{\sqrt{2}\, m_0c^2} \left\{ \frac{ea}{w_1} \sin\left(\frac{w_1 L}{2}\right) - \frac{cp'_{1x}}{(w_1+k_w)} \sin[(w_1+k_w)\frac{L}{2}\ ] \right\} \tag{5.22}$$

$$M^{-}_{\downarrow\downarrow} = \frac{2e\sqrt{\pi}}{\sqrt{\omega}} \frac{\frac{1}{s_2}\sin Rs_2}{\sqrt{2}\, m_0c^2} \left\{ \frac{ea}{w_2} \sin\left(\frac{w_2 L}{2}\right) - \frac{cp_{2x}}{(w_2+k_w)} \sin[(w_2+k_w)\frac{L}{2}\ ] \right\} \tag{5.23}$$

where

$$\begin{aligned} w_1 &\equiv \frac{p_1}{\hbar} - \frac{p'_1}{\hbar} - k_w - k_z \\ w_2 &\equiv \frac{p_2}{\hbar} - \frac{p'_2}{\hbar} - k_w - k_z \\ s_1 &\equiv \frac{p_{1x}}{\hbar} - \frac{p'_{1x}}{\hbar} \mp k_x \\ s_2 &\equiv \frac{p_{2x}}{\hbar} - \frac{p'_{2x}}{\hbar} \mp k_y \end{aligned} \tag{5.24}$$

These are the relevant matrix elements for the calculation of gain because as it turns out $M^{-}_{\downarrow\uparrow}$ and $M^{+}_{\uparrow\downarrow}$ are very small and completely negligable and $M^{+}_{\uparrow\uparrow}$, $M^{+}_{\downarrow\downarrow}$, $M^{+}_{\downarrow\uparrow}$, $M^{-}_{\uparrow\downarrow}$ are associated with absorption and we will not need them in the calculation of gain in this chapter.

We only consider forward emission because the gain for the backward emission is very very small. The question of which matrix elements contribute to emission can easily be answered by examining the

expressions for $w_{1,2,3,4}$. The peak of the function $\frac{1}{w}\sin(wL/2)$ occurs at w = 0, therefore by equating the expressions for $w_{1,2,3,4}$ to zero we can obtain the wavenumber of the emitted photon. In the case of emission, $(p_1-p_1') > 0$ and also $(p_1-p_1') > k_w$ therefore from (5.24) k_z turns out to be positive as it should be. For some of the conditions $w_{1,2,3,4}$ =0, k_z turns out to be negative and this means absorption. This way one can figure out the matrix elements that contribute to emission by examining the argument ($w_{1,2,3,4}$) of the function $\frac{1}{w}\sin\frac{wL}{2}$.

To calculate the transition rates we can use the Fermi's Golden rule because transitions are from a discrete level to a continuum. Therefore, the probability of emission of a single photon per unit time will be

$$P = \int \frac{2\pi}{\hbar} M^2 \rho(\omega)\, dp' \qquad (5.25)$$

Here the integral is over $p' \equiv \frac{p_1'+p_2'}{2}$ thus we take care of the density of final states of the electron. $\rho(\omega)$ is the density of final states for the photons. M^2 is the average of the mod squares of the matrix elements that contribute to emission

$$M^2 = \frac{1}{2}\left\{ |M_{\uparrow\uparrow}^{-}|^2 + |M_{\downarrow\downarrow}^{-}|^2 + |M_{\downarrow\uparrow}^{-}|^2 + |M_{\uparrow\downarrow}^{+}|^2 \right\} \qquad (5.26)$$

This averaging over the spin polarizations is necessary because of the experimental FEL set-up inwhich the electrons are not polarized before they enter the wiggler and their polarizations are not measured when they exit the wiggler. M^2 will be approximately

$$M^2 \cong \frac{4e^2\pi}{\omega}\frac{G(Rs)}{2m_0c^2\gamma^2}\left\{e^2a^2\, G(Lw/2) + c^2p_x^2\, G[(w+k_w)L/2]\right\} \qquad (5.27)$$

where

$$G(wL/2) \equiv \frac{\sin^2(wL/2)}{w^2} \tag{5.28}$$

$$G(Rs) \equiv \frac{\sin^2(Rs)}{s^2} \tag{5.29}$$

with

$$w \equiv \frac{p}{\hbar} - \frac{p'}{\hbar} - k_w - k_z$$
$$s \equiv \frac{p_x}{\hbar} - \frac{p'_x}{\hbar} \mp k_x \tag{5.30}$$

and

$$p \equiv \frac{p_1+p_2}{2} \quad , \quad p_x \equiv \frac{p_{1x}+p_{2x}}{2} \tag{5.31}$$

During the calculation of M^2 we did not integrate over p'_x because p_{1x} and p_{2x} are constants of motion. When a photon is emitted in a direction other than the wiggler axis the transverse momentum of the electron will obviously change due to recoil in the transverse direction but this electron after the transition can now be considered as a different electron with a different initial momentum p_{0z}. At the end, one has to integrate over the initial p_{0z} distribution to come up with the correct gain expression anyway. Therefore the calculation does not contradict the interpretation of p_{1x}, p_{2x} being the constants of motion (Eigenvalues).

Using (5.27) the transition rates can be calculated. The probability of emission of a single photon at the fundamental frequency will be

$$P_{\substack{\text{spon.} \\ \text{emiss.}}} = \frac{1}{\hbar c} \frac{4\pi e^2}{\omega\gamma^2} K^2 \, G(Lw/2) \tag{5.31}$$

And the probability of a single photon emission at the harmonic frequency will be

$$P^{har}_{spon.\ emiss.} = \frac{1}{\hbar c}\frac{4\pi e^2}{\omega\gamma^2}\left(\frac{cp_x}{m_0c^2}\right) G[(w+k_w)L/2] \qquad (5.32)$$

Here by the "harmonic frequency" we are refering to the frequency given by (5.15) which is approximately equal to the 1st harmonic of (5.13). The other frequency (5.16) is very weak and cannot be observed. Eq.(5.14) is almost equal to (5.13) therefore it was included as the fundamental frequency.

In order to arrive at (5.31) and (5.32) we have used the following information. Since p_x is a constant of motion as explained above, $p_x - p'_x$ was considered zero and this makes G(Rs) a Dirac-delta function centered at $k_x=0$. Consequently the density of final states for photons which is equal to $\frac{\omega^2 d\omega\ d\Omega}{(2\pi c)^3}$ in 3-dimensions will reduce to $\frac{d\omega}{2\pi c}$.

The physical explanation of this formal result is as follows. The emission cone of the synchrotron-radiation is very narrow due to relativistic electron energies and also the laser cavity does not support the photons emitted off-axis. The combined effect of these factors will be a laser cavity almost perfectly 1-dimensional so that the 1-D version of the density of final states is used.

We did not multiply $\frac{\omega}{2\pi c}$ by two to account for the two polarizations of photons because only left-circularly photons are emitted ($M^+_{\uparrow\downarrow}$ is small). The physical explanation of this is of course given by the sense of winding of the helical wiggler. An oppositely wound wiggler would cause the emitted photons to be right-circularly polarized.

We also used the fact that G(wL/2) is almost like a Dirac-delta function since it is very sharp around the peak.

Calculation of the Gain

In Chapter III we have defined the gain of the FEL as the difference between the transition rates for emission and absorption of a single photon integrated over the initial momentum distribution.

$$G = \frac{N_e}{V} \int d^3p\, f(p) \int \frac{d^3p'}{(2\pi)^3} \left\{ |M_{emiss}|^2 - |M_{abso}|^2 \right\} \tag{5.33}$$

Since the difference $|M_{emiss}|^2 - |M_{abs}|^2$ is small, it can be written as

$$|M_{emiss}|^2 - |M_{abs}|^2 \cong \delta \frac{d}{d\omega} |M_{emiss}|^2 \tag{5.34}$$

where

$$\delta \equiv \omega_{emiss} - \omega_{abs} \tag{5.35}$$

$$\cong \frac{4(\hbar k_w / m_0 c)\gamma\, \omega}{[1 + K^2 + K_{0\perp}^2 + 2\gamma K_0 + \gamma^2 (K_0/K)]}$$

for the derivative of the transition rate with respect to ω we have

$$\frac{d}{d\omega} |M_{emiss}|^2 = \left(\frac{e^2 a^2\, 4\pi e^2}{\omega_0 2 (m_0 c^2) \gamma^2} \right) \frac{dG}{d\omega} \tag{5.36}$$

since the derivative of the lineshape function $G(\omega)$ is given by

$$\frac{d\, G(wL/2)}{d\omega} = 2 \frac{\sin(wL/2)}{w} \frac{d}{dw} \left(\frac{\sin(wL/2)}{w} \right) \frac{dw}{d\omega} \tag{5.37}$$

and finally

$$\frac{dw}{d\omega} = \frac{[1 + K^2 + K_{0\perp}^2 + 2\gamma K_0 + \gamma^2 (K_0/K)]}{2\gamma^2} \tag{5.38}$$

$$\frac{d}{dw}\left(\frac{\sin(wL/2)}{w}\right) = \frac{1}{w^3}\,[-1 + \cos wL + \frac{wL}{2}\sin wL\,] \tag{5.39}$$

combining all of these we can write

$$G_{fund.} = \frac{N_e}{V}\int d^3p\; f(p)\left\{-16\pi\frac{k_w}{\gamma}\left(\frac{e^2}{m_0c^2}\right)\frac{K^2}{[1+K^2+K_{0\perp}^2+2\gamma K_0+\gamma^2(K_0/K)}\,\frac{dG(w)}{d\omega}\right\} \tag{5.40}$$

and for the harmonic frequency

$$G_{har} = \frac{N_e}{V}\int d^3p\; f(p)\left\{-16\pi k_w\gamma\left(\frac{e^2}{m_0c^2}\right)\frac{K}{[1+K^2K_{0\perp}^2+2\gamma K_0+\gamma^2(K_0/K)]}\,\frac{dG(w+k_w)}{d\omega}\right\} \tag{5.41}$$

Now assuming a gaussian initial momentum distribution (which is the correct distribution in most accelerators) we obtain the final expressions for gain

$$G_{fund.} = \frac{N_e}{V}\,e^{-(p_{0m}-p_0)^2/2\sigma_p^2}\;16\pi\,\frac{k_w}{\gamma}\left(\frac{e^2}{m_0c^2}\right)\frac{K^2}{[1+K^2+K_{0\perp}^2+2\gamma K_0+\gamma^2(K_0/K)]}$$
$$\times\,\frac{1}{(\gamma w)^3}\,[1-\cos Lw - \frac{1}{2}\,Lw\sin Lw\,] \tag{5.42}$$

$$G_{har} = \frac{N_e}{V}\,e^{-(p_{0m}-p_0)^2/2\sigma_p^2}\;16\pi k_w\gamma\left(\frac{e^2}{m_0c^2}\right)\frac{K}{[1+K^2+K_{0\perp}^2+2\gamma K_0+\gamma^2(K_0/K)]}$$
$$\times\,\frac{1}{[\gamma(w+k_w)]^3}[1-\cos L(w+k_w)-\frac{1}{2}\,L(w+k_w)\sin L(w+k_w)] \tag{5.43}$$

where p_0 is the central momentum which gives rise to the peak in the spontaneous emission line-shape (p_0 is the momentum which defines the FEL resonance) and p_{0m} is the momentum that corresponds to the peak of

the "gain-curve". In atomic lasers $p_{0m} = p_0$ but in the case of FEL they differ from each other by

$$p_0 - p_{0m} = 2.6 \frac{c}{L} \tag{5.44}$$

Eq.(5.44) will be discussed in more detail in Chapter VII. σ_p is the halfwidth of the initial momentum distribution and depends on the type of accelerator being used in the FEL operation. To arrive at the expressions (5.42) and (5.43) we have used again the sharpness of the gain cuve. In other words we have approximated $\int \frac{[1-\cos Lw - (1/2)\sin Lw]}{w^3}$ as a Dirac-delta function centered at p_{0m}.

$$\int_{-\infty}^{\infty} \frac{[1-\cos Lw - (1/2)Lw\sin Lw]}{w^3} e^{-(p-p_0)/2\sigma_p^2} dp \cong e^{-(p_{0m}-p_0)/2\sigma_p^2} \times \frac{[1-\cos lw-(1/2)Lw\sin Lw]}{w^3} \tag{5.45}$$

The expression for G_{fund}, (5.42), seems to be equivalent to the classical gain expression given in (1.35) if we ignore $2\gamma K_0 + \gamma^2(K_0/K)$ term in the denominator of (5.42) (note that $Lw \equiv \nu$). Therefore one could argue that classical and quantum mechanical gain expressions are not much different since $2\gamma K_0 + \gamma^2(K_0/K)$ is small. But this would be a misleading conclusion because most of the quantum mechanical information is buried in the line-shape function. Let us now examine the spontaneous-emission line-shape function and its derivative gain-curve in more detail.

Lineshape Broadening and Gain Depreciation due to Quantum Mechanical Effects

During the calcualtion of gain we have averaged over the spins and

also for p we have used the average $\frac{p_1+p_2}{2}$. But in reality up-spin electrons and down-spin electrons emit slightly different frequencies (i.e., the central frequencies of the spontaneous emission line-shapes for up-spin and down-spin electrons are different) as shown in (5.13) and (5.14). Also these line-shapes are slightly broader compared to the classical line-shape given by the classical theory (classical theory cannot predict the seperation of up-spin and down-spin line-shapes). These line-shapes are shown in Figure 14. The classical total-relative-bandwidth of the FEL is given by

$$\left(\frac{d\omega}{\omega}\right)_{classical} = \frac{\lambda_w}{2L_w} \tag{5.46}$$

where L_w is the wiggler length and λ_w is the wiggler wavelength. This linewidth can also be called the homogeneously broadened linewidth since it refers to the width of the spontaneous emission line-shape. The actual FEL laser line-width is of course much smaller than this and is determined by the cavity properties as we shall discuss in Chapter VIII. The inhomogeneous-broadening of the spontaneous emission line-shape will be discussed in Chapter VII, here we shall concentrate on the further broadening of the homogeneously broadened spontaneous emission line-shape due to quantum mechanical effects.

Quantum mechanical broadening is basically due to $p_{1,2x}$ which were discovered from the 2-D solutions of the Dirac equation for an electron moving in a helical wiggler. This also means that the 1-D Quantum theory cannot predict a broadening. The homogeneously broadened width $\frac{\lambda_w}{2L_w}$ is further broadened by a factor of $\frac{2cp_{1,2x}}{\Delta E}$ where ΔE is the energy acceptance of the FEL resonance. ΔE can easily be calculated from (5.46).

$$\Delta E = \frac{E}{2N}$$

where E is the average energy of the electron beam and N is the number of magnet poles in the wiggler. Therefore the quantum mechanical expression for spontaneous emission linewidth will be

$$\left(\frac{\Delta\omega}{\omega}\right)_{QM} = \frac{\lambda_w}{2L_w}\left\{1 + \frac{4N\gamma}{E}\left(\frac{(m_0c^2)(\hbar ck_w)}{K}\right)^{1/2} + \frac{c\delta k}{\omega_0}\right\} \qquad (5.48)$$

The 3rd term in (5.48) has to be there since $\left(\frac{\Delta\omega}{\omega}\right)_{QM}$ is the total width including both up-spin and down-spin line-shapes. δk can easily be calculated from (5.13) and (5.14).

$$\delta k = \frac{4\gamma^3 K_0 k_w}{[1 + K_0^2 + K_{0\perp}^2 + 2\gamma K_0 + \gamma^2(K_0/K)]} \qquad (5.49)$$

As we mentioned earlier these quantum mechanical effects will be observable in the x-ray FEL based on accelerators with E > 1GeV. One such FEL is under construction at Stanford University. The SXRC (Stanford X-Ray Center) FEL parameters are listed in Table II. Using these parameters we find that $\delta k = 0.9\ cm^{-1}$, $\frac{2cp_{1,2x}}{\Delta E} = 1.74\ x10^{-2}$ δk is still unobservable since the instrument width in this set-up is 4 cm^{-1}, but 1.74 % broadening due to $p_{1,2x}$ is certainly observable and its effect on gain is even more noticable since the gain is given by the slope of the lineshape.

The calculation of this gain depreciation effect due to 2-D quantum mechanical effects involve many details of the electron beam, the number of photons in the cavity and the effective interaction length. All these concepts are reserved for Chapter VII. Here we shall present the results only.

For the above mentioned SXRC FEL (Table II) 1.74 % broadening in the spontaneous emission linewidth translates into 9.366 % decrease in gain magnitude. For the Original Stanford experiment or the other existing FELs quantum mechanical gain depreciation would be unobservable but as we mentioned in Chapter VII, other quantum mechanical effects such as photon-number fluctuations in the cavity, have macroscopic consequences in the operation of all the FELs including the long wavelength devices. The quantum mechanical gain-depreciation is shown in Figure 15.

Discussion

The first new result of formulating a 2-D Dirac theory of the FEL is the appearance of an harmonic given by (5.15) and (5.43). This result can be explained physically by recalling that the harmonic frequency is generated by a down-spin electron making a radiative transition to an up-spin state. The probability of this transition should increase when there is an additional transverse momentum such as $p_{1,2x}$. In the 1-D quantum theory the probability of transition is considerably smaller since in a 1-D theory there is less chance of a spin-flip.

The second result we obtain from the quantum theory is that the spontaneous emission linewidth is broadened and the centers of $\uparrow\uparrow$ and $\downarrow\downarrow$ line-shapes are seperated.

Third result concerns gain. Gain is decreased by a larger factor than the broadening factor. The numerical value for the SXRC FEL is 9.366 % which is caused by the quantum mechanical transverse momentum effects.

The most important conclusion of this chapter is that the quantum mechanical transverse momentum effects are greater than the quantum

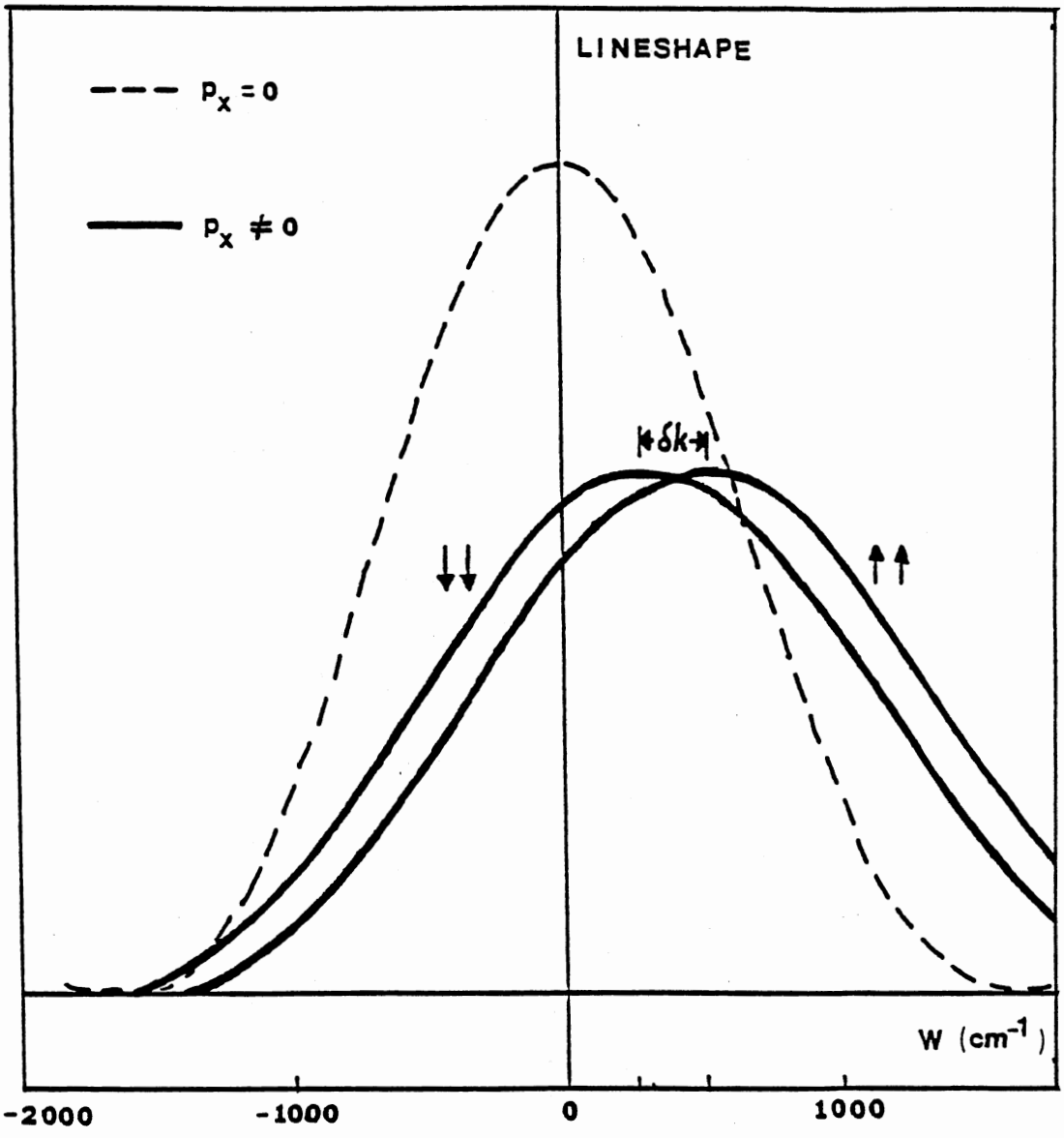

Figure 14. Lineshape broadening due to quantum mechanichal transverse momentum effects. The difference is exaggerated.

TABLE II

PARAMETERS OF THE STANFORD SXRC FEL

Parameter description	Symbol	Numerical value
Wiggler wavelength	λ_w	6.4 cm
Wiggler length	L_w	27 m
Electron beam energy	E	1 GeV
Relativistic factor	γ	2×10^3
Laser wavelength	λ	285 A^0
Wiggler strength	K	2.3
Energy acceptance	ΔE	1.184×10^6 eV

mechanical recoil effects by a factor of γ .

Since the quantum recoil effects are very small for most of the existing FEL devices, the general understanding among the FEL researchers was that the quantum theory of the FEL was unnecessary. Now with the discovery of 2-D quantum effects we can claim that a quantum theory of the FEL is absolutely essential to understand the start-up and saturation behaviour of the short-wavelength FELs (x-ray and vuv region) since these FELs have γ- factors greater than 10^3 .

In this chapter we have carried out a 1st order perturbation calculation, namely, we have calculated the probabilities of emission and absorption of a single photon from a wiggling electron. From these probabilities we have obtained the gain. Throughout the calculation we assumed a uniform wiggler even though we have already derived the solutions of the Dirac equation for an electron moving in a tapered wiggler in Chapter IV. The reason is that in the presence of a tapered wiggler the frequency spectrum and the radiation amplitude continuously shift thereby making the application of 1st order perturbation theory developed in this chapter questionable. For a proper quantum mechanical treatment of tapered FELs in general and strong-signal regime in particular we need a theory where the radiation field is included in the Dirac Hamiltonian ab initio. As we mentioned in Chapter IV this possibility is dealt with in Appendix A.

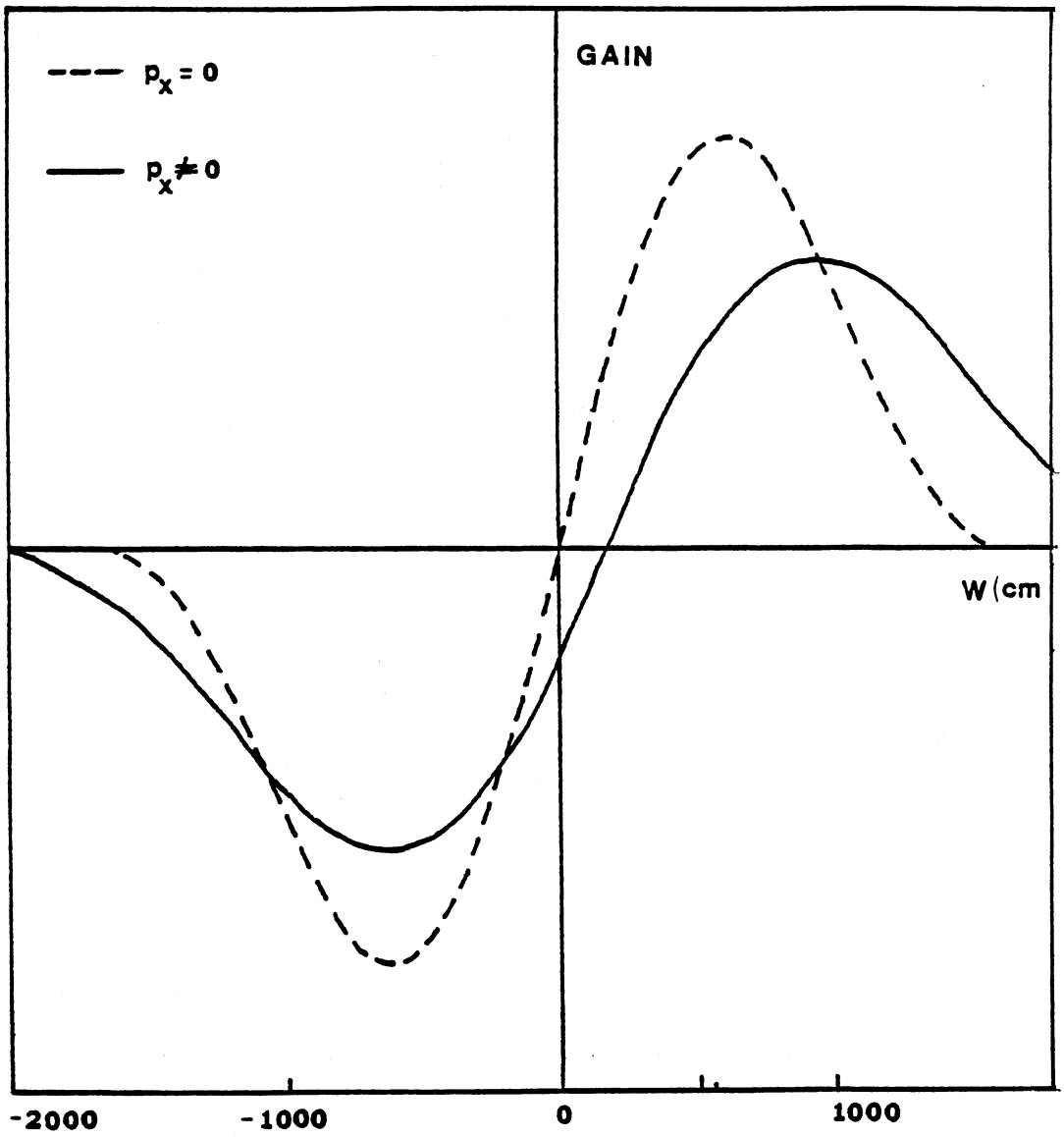

Figure 15. Gain curve. The difference is exaggerated.

REFERENCES

[1] W. Becker, Phys.Lett. A65, 317 (1978).

[2] G. Dattoli and A. Renieri, in "Laser Handbook Vol:4", 1. eds: M.L. Stitch and M. Bass (North Holland, New York) (1985).

[3] S. Saritepe and N.V.V.J. Swamy, Phys.Lett. A113, 69 (1985).

[4] W. Becker and H. Mitter, Z.Physik, B35, 399 (1979).

CHAPTER VI

QUANTUM THEORY OF THE FEL : EFFECTS OF AN AXIAL GUIDE FIELD

Introduction

Efficiency enhancement is the central problem in FEL research and development. Improvements by good engineering techniques are not enough and more innovative and novel techniques are needed. In this chapter we shall present a particular efficiency enhancement mechanism which relies on a magnetic axial guide field to increase the gain.

In the short-wavelength FELs (x-ray, vuv) conventional mirrors cannot be used and special mirrors available can only provide reflectivities less than 50%, therefore one has to have a very high gain and a long wiggler so that the saturation level is reached before the electron pulse exits the wiggler. The problem is that the gain is inversely proportional to γ^3 and as the energy of the beam increases (we have no choice but to have E > 1 GeV to achieve x-ray wavelengths since other alternative mechanisms such as frequency up-conversion by compton backscattering [1] come with even lower efficiencies) the gain decreases sharply. It is essential to have a mechanism that increases the gain in these short wavelength FELs.

For the long wavelength FELs (visible, fir, microwave, mm) the problem arises from the space charge effects. In the highly

relativistic electron beams, space-charge effects are neutrilized by the self-pinching effects but when the relativistic factor γ is less than 10, space-charge effects become dominant, especially if the electron density is high. Since a high current density is the first requirement to have a sufficient gain in the FEL, a gain enhancement mechanism is needed. Here the emphasis is on the confinement of the beam to achieve sufficient current densities rather than obtaining substantial increases in gain.

There are basically two ways to increase the gain. The first one is called tapering and we have briefly discussed it in Chapter IV. The goal is to keep electrons in FEL resonance, as many as possible. This goal is achieved either by decreasing λ_w along the wiggler or by increasing the wiggler field amplitude along the wiggler. We will present numerical calculations regarding the λ_w-tapering in Chapter VII.

The other method for the gain enhancement is to use an axial magnetic guide field along the wiggler axis. In such a field, electrons' helical gyro-motion along the axial guide field lines is superimposed on their helical motion due to wiggler. If the gyro-motion (cyclotron motion) radius is smaller than the wiggling radius the combined orbit will look like the one in Figure 16. As the axial field amplitude is increased electrons execute orbits with higher cyclotron frequencies and at some point this frequency becomes as large as the wiggling frequency and a gyro-resonance occurs. The gyro-resonance represents an instability since the electrons at gyro-resonance have large transverse velocities. As a result, the emittance of the electron beam blows-up and the FEL interaction ceases. In the next section we

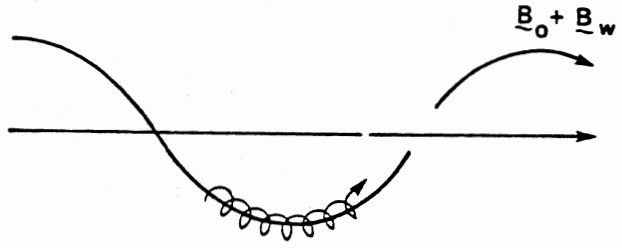

Figure 16. Schematic representation of single-particle orbits

will present the classical equations of motion for an electron in a wiggler and an axial field and report its effects on gain based on a classical calculation. Our main objective in this chapter though is to derive the solutions of the Dirac equation (2-D) for the motion of an electron in such a field and calculate the small-signal gain quantum mechanically.

A quantum mechanical approach to axial-field effects may seem to be totally irrelevant at first glance since most of the axial-field FELs use $\gamma < 10$ electron beams. As we explained above, the axial-magnetic guide field is not only used to confine the particles to neutrilize the space-charge effects but to enhance gain as well. Therefore it can be used in the short-wavelength ($\gamma > 10^3$) FELs to enhance gain, even though the electron beam in such a device would not be space-charge dominated.

A Dirac theory of the FEL is absolutely necessary to understand the physics of short wavelength (x-ray, vuv) FELs and since, in the very near future, axial-guide fields can be employed in such FELs to enhance gain, an extension of our theory to include axial-field effects is in order.

Classical Orbits And Gain

Consider an electron moving in a magnetic field of the form [2]

$$\vec{B} = B_0\hat{z} + B_w(\cos k_w z\ \hat{x} + \sin k_w z\ \hat{y}) \tag{6.1}$$

Where B_0 and B_w are the wiggler and the axial-guide field amplitudes respectively. In order to eliminate explicit coordinate dependence from the equations of motion, let us change the coordinate system to

$$\hat{e}_1 = -\hat{x}\ \sin k_w z + \hat{y}\ \cos k_w z \tag{6.2}$$

$$\hat{e}_2 = -\hat{x}\ \cos k_w z - \hat{y}\ \sin k_w z \tag{6.3}$$

$$\hat{e}_3 = \hat{z} \tag{6.4}$$

The classical equation of motion for an electron is

$$\frac{d}{dt}(\gamma\vec{v}) = -\frac{e}{m_0 c}\vec{v} \times \vec{B} \tag{6.5}$$

Where γ is the relativistic factor $\gamma = 1/\sqrt{1-(v/c)^2}$. In the new coordinate system the magenetic field (6.1) will look like

$$\vec{B} = B_0\ \hat{e}_3 - B_w\ \hat{e}_2 \tag{6.6}$$

After expressing the velocity $\vec{v}$ in terms of the orthogonal basis vectors $\hat{e}_1$, $\hat{e}_2$ and $\hat{e}_3$ and using

$$\frac{d\hat{e}_1}{dt} = k_w v_3\ \hat{e}_2 \quad , \quad \frac{d\hat{e}_2}{dt} = -k_w v_3\ \hat{e}_1 \tag{6.7}$$

one can seperate the equation of motion (6.5) into its components.

$$\gamma\frac{dv_1}{dt} = \gamma k_w v_2 v_3 - \frac{eB_0}{m_0 c}v_2 \tag{6.8}$$

$$\gamma\frac{dv_1}{dt} = -\gamma k_w v_1 v_3 - \frac{eB_w}{m_0 c}v_3 + \frac{eB_0}{m_0 c}v_1 \tag{6.9}$$

$$\gamma\frac{dv_3}{dt} = \frac{eB_w}{m_0 c}v_2 \tag{6.10}$$

or in a more simplified form

$$\dot{v}_1 = v_2(k_w v_3 - \Omega_0) \tag{6.11}$$

$$\dot{v}_2 = -\Omega_w v_3 - v_1(k_w v_3 - \Omega_0) \tag{6.12}$$

$$\dot{v}_3 = \Omega_w v_2 \tag{6.13}$$

where we defined

$$\Omega_0 \equiv \frac{|e|B_0}{\gamma m_0 c} \quad , \quad \Omega_w \equiv \frac{|e|B_w}{\gamma m_0 c} \tag{6.14}$$

since the total energy is conserved the following is a constant of the motion

$$v^2 \equiv v_1^2 + v_2^2 + v_3^2 \tag{6.15}$$

There is another constant of motion [2], [3], given by

$$u \equiv v_1 - k_w \frac{[v_3 - (\Omega_0/k_w)]^2}{2\Omega_w} \tag{6.16}$$

By means of these constants v and u the equation of motion can be written as a single differential equation for the axial velocity

$$\left(\frac{dx}{d\tau}\right)^2 + \phi(x) = 0 \tag{6.17}$$

where

$$\phi(x) \equiv x^4 + 4\varepsilon\beta_0(\varepsilon\beta_0+\beta_u)x^2 + 8\varepsilon^2\beta_0^3 x + 4\varepsilon^2\beta_0^2(\beta_0^2+\beta_u^2-\beta_v^2) \tag{6.18}$$

here $x \equiv (v_3/c)-(\Omega_0/k_w c)$

$$\varepsilon \equiv \frac{B_w}{B_0} \quad , \quad \beta_v \equiv \frac{v}{c} \quad , \quad \beta_u \equiv \frac{u}{c} \tag{6.19}$$

$$\beta_0 \equiv \frac{\Omega_0}{k_w c} \quad , \quad \tau \equiv \Omega_0 t/2$$

The conditions which lead to stable small oscillations in the axial velocity can be investigated by consideration of the roots of the pseudopotential $\phi(x)$. This was done in references [2] and [4]. Here we report the results.

The trajectories with constant axial velocity can be shown to satisfy an energy conservation equation

$$v_{//}^2 + v_{\perp}^2 = v^2 \tag{6.20}$$

$$\Omega_0 \equiv \frac{|e|B_0}{\gamma m_0 c} \quad , \quad \Omega_w \equiv \frac{|e|B_w}{\gamma m_0 c} \tag{6.14}$$

since the total energy is conserved the following is a constant of the motion

$$v^2 \equiv v_1^2 + v_2^2 + v_3^2 \tag{6.15}$$

There is another constant of motion [2], [3], given by

$$u \equiv v_1 - k_w \frac{[v_3 - (\Omega_0/k_w)]^2}{2\Omega_w} \tag{6.16}$$

By means of these constants v and u the equation of motion can be written as a single differential equation for the axial velocity

$$\left(\frac{dx}{d\tau}\right)^2 + \phi\,(x) = 0 \tag{6.17}$$

where

$$\phi\,(x) \equiv x^4 + 4\varepsilon\beta_0(\varepsilon\beta_0+\beta_u)x^2 + 8\varepsilon^2\beta_0^3 x + 4\varepsilon^2\beta_0^2(\beta_0^2+\beta_u^2-\beta_v^2) \tag{6.18}$$

here $x \equiv (v_3/c)-(\Omega_0/k_w c)$

$$\varepsilon \equiv \frac{B_w}{B_0} \quad , \quad \beta_v \equiv \frac{v}{c} \quad , \quad \beta_u \equiv \frac{u}{c} \tag{6.19}$$

$$\beta_0 \equiv \frac{\Omega_0}{k_w c} \quad , \quad \tau \equiv \Omega_0 t/2$$

The conditions which lead to stable small oscillations in the axial velocity can be investigated by consideration of the roots of the pseudopotential $\phi(x)$. This was done in references [2] and [4]. Here we report the results.

The trajectories with constant axial velocity can be shown to satisfy an energy conservation equation

$$v_{//}^2 + v_{\perp}^2 = v^2 \tag{6.20}$$

here $v_{//}$ is the axial velocity and is a special solution for v_3 . $v_\perp$ is given by

$$v_\perp = \frac{\Omega_w v_{//}}{\Omega_0 - k_w v_{//}} \tag{6.21}$$

and can be interpreted as the total transverse velocity. (6.20) constitutes a quartic equation for $v_{//}$ in terms of B_w , B_0 , k_w and γ . The roots of this equation contain one orbit describing motion antiparallel to B_0 and three trajectories (of which only two are stable) corresponding to motion parallel to the axial guide field. These orbits are shown in Figure 17 which is a plot of $\frac{v_{//}}{c}$ versus β_0 . In Figure 17, also included, are the curves obtained for a realizable wiggler [4]. As can be seen there are considerable differences between the actual orbits in a realizable wiggler and the orbits in an ideal wiggler such as the one given by (6.1). Nonetheless, one can define a region of unstability. For the group-I trajectories, the orbit becomes unstable when

$$\beta_0 = \frac{(v_{//})/c}{(1 + \epsilon^{2/3})} \tag{6.22}$$

in other words when

$$B_0 = \frac{\gamma m_0 v_{//} ck_w}{|e|(1 + \epsilon^{2/3})} \tag{6.23}$$

or when $$\Omega_0 = k_w v_{//} \tag{6.24}$$

Once the equations of motion are known one can go through the theory based on Vlasov-Maxwell equations [4] [5] and derive the expression for gain

$$G \cong \beta_\perp^2 \frac{\omega_p^2 L^3 k}{16\gamma\gamma_{//}^2 v_{//}^2} \left\{1 - \frac{\Omega_0 \beta_\perp^2 \gamma_{//}^2}{[\Omega_0(1+\beta_\perp^2) - k_w v_{//}]}\right\} \frac{d}{d\theta} \left(\frac{\sin\theta}{\theta}\right)^2 \tag{6.25}$$

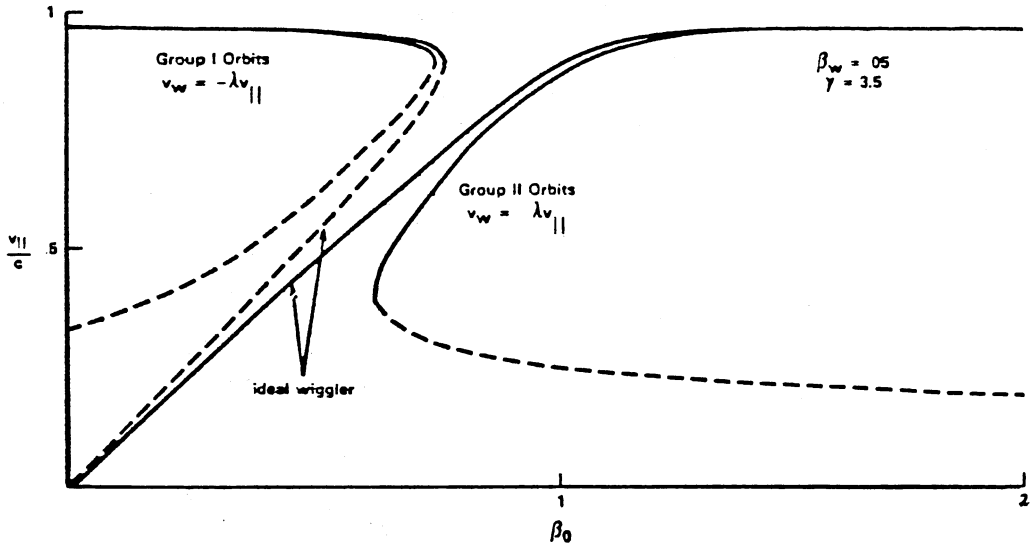

Figure 17. Graph of the axial velocity versus axial field

where $\beta_\perp \equiv v_\perp/v_{//}$, $\gamma_{//} = 1/\sqrt{1-\beta_z^2}$

also, ω_p is the beam-plasma frequency and k is the wavenumber of the emitted radiation. Here

$$\theta \equiv \left(\frac{\omega}{v_{//}} - (k+k_w)\right)\frac{L}{2} \tag{6.26}$$

Based on (6.25), the maximum gain is plotted in Figure 18. It is clear that the gain is considerably enhanced with the introduction of an axial magnetic guide field if the amplitude of the axial field is carefully chosen. One can achieve very high gain at the expense of losing electrons to unstable orbits. In general an optimization of the FEL parameters is needed for each application. In this regard, injection of the electrons into the wiggler becomes the most important technical problem. In other words, one has to devise the injector very carefully in order to launch most of the electrons into stable orbits.

Dirac Electron in a Helical Wiggler and an Axial Guide Field

The magnetic field given in (6.1) can be derived from the vector potential $\vec{A}$

$$\vec{B} = \vec{\nabla} \times \vec{A} \tag{6.27}$$

where

$$\vec{A} = \left(a\cos k_w^* z - \frac{B_0 c}{2}\, y\right)\hat{x} + \left(a\sin k_w^* z + \frac{B_0 c}{2}\, x\right)\hat{y} \tag{6.28}$$

where one has to identify $cB_w \equiv ak_w$. Note that we write k_w with a star to indicate that the wiggler can be tapered as described in Equation (4.3). The Dirac equation for an electron moving in this combined wiggler and guide field is

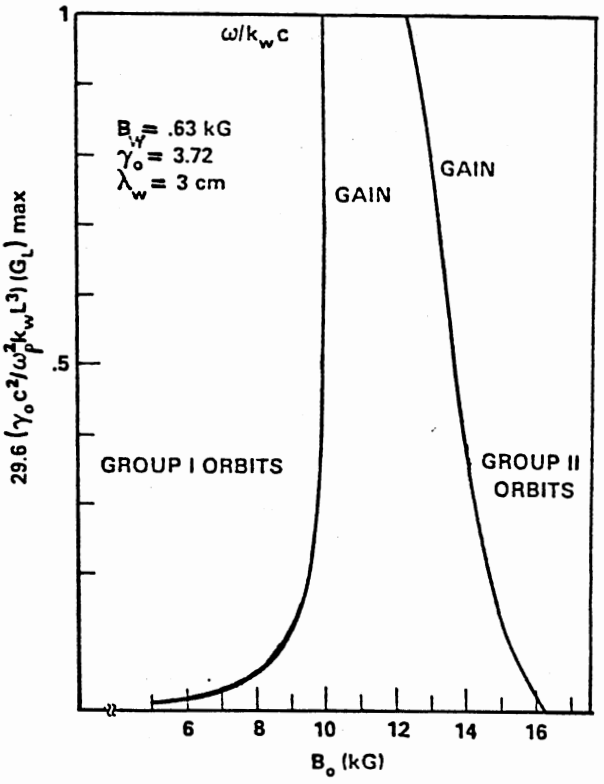

Figure 18. Dependence of small-signal gain on guide field

$$[\rho_1\sigma_x(cp_x-eacosk_w^*z+\frac{B_0ce}{2}y)+\rho_1\sigma_y(cp_y-easink_w^*z-\frac{B_0ce}{2}x)+\rho_1\sigma_z cp_z-E\ ]\Psi = 0 \tag{6.29}$$

In 2x2 form

$$\begin{bmatrix} m_0c^2-E & c\vec{\sigma}\ \vec{P}' \\ c\vec{\sigma}\ \vec{P}' & -(m_0c^2+E) \end{bmatrix}\begin{bmatrix} \Psi_1 \\ \Psi_2 \end{bmatrix} = \begin{bmatrix} 0 \\ 0 \end{bmatrix} \tag{6.30}$$

where

$$\vec{P}' = (p_{\sim x} - \frac{ea}{c}\cos k_w^* z + \frac{eB_0}{2}y)\hat{x} + (p_{\sim y} - \frac{ea}{c}\sin k_w^* z - \frac{eB_0}{2}x)\hat{y} + p_{\sim z}\hat{z}$$

is the canonical momentum.

Dirac equation in 4x4 form will look like

$$\begin{bmatrix} m_0c^2-E & 0 & cp_{\sim z} & cp_{\sim -}+\frac{B_0e}{2}(y+ix)c - ea\,e^{-ik_w^*z} \\ 0 & m_0c^2-E & cp_{\sim +}+\frac{eB_0}{2}(y-ix)c - ea\,e^{ik_w^*z} & -cp_{\sim z} \\ cp_{\sim z} & cp_{\sim -}+\frac{eB_0}{2}(y+ix)c - ea\,e^{-ik_w^*z} & -m_0c^2-E & 0 \\ cp_{\sim +}+\frac{eB_0}{2}(y-ix)c - ea\,e^{ik_w^*z} & -cp_{\sim z} & 0 & -m_0c^2-E \end{bmatrix}\begin{bmatrix} \phi_1 \\ \phi_2 \\ \phi_3 \\ \phi_4 \end{bmatrix} = 0 \tag{6.32}$$

where $p_- \equiv p_x - ip_y$, $p_+ \equiv p_x + ip_y$

let $p_{\sim y} = 0$ as we did in Chapter IV and $\omega_c = \frac{eB_0}{2m_0}$ is the cyclotron frequency then the Dirac equation in 4x4 form can be written as

$$\begin{bmatrix} A & 0 & B & C \\ 0 & A & C' & -B \\ B & C & A' & 0 \\ C' & -B & 0 & A' \end{bmatrix} \begin{bmatrix} \phi_1 \\ \phi_2 \\ \phi_3 \\ \phi_4 \end{bmatrix} = 0 \tag{6.33}$$

where $A \equiv m_0c^2 - E$, $A' \equiv -m_0c^2 - E$

$B \equiv cp_z$

$C \equiv (cp_x - im_0c\,\omega_c x) - ea\, e^{-ik_w^* z}$

$C' \equiv (cp_x + im_0c\,\omega_c x) - ea\, e^{ik_w^* z}$

The solution must satisfy certain requirements. First of all it must reduce to the 2-D solutions (4.49) and (4.56) when the axial field is switched off. Secondly it should not contradict any assumptions that were adopted in Chapter IV, namely solutions must be of the form

$$\Psi^{\uparrow} = \begin{bmatrix} f_1(z)\, e^{i/\hbar\, h_1(x)} \\ f_2(z)\, e^{i/\hbar\, h_2(x)}\, e^{-ik_w^* z} \\ f_3(z)\, e^{i/\hbar\, h_1(x)} \\ f_4(z)\, e^{i/\hbar\, h_2(x)}\, e^{ik_w^* z} \end{bmatrix} \tag{6.34}$$

$$\Psi^{\downarrow} \equiv \begin{bmatrix} g_1(z)\, e^{i/\hbar\, h_1'(x)}\, e^{-ik_w^* z} \\ g_2(z)\, e^{i/\hbar\, h_2'(x)} \\ g_3(z)\, e^{i/\hbar\, h_1'(x)}\, e^{-ik_w^* z} \\ g_4(z)\, e^{i/\hbar\, h_2'(x)}\, e^{-ik_w^* z} \end{bmatrix} \tag{6.35}$$

one can substitute these in (6.33) and obtain sets of coupled

differential equations like we did in Chapter IV and try to come up with a solution to these equations. We have done this and found a particular solution. For the sake of succinctness we present the form of x-dependence of the solution here and show how it works

$$\begin{aligned} \text{let} \qquad h_1(x) &\equiv \left(p_{1x} + \tfrac{1}{2}\, im_0 c\, \omega_c x\right)x \\ h_2(x) &\equiv \left(p_{1x} - \tfrac{1}{2}\, im_0 c\, \omega_c x\right)x \\ h_1'(x) &\equiv \left(p_{2x} + \tfrac{1}{2}\, im_0 c\, \omega_c x\right)x \\ h_2'(x) &\equiv \left(p_{2x} - \tfrac{1}{2}\, im_0 c\, \omega_c x\right)x \end{aligned} \tag{6.36}$$

where p_{1x} and p_{2x} are c-numbers.

Then substituting (6.34) in (6.33) we obtain

$$\begin{aligned} &A f_1 + B f_3 + (cp_{1x} - im_0 c\omega_c x) e^{ik_w^* z} f_4 + im_0 c\omega_c x\, e^{ik_w^* z} f_4 - eaf_4 = 0 \\ &A f_2 + (cp_{1x} + im_0 c\omega_c x) f_3 e^{-ik_w^* z} - eaf_3 - B f_4 - \hbar c k_w f_4 - im_0 c\omega_c x f_3 e^{-ik_w^* z} = 0 \\ &B f_1 + (cp_{1x} - im_0 c\omega_c x) e^{ik_w^* z} f_2 - eaf_2 + A' f_3 + im_0 c\omega_c x\, e^{ik_w^* z} = 0 \\ &(cp_{1x} + im_0 c\omega_c x) f_1 e^{-ik_w^* z} - eaf_1 - Bf_2 - \hbar c k_w f_2 + A' f_4 - im_0 c\omega_c x f_1 e^{-ik_w^* z} = 0 \end{aligned} \tag{6.37}$$

functions containing x cancel out and we obtain a set of equations identical to (4.7). Similarly substituting (6.35) in (6.33) we obtain a set of equations corresponding to down-spin electron and this set is identical to (4.8). Therefore one is led to the conclusion that the z-dependence of the solutions of the Dirac equation for the motion of an electron moving in a combined field of wiggler and axial guide field, will be the same as that of the electron moving in a wiggler only.

Explicitly the solutions will be

$$\Psi^{\uparrow} = N_1 \begin{bmatrix} \phi_{11} e^{i/\hbar\, p_{1x}^{+} x} \\ \phi_{12} e^{i/\hbar\, p_{1x}^{-} x} \\ \phi_{21} e^{i/\hbar\, p_{1x}^{+} x} \\ \phi_{22} e^{i/\hbar\, p_{1x}^{-} x} \end{bmatrix} \left\{ ce_{\nu}(z, p_{1x}) + i se_{\nu}(z, p_{1x}) \right\} \tag{6.38}$$

where $$p_{1x}^{+} \equiv \left(p_{1x} + \frac{1}{2} i m_0 c\, \omega_c x\right)$$

$$p_{1x}^{-} \equiv \left(p_{1x} - \frac{1}{2} i m_0 c\, \omega_c x\right)$$

and
$$\begin{aligned} \phi_{11} &\equiv 1 \\ \phi_{12} &\equiv K_1 e^{ik_w^{*} z} \\ \phi_{21} &\equiv \frac{[c p_{1x} e^{ik_w^{*} z} - ea] K_1 + c p_1}{E + m_0 c^2} \\ \phi_{22} &\equiv \frac{[c p_{1x} e^{-ik_w^{*} z} - ea] - c(p_1 + \hbar k_w) K_1}{E + m_0 c^2}\, e^{ik_w^{*} z} \end{aligned} \tag{6.39}$$

here all the parameters are the same as in (4.50)-(4.55) except K_1 and p_1. Modification of K_1 and p_1 due to the presence of axial guide field will be discussed in the next section. Similarly the down-spin solution will be

$$\Psi^{\downarrow} = N_2 \begin{bmatrix} \Phi_{11} e^{i/\hbar\, p_{2x}^{+} x} \\ \Phi_{12} e^{i/\hbar\, p_{2x}^{-} x} \\ \Phi_{21} e^{i/\hbar\, p_{2x}^{+} x} \\ \Phi_{22} e^{i/\hbar\, p_{2x}^{-} x} \end{bmatrix} \left\{ ce_{\nu}(z, p_{2x}) + i se_{\nu}(z, p_{2x}) \right\} \tag{6.41}$$

where $p_{2x}^{+} \equiv (p_{2x} + \frac{1}{2} i m_0 c \omega_c x)$

$p_{2x}^{-} \equiv (p_{2x} - \frac{1}{2} i m_0 c \omega_c x)$

and $\Phi_{11} \equiv K_2 e^{-ik_w^* z}$

$\Phi_{12} \equiv 1$

$$\Phi_{21} \equiv \frac{[cp_{2x} e^{ik_w^* z} - ea] + (cp_2 + \hbar c k_w) K_2}{E + m_0 c^2} e^{-ik_w^* z}$$

$$\Phi_{22} \equiv \frac{[cp_{2x} e^{-ik_w^* z} - ea] K_2 - cp_2}{E + m_0 c^2}$$

where all the parameters are the same as (4.58)-(4.62) except K_2 and p_2. Modification of K_2 and p_2 will be discussed in the next section.

Solutions (6.38) and (6.41) indeed reduce to 2-D solutions of the 4'th Chapter when $\omega_c \to 0$ ($B_0 \to 0$) . Also note that these solutions are not exact since the 2-D solutions of electron moving in a wiggler only, were derived using the power series expansions of Mathieu functions. Equations (6.38) and (6.41) are the extensions of those 2-D solutions thus are also approximate. But the approximation error is small and these solutions are sufficient to describe the motion of an electron moving in a combined helical wiggler and an axial guide field. 2-D solutions (3-D preferably) are absolutely necessary to investigate the effects of an axial guide field quantum mechanically since in the 1-D quantum theory transverse momentum compenents are ignored and since the basic contribution of an axial guide field is to introduce an additional transverse motion to the electron.

Stability from a Quantum Mechanical Point of View

The physically relevant quantitiy in Relativistic Quantum Mechanics is the current density. It is given in terms of the wavefunctions (spinors) and the Dirac-γ matrices

$$j_z^{\uparrow} = \bar{\Psi}^{\uparrow}\gamma^3\Psi^{\uparrow} \tag{6.44}$$

$$j_z^{\downarrow} = \bar{\Psi}^{\downarrow}\gamma^3\Psi^{\downarrow} \tag{6.45}$$

Using (6.38) and (6.41) we can find these current densities for an electron moving in a combined field of a wiggler and an axial guide field.

$$j_z^{\uparrow} = \frac{1}{N_1^2}(\phi_{11}^*\phi_{21} - \phi_{21}^*\phi_{11})e^{-m_0\omega_c\frac{x}{\hbar}^2} + \frac{1}{N_1^2}(\phi_{22}^*\phi_{12} - \phi_{12}^*\phi_{22})e^{-m_0\omega_c\frac{x}{\hbar}^2} \tag{6.46}$$

$$j_z^{\downarrow} = \frac{1}{N_2^2}(\Phi_{11}^*\Phi_{21} - \Phi_{21}^*\Phi_{11})e^{-m_0\omega_c\frac{x}{\hbar}^2} + \frac{1}{N_2^2}(\Phi_{22}^*\Phi_{12} - \Phi_{12}^*\Phi_{22})e^{m_0\omega_c\frac{x}{\hbar}^2} \tag{6.47}$$

A close examination of the explicit expressions for ϕ_{ij} and Φ_{ij} will reveal that

$$j_z^{\uparrow} \cong \frac{4}{2\gamma}\left\{\frac{cp_1}{E+m_0c^2}\cosh(m_0\omega_c\frac{x}{\hbar}^2) - \frac{(ea-cp_{1x}\cosh_w z)}{E+m_0c^2}\sinh(m_0\omega_c\frac{x}{\hbar}^2)\right\} \tag{6.48}$$

$$j_z^{\downarrow} \cong \frac{4}{2\gamma}\left\{\frac{cp_2}{E+m_0c^2}\cosh(m_0\omega_c\frac{x}{\hbar}^2) - \frac{(ea-cp_{2x}\cosh_w z)}{E+m_0c^2}\sinh(m_0\omega_c\frac{x}{\hbar}^2)\right\} \tag{6.49}$$

As can be seen from (6.48) and (6.49) the probability-current density can become unstable. The quantum mechanical equivalent of an unstable classical orbit can be described as a solution to the Dirac equation which gives an infinite or a negative current density.

The condition $j < 0$ is reached when

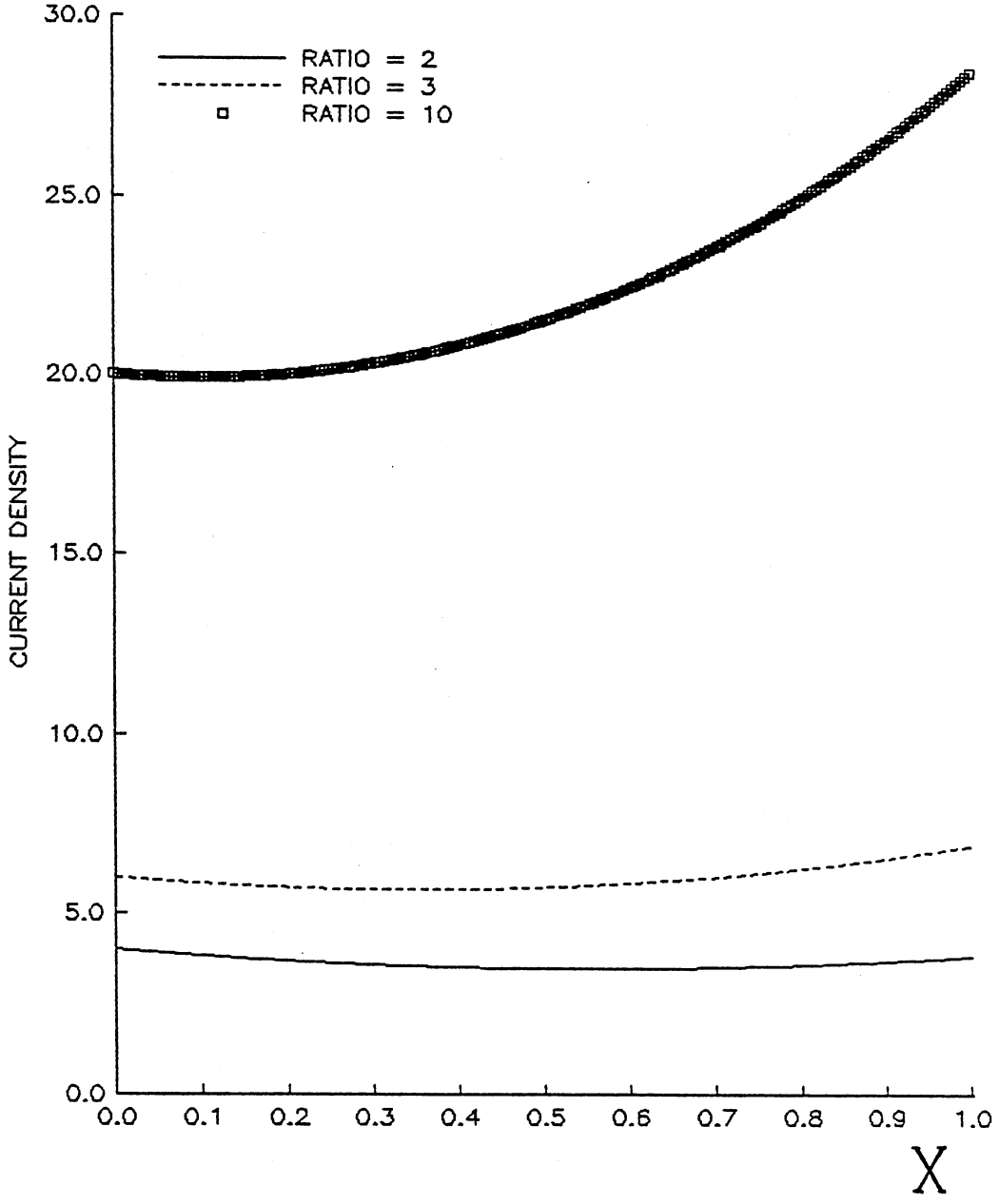

Figure 19. Current density versus axial guide field strength

$$cp_{1,2}\cosh(m_0\omega_c \frac{x^2}{\hbar}) = (ea-cp_{1,2}\cos k_w z)\sinh(m_0\omega_c \frac{x^2}{\hbar})$$

but since $[\tanh()]_{max} = 1$, this condition is reached only when $cp_{1,2} \cong ea$ which means that the slow electrons will be unstable. This conclusion is in complete agreement with the classical theory. The other condition $j \to \infty$ (or very large) will be met when ω_c reaches a certain value. In Figure 19 we have plotted probability current density versus $X \equiv m_0\omega_{ch}\frac{x^2}{\hbar}$. The parameter RATIO is defined as $(cp_{1,2}/ea)$ and we have only plotted the probability-current-densities for low RATIOs. Higher RATIO curves will be very similar to RATIO=10 curve, only lifted up in the vertical scale. Note also that j(X) quickly takes off and blows-up when X >1 therefore X = 1 is taken as the cut-off value. From this cut-off value we can calculate the maximum ω_c (hence the maximum B_0) that is allowed.

$$(\omega_c)_{max} = \frac{\hbar}{m_0 R^2} \tag{6.51}$$

Here we replaced x with R the effective radius of the wiggling motion since the radius of the motion of an electron in a combined wiggler and axial field is given dominantly by the radius of the wiggling motion (especially so when B_0 is strong). This radius is given by

$$R = \frac{v_\perp m_0}{eB_0} = \frac{ea/c\gamma}{eB_0} = \left(\frac{B_w}{B_0}\right)\frac{1}{k_w\gamma} \tag{6.52}$$

substituting this in (6.51) we obtain

$$(\omega_c)_{max} = \frac{\hbar}{m_0}\left(\frac{B_0}{B_w}\right)^2 \gamma^2 k_w^2 \tag{6.53}$$

since $\omega_c \equiv \frac{eB_0}{2m_0}$ we can write

$$(\omega_c)_{max} = (\omega_c)^2_{max}\left(\frac{4m_0\hbar}{e^2}\right)\left(\frac{k_w\gamma}{B_w}\right)^2 \tag{6.54}$$

$$(\omega_c)_{max} = \left(\frac{e^2}{4hm_0}\right)\left(\frac{B_w}{\gamma k_w}\right)^2 = \left(6.6744\ x10^{25}\ \frac{B_w^2}{\gamma^3 ck_w^3}\right)\gamma ck_w \qquad (6.55)$$

$$(\omega_c)_{max} \cong (10^{-2}c)\ \gamma k_w \qquad (6.56)$$

This expression is close to (6.24) considering the fact that $v_{//} \sim 10^{-2}c$ for the nonrelativistic electrons. Thus it is possible to predict the unstability region from the Dirac solutions but the predicted value $(\omega_c)_{max}$ is not as clear-cut as in classical theory.

Another conclusion that we can infer from this quantum mechanical analysis is that all the electrons entering the wiggler with relativistic speeds will follow the group-I trajectories. First of all, Dirac equation does not predict a group-II trajectory since the current density blows-up when $(eB_0/m_0\gamma) > ck_w$, consistent with the conclusion drawn for group-I orbits in classical theory. As mentioned by Friedland [4], an electron can be launched on a group-II orbit by injecting it at a nonrelativistic speed and then bringing it up in energy adiabatically. This of course is not relevant from a Dirac equation point of view.

In the Dirac equation formulation the spins of the electrons are naturally included. The presence of an axial guide field brings interesting possibilities regarding the spin-polarization of electrons. As we know from (4.48) and (4.60) the effective longitudinal momenta, p_1 and p_2 for up-spin and down-spin electrons respectively, are different. The presence of an axial guide field makes this difference even greater. For the combined field of wiggler and an axial field the expressions for p_1 and p_2 are given by (assuming that $\vec{B} = B_0\hat{z}$)

$$cp_1 \cong -\frac{1}{2}\hbar ck_w - \frac{eB_0 h}{2m_0\gamma} + \left(c^2(p_{0z}+\frac{1}{2}\hbar k_w)^2 - e^2a^2 + p_{0\perp}^2 - c^2p_{1x}^2 - \frac{c^2e^2B_0^2}{k_w^2}\right)^{1/2} \quad (6.57)$$

$$cp_2 \cong +\frac{1}{2}\hbar ck_w + \frac{eB_0 h}{2m_0\gamma} + \left(c^2(p_{0z}-\frac{1}{2}\hbar k_w)^2 - e^2a^2 + p_{0\perp}^2 - c^2p_{2x}^2 - \frac{c^2e^2B_0^2}{k_w^2}\right)^{1/2} \quad (6.58)$$

The physical explanation for this is simply that the spin-magnetic moment of the up-spin electron is aligned with the axial field resulting in a lower energy whereas the down-spin electron's spin-magnetic moment is antiparallel to $\vec{B}$ resulting in a higher energy. Therefore the slight difference between the relativistic factors γ_1 and γ_2 corresponding to p_1 and p_2 will be a little bigger. This change is very small and does not change the electron dynamics very much, it's effect on emitted frequencies and the rates for these emissions however cannot be neglected. Obviously the harmonic frequency which is emitted by those down-spin electrons making a transition from p_2 to p_1' (ie, accomponied by a spin-flip) is increased since the spin-flip energy gap is greater. But the probability of this emission is decreased as we shall calculate in the next section. The physical reasoning behind this is that when an axial field is present the problem becomes rather 1-Dimensional since the effect of an axial field is to confine the transverse motion of the electrons ($B_0 \cong B_{0max}$ case is an exception). Since in 1-D theory the rate for harmonic frequency generation is absolutely small, the rate calculated from a 2-D theory in the presence of an axial field will also be small. The implications of this, regarding the spin-polarizations of the electrons, is that the spin-polarization of the beam is preserved whereas a wiggler without an axial field would polarize the beam in the favor of either up-spin or down-spin. This phenomenon does not promise anything novel as far as

the FELs are concerned but it may have very important applications in electron accelerators in general. The electron (or positron) beam can be polarized for instance by using a helical wiggler and then by switching on the axial field the achieved polarization can be preserved against the thermal de-polarization effects.

Effects of Axial Field on Gain

As mentioned in the previous sections, the guide field enhances the gain. Now we shall calculate this effect from the matrix elements calculated by using the Dirac solutions (6.38) and (6.41). Since the z-dependence of these solutions are identical to (4.49) and (4.56) the calculation of matrix elements are very much simplified given the knowledge of matrix elements in Chapter V. In fact, the $e^{\mp m_0 \omega_c \frac{x^2}{\hbar}}$ term drop out in the calculation of matrix elements and therefore the matrix elements have the same form as those in Chapter V. The only difference is in the expressions for η_1 and η_2 and consequently in p_1 and p_2. The axial field will modify the expressions for η_1^2 and η_2^2 as follows

$$\eta_1^2 \equiv m_0^2c^4 - E^2 + e^2a^2 + \frac{e^2B_0^2c^2}{k_w^2} + c^2p_{1x}^2 \tag{6.59}$$

$$\eta_2^2 \equiv m_0^2c^4 - E + e^2a^2 + \frac{e^2B_0^2c^2}{k_w^2} + c^2p_{2x}^2 \tag{6.60}$$

This is a direct consequence of the conservation of energy. As the energy shared by the transverse momentum increases the energy in the z-direction should decrease. The explicit expressions for p_1 and p_2 in the presence of an axial field are already given in (6.57) and (6.58).

In order to calculate gain we do not need to go through the same

steps again, we just have to replace e^2a^2 in matrix elements and other expressions with $(e^2a^2+\frac{B_0^2e^2c^2}{k_w^2})$. Note however that "ea" in Dirac equation solutions should not be replaced with $(ea+\frac{B_0ec}{k_w})$. Just as we interpreted $c^2p_{1,2x}^2$ as a quantum mechanical correction to e^2a^2 we can also interpret $(eB_0c/k_w)^2$ as a classical correction term due to an axial field. There is a fundemental difference between these corrections though. $c^2p_{1,2x}^2$ broadens the spontaneous emission lineshape whereas $(eB_0c/k_w)^2$ has the opposite effect. $c^2p_{1,2x}^2$ causes a broadening since it is a quantum mechanical correction, a noise, hence the inclusion $c^2p_{1,2x}^2$ as an inhomogeneous broadening mechanism. $(eB_0c/k_w)^2$ on the other hand is a classical correction term and does not fluctuate. On the contrary, the axial field confines the electrons closer to the axis (except when $B_0 \cong B_{0max}$) thus reducing the emittance of the beam resulting in a sharper lineshape and therefore in a larger gain. The gain expressions will be

$$G_{fund.}=\frac{N_e}{V}\,e^{-(p_{0m}-p_0)^2/2\sigma_p^2}\;16\pi\frac{k_w}{\gamma}\,\frac{K_a^2}{[1+K_a^2+K_{0\perp}^2+2\gamma K_0+\gamma^2(K_0/K_a)]}\left(\frac{e^2}{m_0c^2}\right)$$

$$x\,\frac{1}{(\gamma w)^3}[1-\cos Lw-\tfrac{1}{2}\,Lw\,\sin Lw\,] \qquad (6.63)$$

$$G_{har}=\frac{N_e}{V}\,e^{-(p_{0m}-p_0)^2/2\sigma_p^2}\;16\pi k_w\gamma\,\frac{K_a\left(\frac{hck_w}{m_0c^2}\right)}{[1+K_a^2+K_{0\perp}^2+2\gamma K_0+\gamma^2(K_0/K_a)^2]}\left(\frac{e^2}{m_0c^2}\right)$$

$$x\,\frac{1}{(\gamma w)^3}[1-\cos Lw-\tfrac{1}{2}\,Lw\,\sin Lw\,] \qquad (6.64)$$

where $K_a \equiv \left\{ (e^2 a^2 + \frac{e^2 B_0^2 c^2}{k_w^2}) / m_0^2 c^4 \right\}^{1/2}$

note that G_{fund} is proportional to K_a^2 while G_{har} is proportional to K_a . The result being that while G_{fund} is increased due to the presence of an axial field, G_{har} is reduced. There is also a change in the harmonic frequency due to the fact that the axial field increases the energy gap between the spin states. The fundemental and harmonic frequencies generated by wiggling electrons in the presence of an axial field will be given by

$$\omega_{fund} = \frac{2\gamma^2 c k_w}{[1+K_a^2+K_{0\perp}^2+2\gamma K_0+2\gamma^2(K_0/K_a)]} \tag{6.65}$$

$$\omega_{har} = \frac{2\gamma^2 c k_w}{[1+K_a^2+K_{0\perp}^2+2\gamma K_0+2\gamma^2(K_0/K_a)]} + \frac{eB_0}{m_0\gamma} \tag{6.66}$$

Fundemental frequency is also affected by the axial field as can be seen from (6.65) since K of the pure wiggler is replaced by $K_a > K$. The magnitude of $(eB_0/m_0\gamma)$ term in (6.66) can be significant if B_0 is high. Typically $B_0 \sim 1$ T , then ω_{har} is increased by

$$\omega_{har} \rightarrow \omega_{har} + 1.7585 \times 10^{11} / \gamma$$

REFERENCES

[1] F. DeMartini, Phys.Quant.Elec. 7 , 789, Addison-Wesley (1980).

[2] H.P. Freund et al , IEEE J.Quant.Elec, QE-19, 322 (1983).

[3] R.C. Davidson and H.S. Uhm, J.Appl.Phys., 53, 2910 (1982).

[4] L. Friedland, Phys.Fluids, 23, 2376 (1980).

[5] S.H. Gold et al, Phys.Quant.Elec., 9, 741 , Addison-Wesley(1982).

CHAPTER VII

PULSED OPERATION

Introduction

In Chapter VI we assumed a continous electron beam. This assumption is justified for some of the FEL devices [1] where the electron pulse length is larger than the wiggler length. In most FELs though , the pulselength is much shorter (in the order of 1 mm). Figure 20 shows the the time structure of the Stanford SCA accelerator which was used in the original FEL experiments. In an FEL oscillator electron pulses are injected into the resonator to overlap a rebounding optical pulse. The rebounding optical pulse must be closely synchronized with the succession of electron pulses. Figure 21 depicts this schematically. One would expect that the exact synchronism would result in the highest gain but the real situation is surprisingly more complex. It has been discovered that the gain is extremely sensitive to the resonator length and a slight desynchronism is necessary to obtain optimum gain. In figure 22, average power output of the Stanford FEL oscillator is plotted against the cavity length desynchronism. The graph shows that when the cavity length is decreased slightly (10 μm) the average power output reaches a peak. The effect which makes this adjustment necessary is known as "Laser Lethargy " and is one of the unique features of the short-pulse FEL.

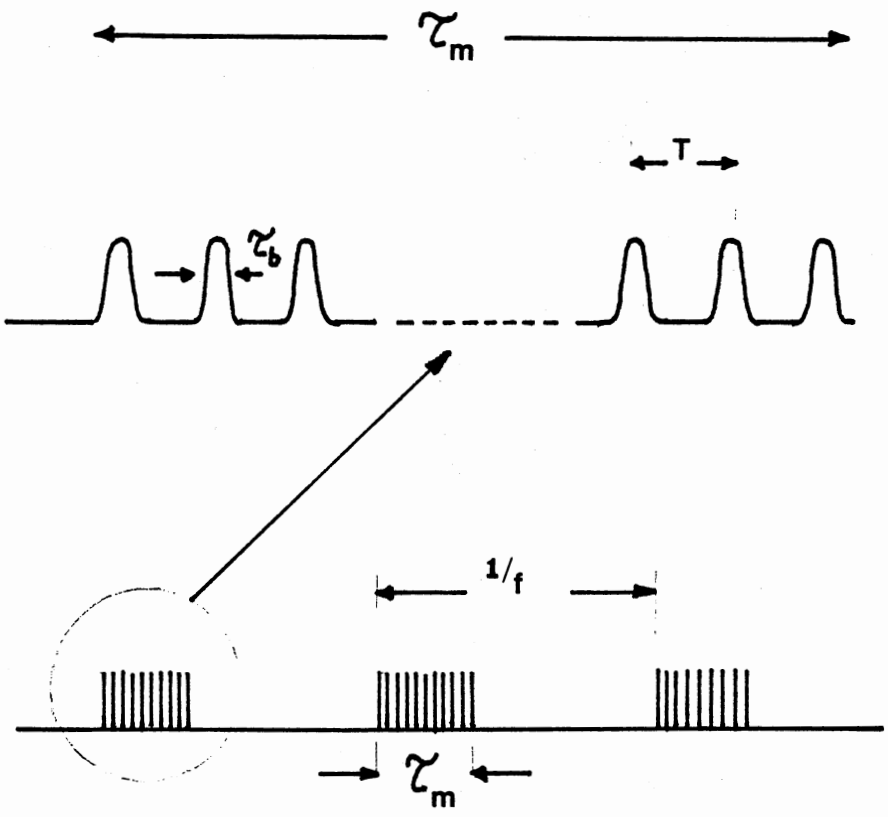

Figure 20. Time structure of the Stanford SCA electron beam.
τ_b = 3.2 ps , τ_m = 1.5-20 ms , f=10-20 Hz , T=769ps

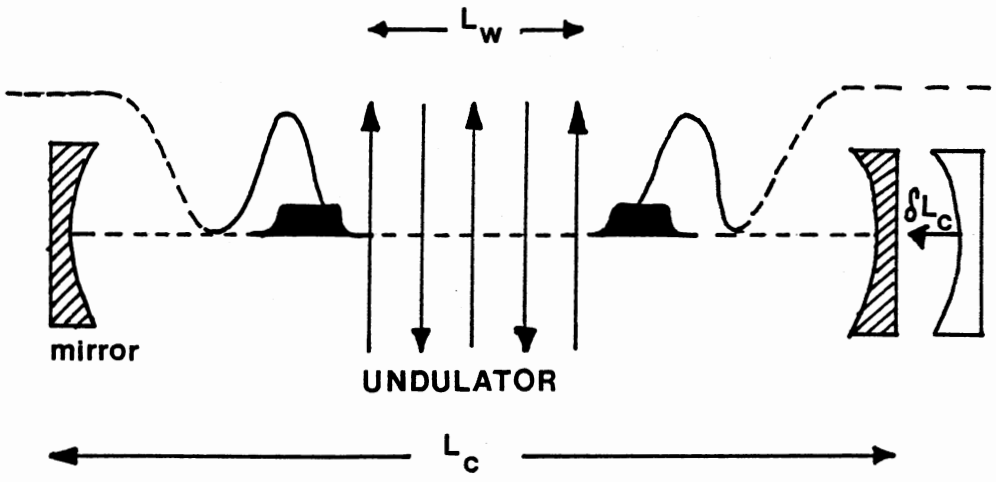

Figure 21. Electron and optical pulses in an FEL

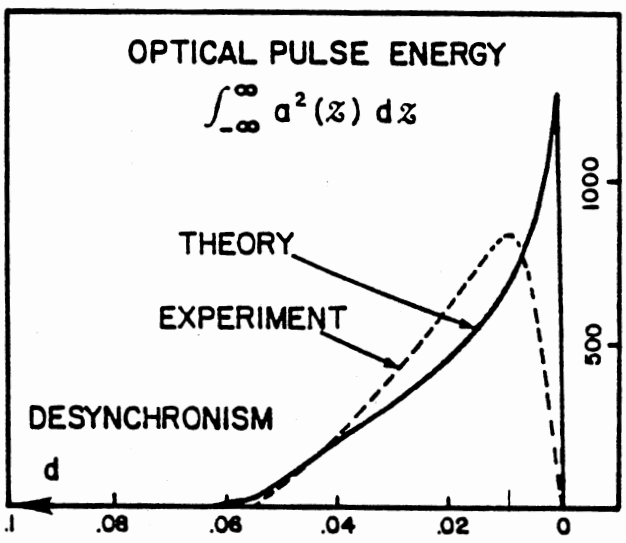

Figure 22. Laser Lethargy effect

Laser Lethargy

From the classical theory of FELs it is known that the light slips ahead of electrons by $N\lambda$ during its interaction with electrons and the wiggler field. Here N is the number of magnet poles in the wiggler and λ is the wavelength of the laser. If this slippage $N\lambda$ is comparable to the electron pulse length Δ then the laser lethargy effect will be observed. Because of the slippage and because there is more gain at the end of the wiggler than at the beginning, the trailing edge of the light pulse is amplified more than the leading edge. The overall effect is that the optical pulse gets shorter and shorter and after several round-trip passes it walks off the gain medium, ie, the electron pulse. This is illustrated in figure 23. A simple cure for this lethargy effect has been prescribed. The resonator length is decreased slightly so that as the center of the optical pulse lags behind the center of electron pulse after several passes, it will not walk out of the gain medium. The initial desynchronism (slight advancement of the optical pulse) compensates the latter retardation due to Laser Lethargy. As the optical pulse builds-up the problem of laser lethargy gets less severe and eventually disappears when the saturation is reached. Figure 24 describes this situation.

Laser lethargy is a serious problem in the start-up of the FEL oscillator and if not corrected the oscillator may never reach the saturation. It is also desirable that the laser reach saturation in the shortest time possible. Our objective in this chapter is to develop a formalism to explain the lethargy effect first and then expand it into a simulational model to study the start-up time of the pulsed-FEL

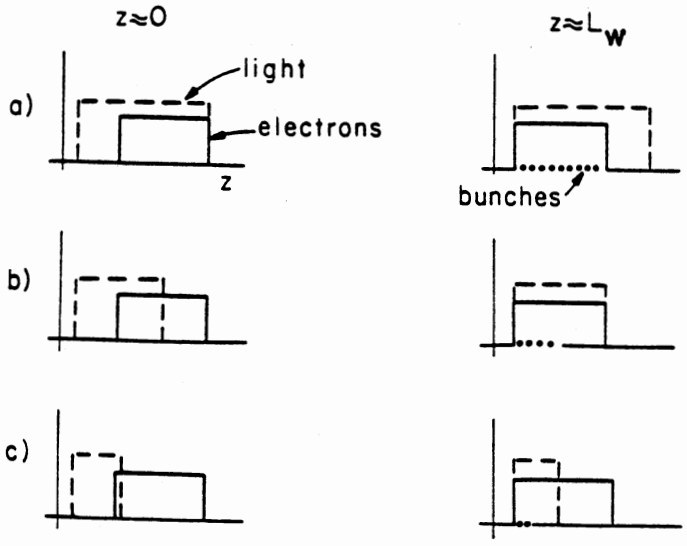

Figure 23. (a) Initial relative positions of light and electron pulses near input and output of wiggler.
(b) configuration shown many passes later
(c) configuration shown after many more passes

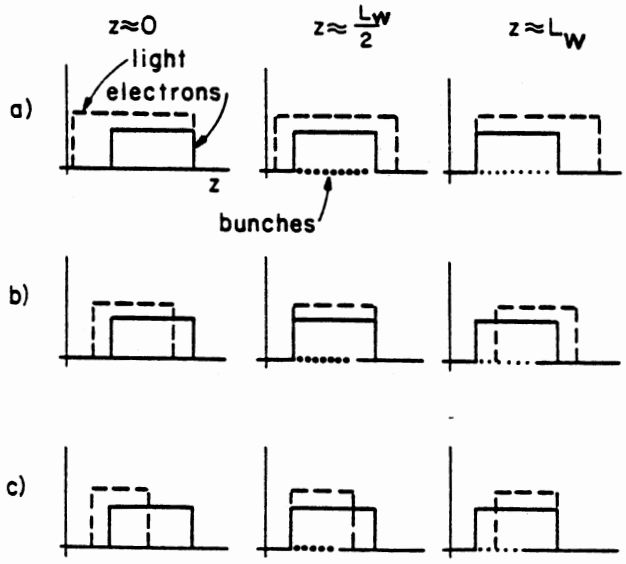

Figure 24. (a) Same as Figure 23, except that the light intensity is high, the system is saturated and the bunches are at a maximum near the center of the wiggler.

oscillator. Our main objective is to demonstrate the importance of quantum mechanical effects in the FEL start-up problem quantitatively and show how quantum mechanics modifies the classical results. We will also study the effects of tapering on the optical pulse shape and the start-up time using this model of the pulsed FEL.

Start-up in the Pulsed Operation

The problem of start-up in the pulsed operation was first studied by Hopf et.al. using the formalism of "Quasi-Bloch " description of the FEL [2]. Later the multimode Hamiltonian picture of pulse dynamics was developed [3]. Concurrently the single-particle electron model [4] was coupled to Maxwell's nonlinear wave equation [5] and this proved to be the most succesful classical description of the pulsed FEL interaction in both weak and strong optical fields [6]. Another comprehensive theory of the start-up of a pulsed-FEL was given by Sprangle, Tang and Bernstein [7]. In these studies one starts with the basic FEL-interaction equations and derives a differential equation for either the average photon number or the signal amplitude. Then by solving this equation numerically one follows the evolution of the photon number (signal amplitude) in time and determines how many round-trips it takes to reach saturation. Colson's analysis [6] is also capable of following the evolution of the pulse shape. In these calculations the laser lethargy effect has been taken care of by including the cavity length in an ad hoc manner. These analyses cannot treat photon number fluctuations which play an important role in the beginning of the start-up. A full explanation of n_T , the number of round-trips to saturation, using an ab initio quantum mechanical calculation remains as

a very complicated problem. Therefore all saturation calculations have to model the early stages of the start-up but unfortunately the start-up time is model dependent and very sensitive to any slight change in the gain during this early stage.

General Theory of Pulse Propagation

We consider as our basic model an optical pulse with a carrier frequency ω_0 and a complex gaussian envelope written in the form

$$E(t) = E_0\, e^{-at^2} e^{i(\omega_0 t+bt^2)} = E_0 e^{-\Gamma t^2} e^{i\omega_0 t} \tag{7.1}$$

the complex gaussian parameter describing this pulse is thus

$$\Gamma = a - ib \tag{7.2}$$

The instantaneous intensity $I(t)$ of this pulse will be

$$I(t) = |E(t)|^2 = e^{-2at^2} = e^{-(4\ln 2)(t/\tau)^2} \tag{7.3}$$

so that the pulsewidth τ, defined in the FWHM fashion, is related to the parameter "a" by

$$\tau_p = (2\ln 2/a)^{1/2} \tag{7.4}$$

The total instantaneous phase of the signal is

$$\phi_{tot}(t) = \omega_0 t + bt^2 = (\omega_0+bt)t \tag{7.5}$$

and therefore the instantaneous carrier frequency in radians per second will be defined as

$$\omega_i(t) = \frac{d\phi_{tot}}{dt} = \omega_0+2bt \tag{7.6}$$

The parameter "b" defines the degree of "chirp" in the signal, that is, the degree of variation of the instantaneous frequency within the pulse.

Figure 25 illustrates a chirped pulse. It is obvious that the functional dependence of the chirp has to be modeled. A linear increase or decrease of the instantaneous carrier frequency within the spatial dimensions of the pulse is a very reasonable model in most cases and as we shall see in the next section, it is the case in FELs to a very good accuracy.

The gaussian envelope is also a valid form for the FEL generated optical pulses. One advantage of gaussian pulse in time is that it Fourier-transforms into a gaussian spectrum in frequency.

$$E(\omega) = E_0 e^{-\frac{(\omega-\omega_0)^2}{4\Gamma}} \tag{7.7}$$

or explicitly

$$E(\omega) = E_0 e^{\left[-\frac{1}{4}\left(\frac{a}{a^2+b^2}\right)(\omega-\omega_0)^2 - i\frac{1}{4}\left(\frac{b}{a^2+b^2}\right)(\omega-\omega_0)^2\right]} \tag{7.8}$$

The power spectrum, or power spectral density is then given by

$$|E(\omega)|^2 = E_0^2\, e^{-\frac{1}{2}\left(\frac{a}{a^2+b^2}\right)(\omega-\omega_0)^2} = E_0^2\, e^{-4\ln 2\left(\frac{\omega-\omega_0}{\Delta\omega}\right)^2} \tag{7.9}$$

where $\Delta\omega$ is the FWHM spectral width (in radians per second) of the optical pulse. This can be converted into a pulse bandwith measured in Hz by writing

$$\Delta f = \Delta\omega \,/\, 2\pi = (\sqrt{2\ln 2}\,/\pi)(a[1+(b/a)^2])^{1/2} \tag{7.10}$$

which indicates that the presence of a frequency chirp as determined by the imaginary parameter ib increases the spectral width $\Delta\omega$ by a ratio $\sqrt{1+(b/a)^2}$ as compared to an unchirped pulse with the same pulsewidth in time. Another useful concept is the "time-bandwidth-product" given by

$$\Delta f\, \tau_p = (2\ln 2/\pi)\sqrt{1+(b/a)^2} \cong 0.44\sqrt{1+(b/a)^2} \tag{7.11}$$

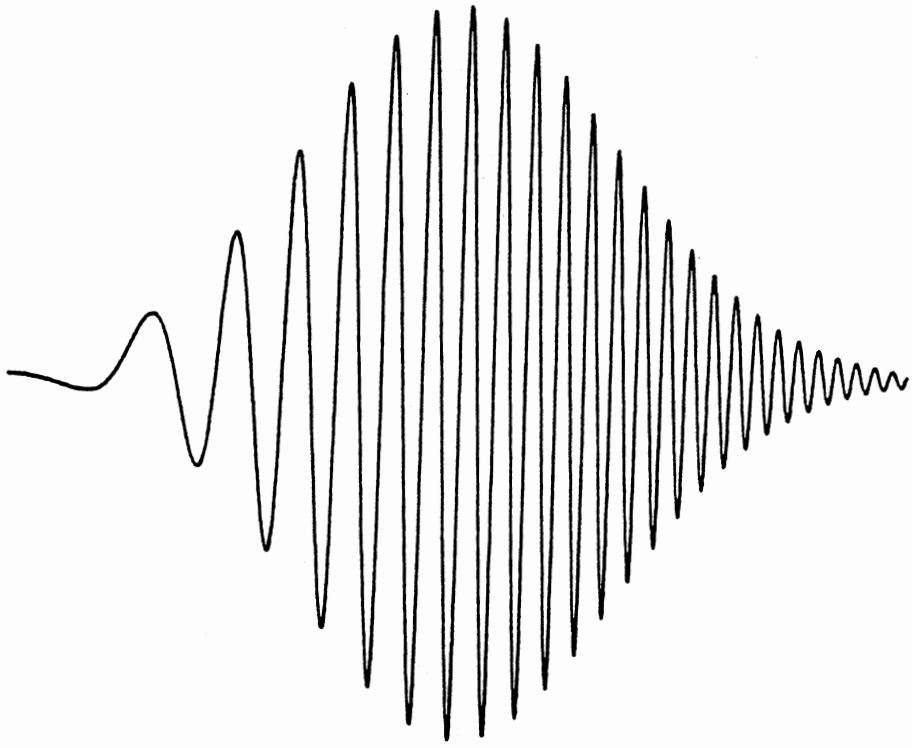

Figure 25. A chirped gaussian signal pulse

FWHM version of a general Fourier theorem says that the time-bandwidth product of any pulsed signal is constrained by the uncertainty principle

$$\Delta f_{rms} \Delta t_{rms} \geq 1/2$$

Therefore pulses with little chirp or other internal substructure (transform limited pulses) will have a time -bandwidth-product close to the value of 0.5 .

The basic wave equation for a 1-D signal in a dispersive medium can be written as

$$\frac{\partial^2 E(z,t)}{\partial z^2} - \mu_0 \varepsilon_0 \frac{\partial^2 E(z,t)}{\partial t^2} = \mu \frac{\partial^2 P(z,t)}{\partial t^2} \tag{7.12}$$

where P(z,t) is the polarization of the medium and

$$E(z,t) = \text{Re } E_0(z,t)\, e^{i[\omega_0 t - k(\omega_0) z]} \tag{7.13}$$

where ω_0 is the carrier frequency, $k(\omega)$ is the wavenumber at this frequency and $E_0(z,t)$ is the complex envelope of the pulsed signal. The polarization P(z,t) can be written in terms of its Fourier transform

$$P(z,t) = \frac{1}{2\pi} \int_{-\infty}^{\infty} P(z,\omega) e^{i\omega t} \, d\omega \tag{7.14}$$

where $P(z,\omega)$ can be written in the form

$$P(z,\omega) = \chi(\omega) \varepsilon_0 E(z,\omega) \tag{7.15}$$

where $E(z,\omega)$ is the Fourier transform of E(z,t) given by

$$E(z,\omega) = \int_{-\infty}^{\infty} E(z,t) e^{-i\omega t} \, dt = \int_{-\infty}^{\infty} E(z,t) e^{i(\omega_0 - \omega)t} dt \tag{7.16}$$

and where $\chi(\omega)$ is the dispersive susceptibility of the propagation system. Using these definitions plus Fourier transform theorems, one can reduce (7.12) into the so called "parabolic equation" [9] for the

pulse envelope $E_0(z,t)$ given by

$$\frac{\partial E_0(z,t)}{\partial z} + \frac{1}{v_g}\frac{\partial E_0(z,t)}{\partial t} - i\frac{k''}{2}\frac{\partial^2 E_0(z,t)}{\partial t^2} = 0 \qquad (7.17)$$

where $k'' = \left.\frac{d^2k(\omega)}{d\omega^2}\right|_{\omega=\omega_0} = \frac{d}{d\omega}\frac{1}{v_g(\omega)}$ ≡ group velocity dispersion

$$k' = \frac{1}{v_g(\omega_0)} \equiv \frac{1}{\text{group velocity}}$$

If $k'' = 0$ then this equation is satisfied by any solution of the form $E_0(z,t) = E_0(z-v_g t)$. If $k'' \neq 0$, however, the $i\frac{k''}{2}\frac{\partial^2 E_0}{\partial t^2}$ term in (7.17) then acts like a generalized complex diffusion term for the pulse envelope $E_0(z,t)$. This diffusion term may lead to pulse broadening, pulse compression and/or pulse reshaping effects depending on the other parameters. One can deduce from (7.17) or from other methods explained in the literature [9] that

$$\frac{1}{\Gamma(z)} = \frac{1}{a(z)-ib(z)} = \frac{1}{\Gamma_0} + 2ik''z = \frac{a(z)+ib(z)}{a^2(z)+b^2(z)} \qquad (7.18)$$

By differentiating $\Gamma(z)$ with respect to distance along the system one can obtain the differential equation

$$\frac{d\Gamma(z)}{dz} = -2ik''\Gamma^2(z) \qquad (7.19)$$

which can be seperated into two equations for "a" and "b"

$$\frac{da(z)}{dz} = -4k''a(z)b(z) \quad , \quad \frac{db(z)}{dz} = 2k''[a(z)^2 - b(z)^2] \qquad (7.20)$$

integrating these equations one obtains

$$a(z) = \frac{a_0}{(1+2k''zb_0)^2+(2k''za_0)^2} \tag{7.21}$$

$$b(z) = \frac{b_0(1+2k''zb_0) + 2k''za_0^2}{(1+2k''zb_0)^2+ (2k''za_0)^2} \tag{7.22}$$

where a_0 and b_0 are the initial pulse parameters. It is instructive to plot b(z) versus a(z) (figure 26) to see how the pulse length changes with increasing z or with k'' . A maximum in a(z) corresponds to a minimum in pulselength. An optical pulse is not always compressed during its passage through a dispersive medium where $k'' \neq 0$ It depends on the length of the dispersive medium (parameter z) as well as on initial conditions a_0 , b_0 and the sign of k''. Figure 27 shows how it is possible to achieve more compression by choosing a large initial chirp. The most important conclusion relevant to our FEL calculations is that all signals with large initial time-bandwidth-products (large chirp, $b_0 \gg a_0$) are potentially compressible.

A physical explanation for pulse compression can be given as follows. Different parts of a chirped pulse, which start out down the line at slightly earlier or later times also have slightly different frequencies. They can then travel slightly more slowly or rapidly down the line because of group velocity dispersion, in such a way that they just exactly catch up with the central portion of the pulse.

Optical model of the FEL and Laser Lethargy

In the previous section the propagation of an optical pulse through a gainless and linear medium has been discussed. In this section we

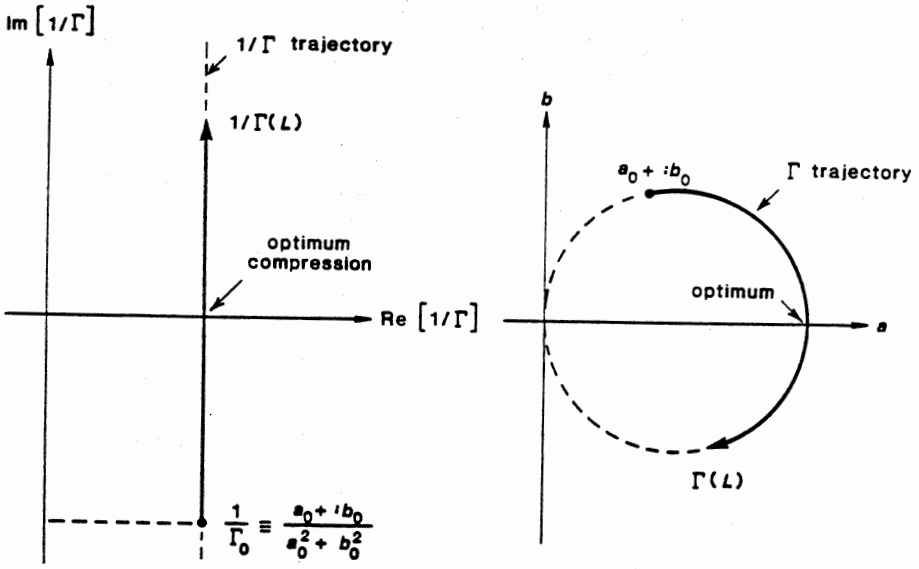

Figure 26. Trajectories for dispersive pulse propagation and pulse compression in the Γ and $1/\Gamma$ planes

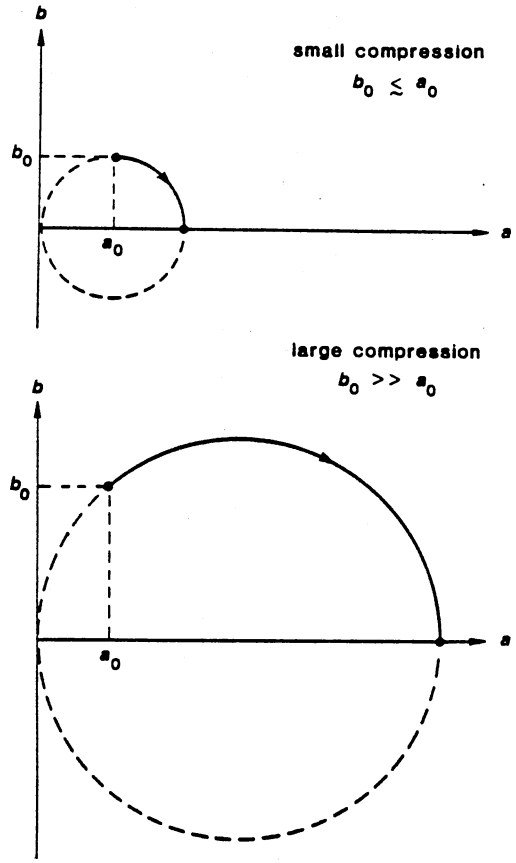

Figure 27. Pulse compression with the same initial pulsewidths but smaller and larger initial time-bandwidth products

will bring the gain into the picture and make connections to FEL theory. We will use all the information derived in chapters IV and V and the results of other researches discussed in literature. Putting all the information about pulse propagation formalism together we come up with a useful model which we call "the Optical Model of the FEL" since all features of the FEL dynamics are represented by optical parameters.

We identify instantaneous carrier frequency ω_i with the frequency corresponding to the peak in the gain curve, not the central frequency of the spontaneous emission lineshape. This distinction does not arise in a conventional laser since its spontaneous emission lineshape and gain curve peak at the same frequency. The unique difference of FEL gain is illustrated in figure 28. We also assume a gaussian shape for the FEL generated optical pulse. The FEL spontaneous emission lineshape (which is the Fourier transform of the optical pulse-in-time-domain) has a $(\sin x / x)^2$ dependence. This functional form is a consequence of assuming a square electron-pulse shape. In the CW operation the entrance and exit of electrons into and out of the interaction region, which spans the whole length of the wiggler L_w , constitutes a square pulse. In the pulsed operation, interaction length should be taken as the actual pulse length Δ , therefore the spontaneous emission lineshape will read

$$f(w(\omega))= \left(\frac{\sin(w\Delta/2)}{w\Delta/2} \right)^2 \qquad (7.23)$$

where w is the same as given in (5.30) . Obviously (7.23) is not the Fourier transform of a gaussian optical pulse. But as Δ gets shorter f(w) gets broader and can be better approximated by a gaussian function. The gaussian approximation is further justified by the fact that in

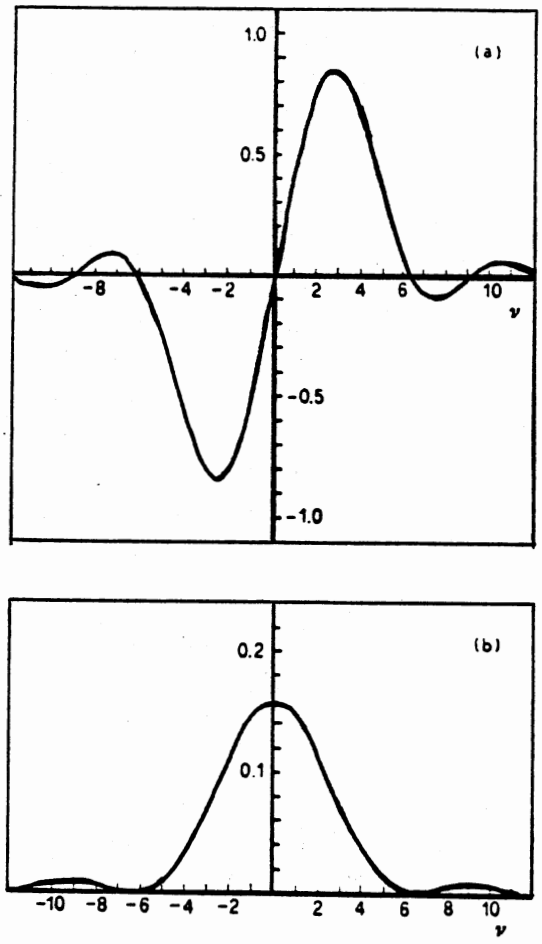

Figure 28. (a) small-signal gain (b) spontaneous spectrum

practice one never has exact square electron-pulses. A real electron-pulse acquires a tail when it is formed in the rf-cavity of the accelerator.

Next step is to identify the optical parameter "b" with a parameter in FEL theory. We know from FEL theory that as electrons radiate and lose energy, if there is no tapering, the central frequency of the lineshape will shift towards a lower frequency. Recall that the central frequency (fundemental) is given by

$$\omega_0' = \frac{2ck_w\gamma^2}{[1+K^2+K_{0\perp}^2+2\gamma K_0+\gamma K_0(\frac{\gamma}{K}+1)]} \tag{7.24}$$

The relevant frequency though is the frequency at which the gain curve peaks. This frequency can be found by the usual algebraic technique of equating the first derivative of the gain function to zero. We obtain the the condition

$$-2Lw\sin Lw + (L^2w^3/2 - 3)\cos Lw + 3 = 0 \tag{7.25}$$

which has a solution

$$Lw = 2.605776573 \quad \text{radians} \tag{7.26}$$

since w can be written as $(\omega_0' - \omega_0)/c$ where ω_0 is the gain-peak frequency, we obtain

$$\omega_0 = \omega_0' - \frac{c}{L}(2.605776573) \tag{7.27}$$

At this point we would like to comment on the significance of the parameter L . It will be the essential parameter in our formalism since we take it as the "effective interaction length" not as the actual length of the wiggler or the electron pulse. The effective interaction length has been discussed in reference [10] in relation to tapering calculations. In this chapter it will assume a greater role when we

discuss the changes in gain function as the laser approaches saturation.

During one pass of the electron-pulse through the wiggler, γ decreases slightly and ω_0 changes accordingly. Quantitatively speaking

$$\Delta\gamma = -\frac{G\, W_{0s}}{(mc^2)} \quad , \quad W_{0s} \equiv \hbar\omega_0 N_p \quad \text{where} \quad N_p: \text{Number of photons that constitute the optical pulse} \tag{7.28}$$

where G is the gain as defined in (1.35)

$$G = -\pi g \frac{d}{d\nu}\left(\frac{\sin(\nu/2)}{\nu/2}\right)^2 \quad , \quad g \equiv \frac{4\pi}{\gamma}\frac{\lambda_0 L_w}{\Sigma}\frac{I}{I_0} F_\xi \left(\frac{\omega}{\Delta\omega}\right)^2 \tag{7.29}$$

here $\nu \equiv Lw$, $\lambda_0 = 2\pi c/\omega_0'$, and other parameters are defined in Chapter I. Since L is the most important parameter in our formalism we would like to show how the gain amplitude depends on L explicitly. First, let us examine the relative bandwidth

$$\left(\frac{\Delta\omega}{\omega}\right) = \frac{\lambda_w}{2L_w} \quad \text{CW operation} \quad , \quad \left(\frac{\Delta\omega}{\omega}\right) = \frac{\lambda}{L} \quad \text{Pulsed operation} \tag{7.30}$$

where λ is the laser wavelength and is given by

$$\lambda = \frac{2\pi c}{\omega_0'}\frac{1}{\left(1 - \frac{2.605776573\, c}{\omega_0' L}\right)} \cong \frac{2\pi c}{\omega_0'}\left(1 + \frac{2.605776573 c}{\omega_0' L} + \ldots\right) \tag{7.31}$$

which can be derived from (7.27). Here L is the effective interaction length and in the pulsed operation it is initially equal to Δ the electron-pulse length. Later, as the optical pulse grows and undergoes distortion and compression, L refers to the instantaneous optical pulse length. In addition to these rather obvious physical interpretations of L we will also incorporate the effects of inhomogeneous line broadening due to the energy and momentum spread in the electron beam, and the

effects of quantum mechanics to L. This way all the relevant features of an FEL will be explained in terms of an effective L. We will also show that even the problem of pulse-propagation in a tapered FEL can be solved with this effective interaction length formalism.

Using (7.30) the amplitude of the gain function can be expressed as

$$|G| = \frac{2\pi^2}{\gamma} \frac{K^2 F}{(1+K^2)} L_w \frac{(L^2 - 0.8294444\ \lambda_0 L + 0.1719945\ \lambda_0^2)}{\lambda_0 \Sigma} \frac{Ir_0}{ec} \alpha_0 \qquad (7.32)$$

where $\alpha_0 \equiv \frac{4}{\nu^3}(1-\cos\nu - \frac{1}{2}\nu \sin\nu)\big|_{\nu=2.605776573} = 0.013157$

In (7.32) the only dynamical variable is L. All other symbols refer to experimental parameters or constants. By taking $W_{0s} = \hbar\omega_0 N_p$, where N_p is the photon number, and by replacing $L_w \cong c\,\Delta t$ in (7.32) we can express $\Delta\gamma$ as

$$\Delta\gamma = -|G| \frac{\hbar\omega_0 N_p}{mc^2} \frac{c}{L_w} \Delta t \Rightarrow \frac{d}{dt}\gamma = -\frac{|G| r_0 N_p \omega_0}{L_w \alpha} \qquad (7.33)$$

where α is the fine structure constant. Therefore the instantaneous carrier frequency will be

$$\omega_i(t) = \omega_0 + \frac{d\omega_0'}{dt} t \qquad (7.34)$$

since $\frac{d\omega_0'}{dt} = \frac{4\gamma_0 c k_w}{[1+K^2+K_{0\perp}^2+2\gamma_0 K_0+\gamma_0 K_0(\frac{\gamma_0}{K} \mp 1)]} \frac{\gamma_0}{} \frac{d\gamma(t)}{dt}\Big|_{\gamma=\gamma_0}$ we have

$$\omega_i(t) \cong \omega_0 - 32\pi^4 \frac{\alpha_0}{\alpha} \frac{K^2 F}{(1+K^2)^2} \frac{r_0[L^2 - 0.8294444\ \lambda_0 L + 0.1719945\ \lambda_0^2]}{\lambda_0 \lambda_w \Sigma\lambda} \frac{Icr_0 N_p}{e} t \qquad (7.35)$$

comparing this to (7.6) we can identify

$$b = -16\pi^4 \frac{\alpha_0}{\alpha} \frac{K^2 F}{(1+K^2)^2} \frac{r_0(1-\frac{0.4147222\lambda_0}{L})[L^2-0.8294\lambda_0 L+0.1719\lambda_0^2]}{\lambda_0^2 \lambda_w \Sigma} \frac{Icr_0 N_p}{e} \tag{7.36}$$

Note that the sign of "b" is negative. The next step is to find the dispersion relation for the medium of electron gas. This FEL dispersion relation is derived in reference [11].

$$\omega = (k + k_w)v - \frac{\omega_p}{\gamma} \quad \text{where} \quad \omega_p = \frac{4\pi\rho e^2}{\gamma m_0} \tag{7.37}$$

ρ is the density of electrons and ω_p defines the invariant plasma frequency for a relativistic system. From (7.37) we can immediately conclude that

$$k'' \equiv \frac{d^2 k(\omega)}{d\omega^2}\bigg|_{\omega=\omega_0} = \frac{d}{d\omega}\frac{1}{v} = 0 \tag{7.38}$$

since v is defined as the average parallel speed and it is independent of ω .

$$v = \langle v(z) \rangle = \left\langle \frac{cK\sqrt{2}}{\gamma} \sin k_w z \right\rangle = \frac{cK}{\gamma\sqrt{2}} \tag{7.39}$$

Therefore, there will not be any pulse broadening or compression due to medium effects.

Now consider the gain function as given in (7.29). The gain variation around ω_0 can be written as

$$\alpha(\omega) = |G| + \frac{\partial G(\omega)}{\partial\omega}\bigg|_{\omega=\omega_0} (\omega - \omega_0) + \frac{1}{2}\frac{\partial^2 G(\omega)}{\partial^2\omega^2}\bigg|_{\omega=\omega_0} (\omega - \omega_0)^2 + \ldots\ldots \tag{7.40}$$

since $\frac{\partial G(\omega)}{\partial\omega}\Big|_{\omega=\omega_0} = 0$, evaluating the third term we have

$$\alpha(\omega) = |G| - \frac{1}{2}(2.0603)g\left(\frac{L}{c}\right)^2(\omega - \omega_0)^2 \tag{7.41}$$

Let us denote

$$K_\alpha \equiv 2(2.0603)g\,(L/c)^2\, z_0 \tag{7.42}$$

where z_0 is the normalized distance $z_0 = \frac{z}{L_w}\frac{1}{4N^2}$

This normalization is necessary because our $\alpha(\omega)$ is unitless hence the (z/L_w) normalization, secondly , in our formulation (λ/L) replaces the $(\lambda_w/2L_w) \equiv (1/2N)$ factor of the original gain expression,and since (7.42) involves an L^2 term the parameter z_0 has to be further normalized.

The primary effects that result when a pulse passes through a linear but frequency dependent gain medium are pulse broadening or shortening, and possibly frequency and time shifting effects that can occur if the gain medium has a linear variation around the carrier frequency. As we have seen in (7.40), the FEL gain does not have such a linear variation around the carrier frequency but it does have a linear variation around the central frequency. As far as the optical pulse is concerned the behaviour around ω_0 is important because this is the frequency which is enhanced and amplified pass after pass.

The first term in (7.40) gives a uniform amplitude gain which applies equally to all frequency components and hence no change in pulse-shape results. The second term however leads to a change in the gaussian pulse parameter [9].

$$a(z) = \frac{a_0(1+ K_\alpha a_0) + K_\alpha b_0^2}{(1+ K_\alpha a_0)^2 + (K_\alpha b_0)^2} \tag{7.43}$$

a_0 and b_0 are the initial pulse parameters. Since K_α is small

compared to $(1/\Gamma_0)$, (7.43) can be written as

$$a(z) \cong a_0[1 - K_\alpha a_0 + K_\alpha (b_0^2/a_0)] \qquad (7.44)$$

A larger a(z) means a shorter pulse. The third term in (7.44) causes a pulse compression whereas the second term causes a pulse broadening. Under the special circumstance of $b_0 > a_0$ the overall effect is a pulse compression. This is the case in FELs. The unique feature of FEL interaction is that the "chirp" is reintroduced at each pass of an electron-pulse. Even though the "chirp" is largely removed at the end of the interaction region as a result of compression, it will be reintroduced by the interaction of the rebounding optical pulse with the fresh electron-pulse.

For the Stanford oscillator the numerical value of b_0 is calculated at 500 kW peak power inside the cavity

$$b_0 = -1.3449235 \times 10^{27} \quad 1/\text{sec}^2$$

The amount of compression depends on the parameter K_α . For the above mentioned radiation level K_α is (at $z = L_w$)

$$K_\alpha = 2(2.0603)g(L/c)^2 (1/4N^2) = 2.683 \times 10^{-29} \quad \text{sec}^2$$

This value of K_α was calculated by taking the initial value of L which is 1 mm for the Stanford oscillator. In reality K_α is smaller at this radiation level because the effective interaction length L is significantly smaller than L_0, the initial parameter. The change in the effective interaction length can be caused by the following processes

a) The increase in the number of photons in the cavity and the approach to saturation point.

b) Laser Lethargy.

c) The amount of desynchronism (the slight change of cavity length)

d) Inhomogeneous Broadening effects

e) Quantum Mechanical effects

f) Tapering effects

We shall now investigate these processes in detail.

a) Photon density and saturation

Before we discuss photon density and saturation we have to look at the peak-gain frequency more closely. In terms of the dimensionless parameter ν the dependence of peak-gain frequency on photon number density is given by [6]

$$\nu_{peak} = 2.605776573 - s\,\frac{d\phi(z)}{dt} \tag{7.45}$$

Here $s = N\lambda/\Delta$ is the slippage (as a result of the synchronism condition the optical pulse advances the electron pulse by $N\lambda$ at the end of the wiggler) and ϕ is the phase of the optical pulse. Eq.(7.45) of course, assumes that L is constant and the position of the gain maximum is changing. In our model the gain curve is normalized, ie, the gain peak always occurs at $\nu = 2.605776573$ radians. The normalization of the gain curve necessarily implies the normalization of the effective interaction length L. In other words the change in the peak-gain frequency due to the increase in photon density will be represented by the change in L so that the gain curve always stays the same (normalized). From (7.6) we identify

$$\phi \leftrightarrow 2bt/\omega_0 \tag{7.46}$$

then (7.45) becomes

$$\nu_{peak} = 2.605776573 + \frac{2N\lambda|b|}{c\omega_0} \tag{7.47}$$

Expressing this result in terms of actual frequencies, using (7.27)

$$\omega_0' - \omega_0 = 2.605776573\frac{c}{L_0} + \frac{2N\lambda|b|}{L_0\omega_0} \equiv \frac{2.605776573\ c}{L} \tag{7.48}$$

Here $L_0 \equiv \Delta$ is the initial interaction length and L is the effective interaction length. Therefore L can be written as

$$L = \frac{L_0}{\left[1 + \frac{2N\lambda|b|}{c\omega_0}\right]} \tag{7.49}$$

since $|b|$ contains N_p (number of photons).

$$\text{let } |b| \equiv b_0 N_p \quad \text{where } b_0 \equiv \frac{16\pi^4\alpha_0 K^2 FIcr_0^2(1-\alpha_1)(L^2-\alpha_2 L+\alpha_3)}{\alpha(1+K^2)^2\ e\ \lambda_0^2\ \lambda_w \Sigma} \tag{7.50}$$

where $\alpha_1 \equiv 0.4147222(\lambda_0/L)$, $\alpha_2 \equiv 0.8294\lambda_0$, $\alpha_3 \equiv 0.1719\ \lambda_0^2$

$\alpha_0 \equiv 0.013157$, $\alpha \equiv 137$

thus L becomes

$$L = \frac{L_0}{\left[1 + \frac{2N\lambda b_0 N_p}{c\omega_0}\right]} \tag{7.51}$$

The number of photons N_p is given by a differential equation [6]

$$\frac{dN_p}{dn} = \Delta N + \left(g(N_p) - Q^{-1}\right) N_p \quad , \text{ here } g \equiv |G| \tag{7.52}$$

where ΔN is the increase in the number of photons in the volume element $L\lambda^2$ and can be calculated from the number of transitions per pass for one electron W_T .

$$\Delta N = \rho FL\lambda^2 W_T \tag{7.53}$$

Here ρ is the electron density. n in Eq.(7.52) is the number of passes, Q the loss factor of the optical cavity which for the Stanford oscillator $Q = 35$ corresponding to a 2.8 % loss per pass.

If $g(N_p)$ were a constant the differential equation would have a simple solution of

$$N_p = \frac{\Delta N}{[g(0)-Q^{-1}]} \left[e^{(g-Q^{-1})n} - 1 \right] \tag{7.54}$$

where we assumed the initial condition $N_p(n=0)=0$. But g is not constant, therefore, (7.54) can only be taken as an approximation. Indeed, it is a good approximation if we restrict its validity to the later stages of the start-up (early stages are dominated by Quantum Mechanical effects). When n is small (7.54) indicates a linear growth in photon number, later the growth becomes exponential and then it saturates. Eq.(7.54) can not however account for the saturation effect since it is based on the wrong assumption that g is constant throughout the start-up process. Since the dependence of g on N_p is a very complicated function the only approach to this problem is by way of numerical calculations. We turn (7.52) into a difference equation and include the effect of decreasing $g(N_p)$ iteratively, ie, feed the values of $N_p(n)$ and $L(n)$ into the expression for $g(L(N_p(n+1)))$, namely into (7.51) . As n increases N_p increases according to (7.54), this causes L to decrease (from (7.51)) hence a decrease in $g(L)$ as given by (7.32). As g gets closer to Q^{-1} the exponential growth subsides and eventually becomes zero. This point where $g=Q^{-1}$ is called saturation point and the number of passes required to get to this level of radiation density will be denoted by n_T .

During this growth an oscillating overshoot can occur for the N_p around N_{ps} the average value of the N_p at saturation. This can only happen if$(g-Q^{-1})_{init}$is in the order of unity or larger. This comes about because of the recursive(self-consistent) relation between g and L

which can be better represented as follows

$$L_{n+1} = \frac{L_0}{\left(1 + \frac{2N\lambda b_0(L_n)N_p(n(L_n))}{c\omega_0}\right)} \qquad n = 1,2,3,... \qquad (7.55)$$

Suppose that $g = Q^{-1}$ condition is reached after the n'th pass and let us denote this level of radiation as N_{ps} . In the n+1'th pass $g < Q^{-1}$ since $L_{n+1} < L_n$. Therefore we have an exponentially decreasing N_p at the n+1'th pass. But then after few passes g becomes greater than Q^{-1} again and N_p grows back to saturation level. This oscillatory saturation behaviour was predicted by numerical calculations based on various methods. The utility of our method is that one does not have to write elaborate computer codes to solve a nonlinear differential equation but instead the solution is implicit in the concept of effective interaction length and one has to write only a computer code to follow the evolution of L_n and N_p as a function of n . We have written such a program (Appendix B) and plotted the graph of N_p versus n. Figure 29 shows the low gain behaviour which is the case in Stanford oscillator FEL. The second curve is just to show what happens when the cavity losses increase for any reason or when g is lower than 0.06 (the experimentally observed initial gain in Stanford FEL) . Under such conditions power grows slowly and the saturation level is much lower than Q=35 case. We have also calculated and plotted the situation, in Figure 30, when the initial gain is increased by a factor of 100. To demonstrate the effect we used Stanford FEL parameters but in general such a high gain FEL would require a storage-ring accelerator with very low emittance electron beam. Our model correctly predicts the oscillatory behaviour.

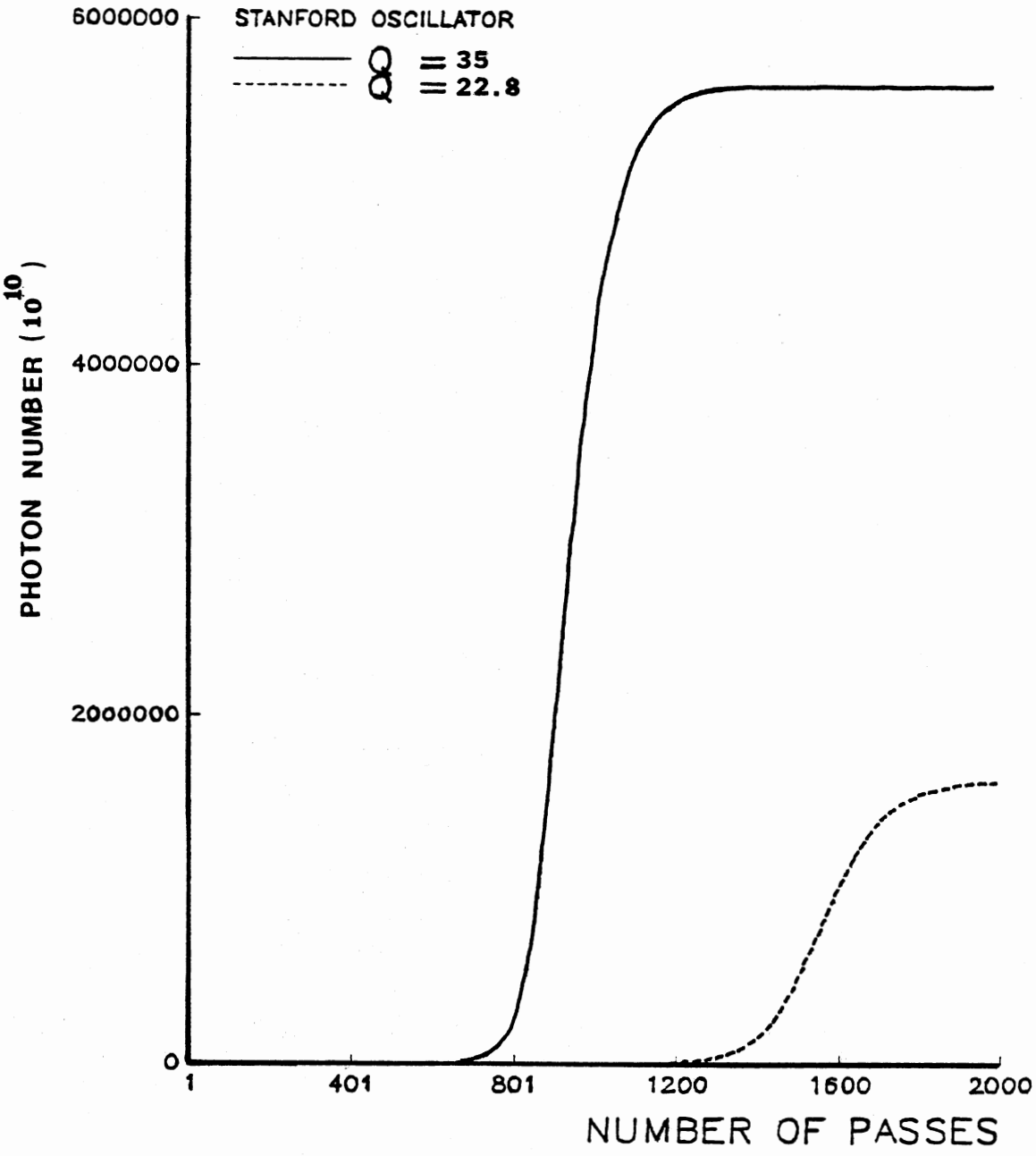

Figure 29. Low gain regime, short pulse effects have not been included.

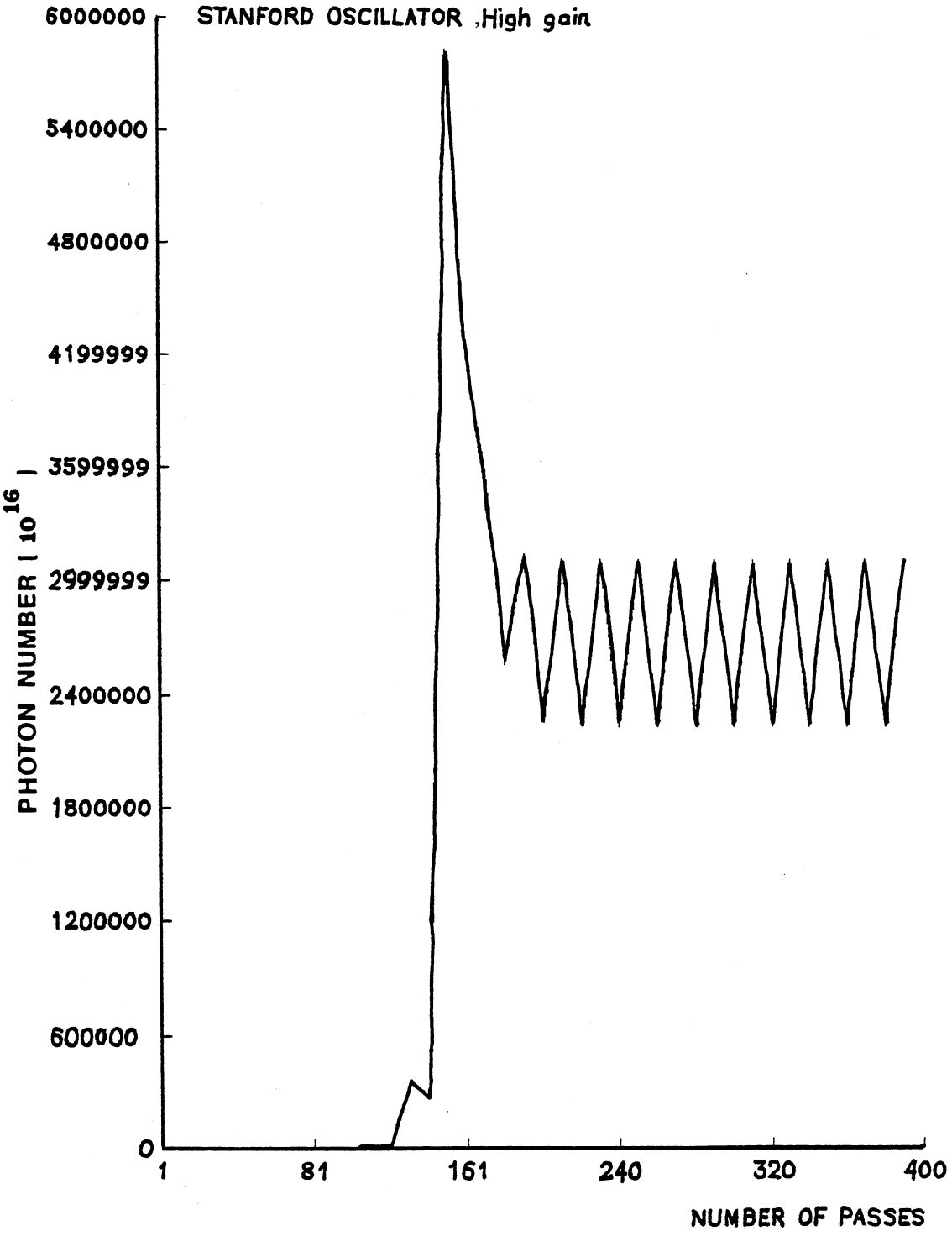

Figure 30. High gain regime, short pulse effects have not been included.

b) Laser Lethargy

So far we have not considered the short pulse effects in our numerical calculations. In a typical FEL like the original Stanford oscillator, electron pulses are 1 mm long as shown in Figure 1 and initially the optical pulselength will also be 1 mm. But as the radiation builds up and coherence is established a chirping develops in the optical pulse and this chirping will cause the optical pulse to be compressed as we explained in the previous section. Now we shall discuss how this change will affect the numerical calculations.

It is obvious that if the optical pulse length changes then ΔN in (7.54) should change because ΔN is proportional to the optical pulselength. Secondly, the loss factor Q should change. Even though Q is mainly a property of the cavity, in the case of pulsed FEL , it also depends on the optical pulselength. Since loss factor is the inverse of the percentage loss of photons per pass, as the optical pulse gets shorter the percent loss should increase proportionally. Therefore Q^{-1} will be modified as

$$Q_{n+1}^{-1} = Q_0^{-1} + [(\delta L_p)_{n+1}/L_0] \tag{7.56}$$

where $(\delta L_p)_{n+1}$ can be calculated from (7.43) .

$$(\delta L_p)_{n+1} = c\sqrt{2\ln 2}\left(\frac{1}{\sqrt{\dfrac{a_n(1+K_\alpha a_n)+K_\alpha b_n^2}{(1+K_\alpha a_n)^2+(K_\alpha b_n)^2}}} - \frac{1}{\sqrt{a_n}}\right) \tag{7.57}$$

$$\cong L_n\left\{\frac{1}{2}K_\alpha a_n\left[-1+(b_n/a_n)^2\right]\right\}$$

As we mentioned above, ΔN Yshould be modified as

$$\Delta N_{n+1} = \Delta N_n (1 - (\delta L_p)_{n+1}/L_0) \tag{7.58}$$

After these effects are included in the numerical simulation we obtained the curve shown in Figure 31. As can be seen, the radiation density grows first and then decreases. This phenomenon which is due to the optical pulse compression is exactly the same thing as the so called Laser Lethargy in the literature. Laser Lethargy is usually explained as the growing of the trailing edge of the optical pulse more than the leading edge due to electron bunching being formed towards the end of wiggler. In this explanation the optical phenomenon of pulse compression is not recognized. Laser Lethargy was thought of being the result of electron dynamics only. What we have shown here is that the Laser Lethargy effect is mostly an optical phenomenon and it can treated as such in the context of pulse-propogation formalism.

c) The amount of desynchronism

It has been experimentally observed that, in the pulsed operation, the saturation level is very sensitive to the variations in cavity length. A slight decrease (desynchronism) in the cavity length L_c was found necessary to obtain the highest saturation level. This sensitivity was explained in the beginning of this chapter. In order to see quantitatively how this desynchronism affects n_T , the number of passes to saturation, and the saturation level N_{ps} , we need to examine its resemblance to slippage. The slippage, as we mentioned before, is the distance which the optical pulse gains over the electron pulse in one transit time. This distance is equal to $N\lambda$ and for short pulses it is comparable to the pulse length. Therefore it is useful to

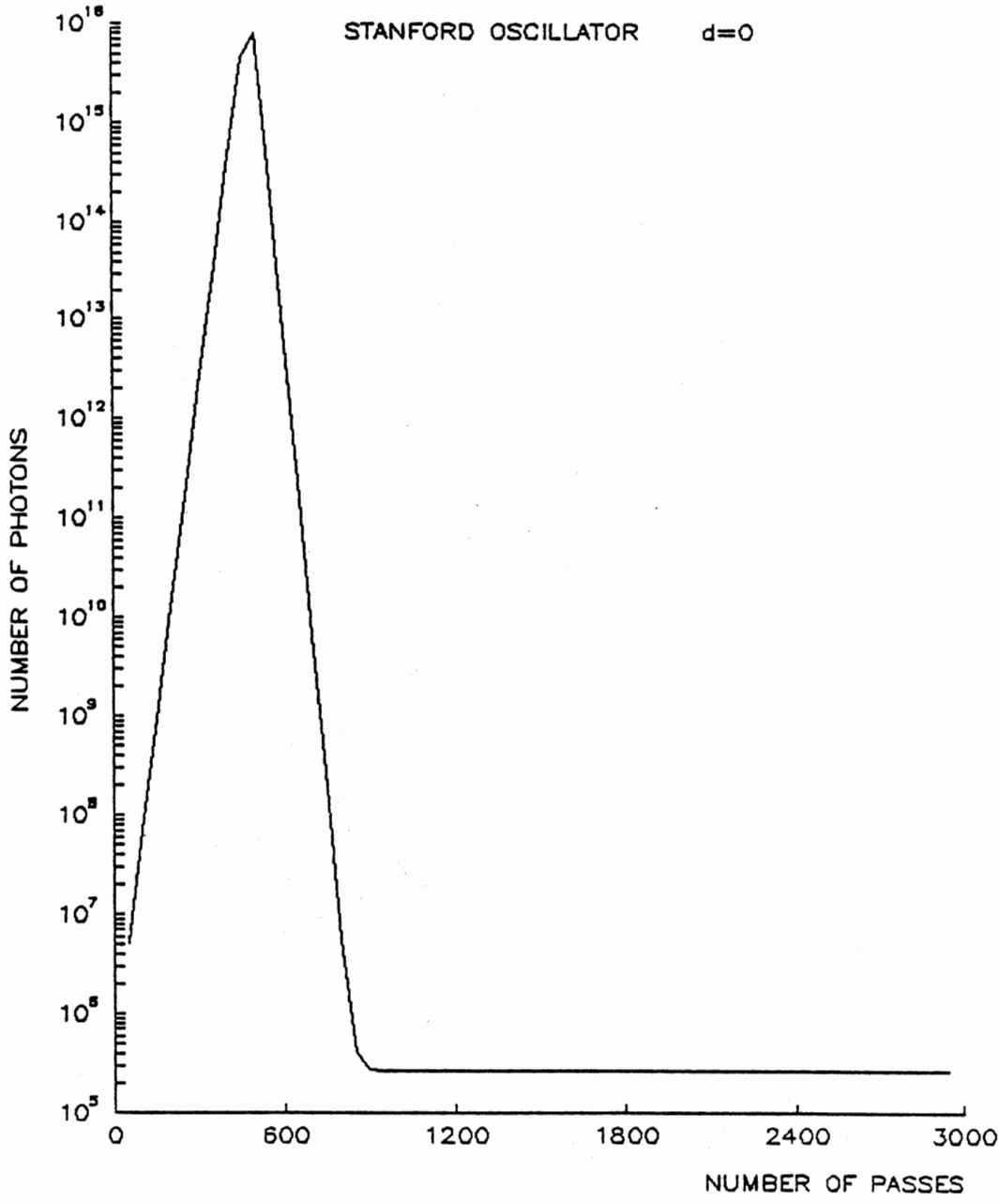

Figure 31. Power evolution under Laser Lethargy effect

normalize this slippage to the original pulse length.

$$s = \frac{N\lambda}{\Delta/2} \tag{7.59}$$

The only effect of slippage s is that all the expressions involving z have to be modified. According to Colson [6], the normalized z_0 has to be replaced by

$$z' = z_0 + s(\tau - \frac{1}{2})\frac{1}{4N^2} \tag{7.60}$$

where τ is the normalized time $\tau = ct/L_w$

The only expression which involves normalized z_0 is (7.42), it will be modified as

$$K_\alpha \equiv 2(2.0603)g(L/c)^2 \left[z_0 + s(\tau - \frac{1}{2})\frac{1}{4N^2}\right] \tag{7.61}$$

At $z = L_w$ and $\tau = 1$

$$K_\alpha \equiv 2(2.0603)g(L/c)^2 \frac{1}{4N^2}(1+s/2) \tag{7.62}$$

Desynchronism is nothing but an additional slippage. By decreasing L_c we are causing the optical pulse to advance the fresh electron pulse before real slippage starts. Let us define this additional slippage as $d \equiv (2\delta L_c/\Delta)$, d stands for desynchronism. We then replace s in (7.60) by $s' = s + 2d$, we have

$$K_\alpha \equiv 2(2.0603)g(L/c)^2 \frac{1}{4N^2}[1+(s+2d)/2] \tag{7.63}$$

The resemblance of d to s also sheds light on its connection to optical pulselength and the loss factor Q . By introducing a desynchronism we are effectively decreasing the Q factor. As the optical pulse gets compressed this loss factor momentarily decreases

because the action of pulse compression is opposed by the action of cavity length detuning(desynchronism). Therefore the Q^{-1} should be further modified as

$$Q_{n+1}^{-1} = Q_0^{-1} + |(\delta L_p)_{n+1}/L_0 - d| \qquad (7.64)$$

The absolute value signs are necessary because $(\delta L_p)_{n+1}/L_0$ can be greater or smaller than d, and in either case Q^{-1} should increase. Initially when N_p is small $\Rightarrow$ $b_n < a_n$ and therefore $(\delta L_p)_{n+1} < 0$. This means that initially there is optical pulse broadening instead of compression. But electron pulselength, during this early evolution stage, is constant, and broadening at this stage will thus cause further loss. Later when $b_n > a_n \Rightarrow (\delta L_p)_{n+1} > 0$, two situations may arise , it can be greater or smaller than $2L_c$. In either case there is additional loss, hence the absolute values. Towards saturation the electron pulse length also changes due to introduction of energy spread by FEL interaction. We shall postpone consideration of this effect to the next section.

It is clear from above discussion that the pulse compression (Laser Lethargy) or counter measures such as desynchronism are relevant only when the initial pulse length Δ is small. In the limit $\Delta \to \infty$ (CW operation) , K_α goes to zero and there is no Laser Lethargy effect and the amount of desynchronism makes no difference. Our numerical calculations are summarized in figures 32, 33 and 34. Figure 32 shows the usual radiation growth curve with different d values. In Figure 33 we plotted the N_{ps} versus d which tells us which d value is the optimum choice. Our theoretical curve is compared with the theoretical curve obtained from Colson. The agreement is very good. This curve

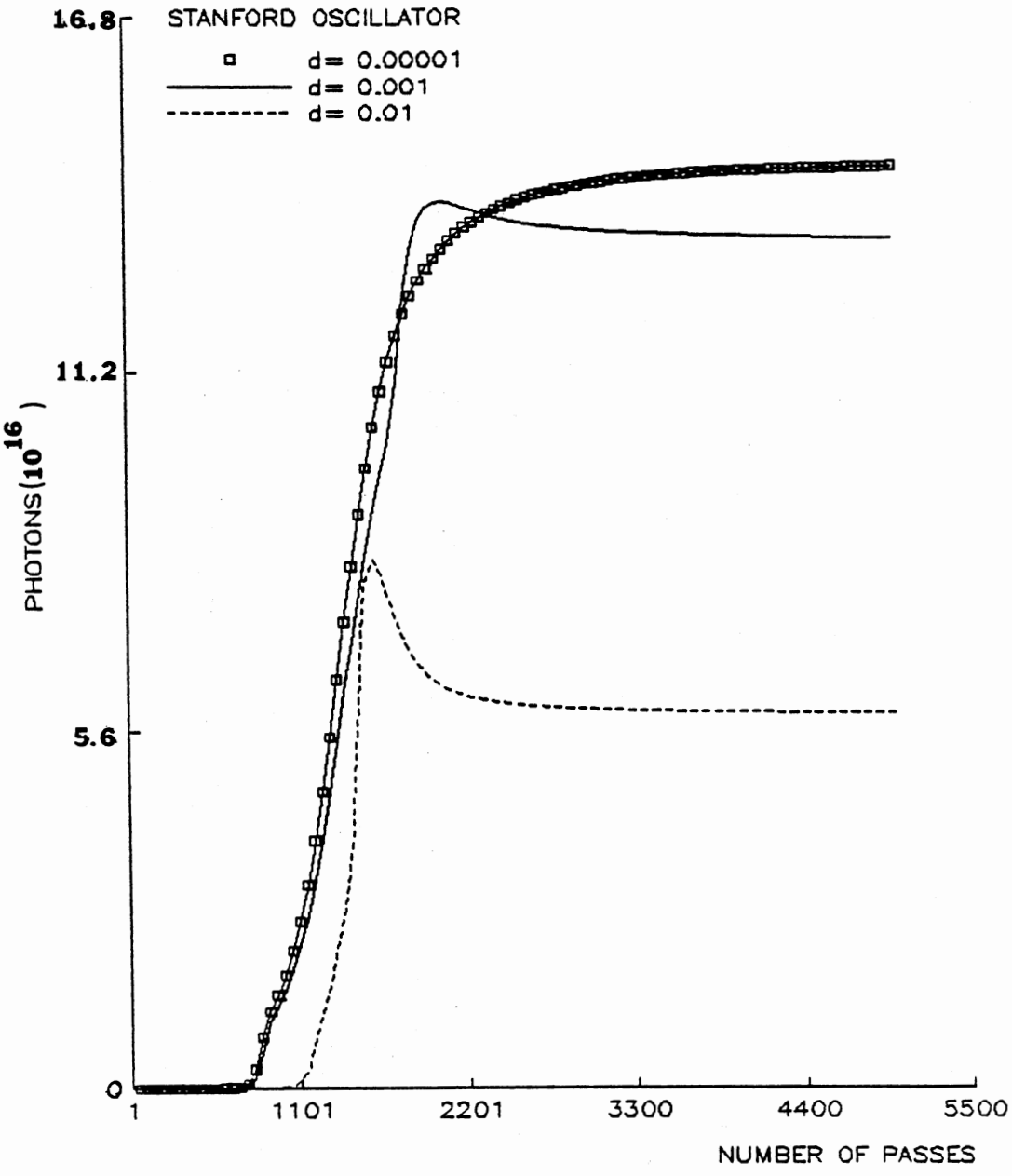

Figure 32. Power growth with different desynchronisms

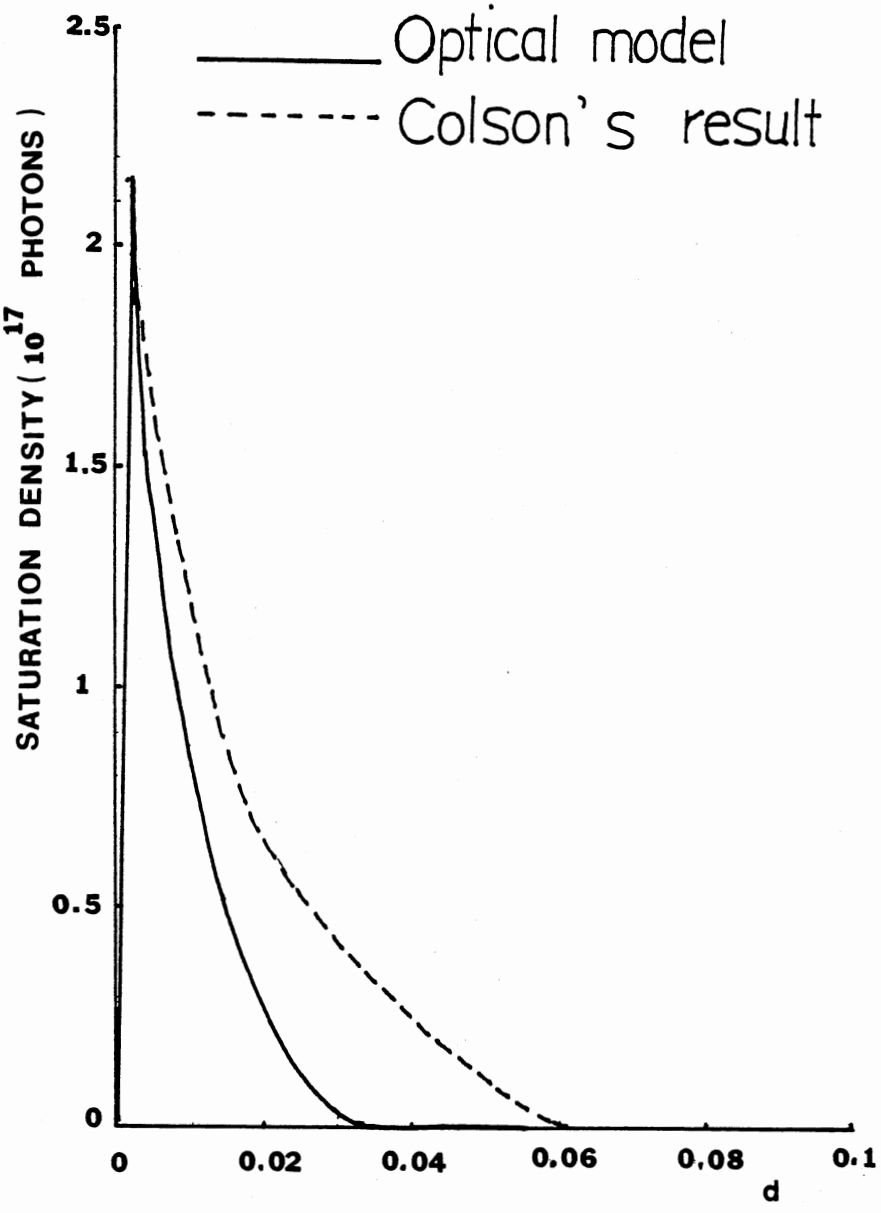

Figure 33. Saturation density versus the amount of desynchronism

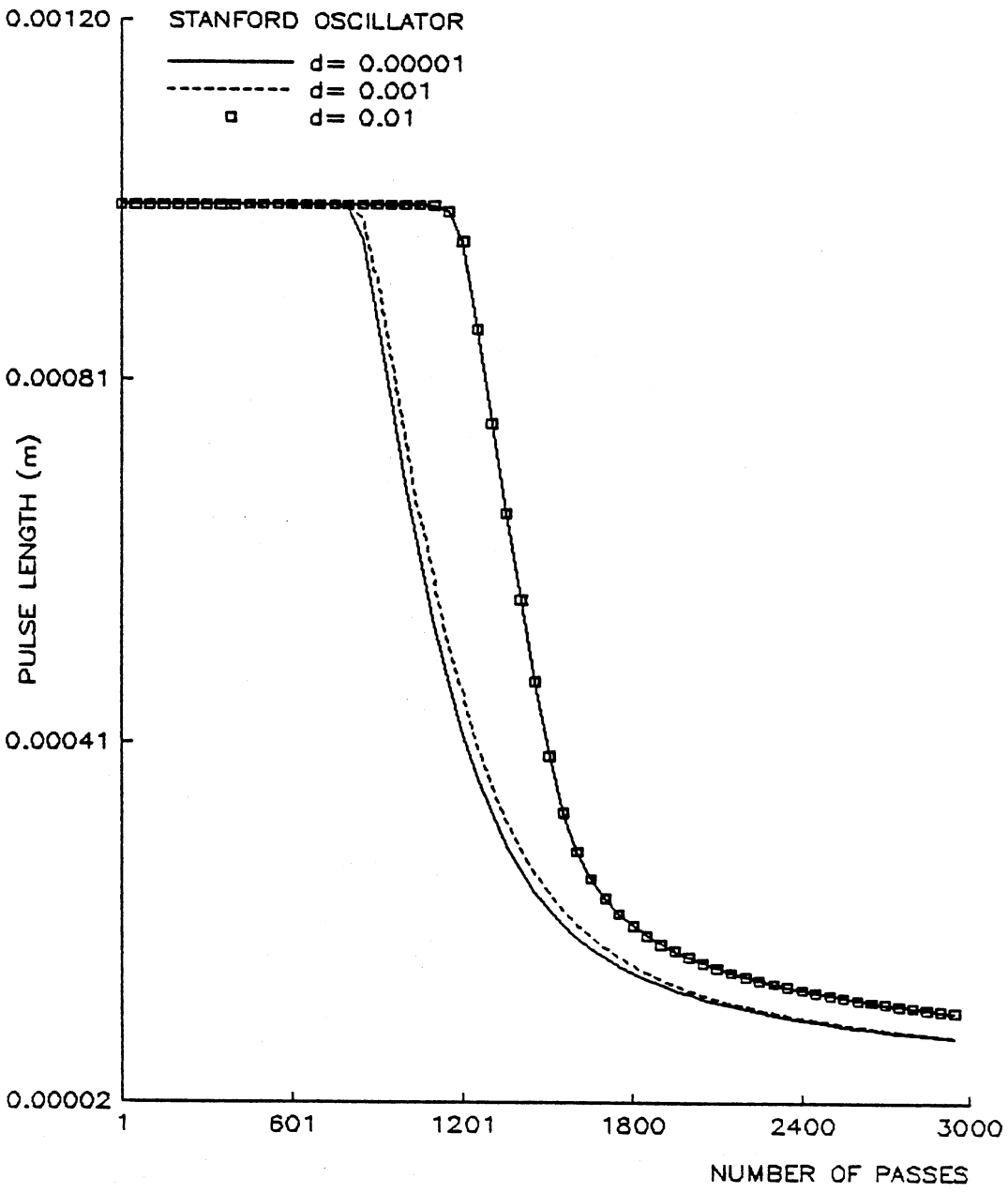

Figure 34. Pulse compression

once again demonstrates the efficacy of our model. The evolution of the optical pulse length is plotted in Figure 34.

d) Inhomogeneous broadening

Until now we have neglected the energy spread and the emittance of the electron beam. A spread in the energy or in the momentum of electrons will introduce a broadening of the emission line. As can be seen from (7.24) the central frequency will be shifted if there is an initial transverse momentum $p_{0\perp}$. $p_{0\perp}$ can also be interpreted as the spread in the transverse momentum and in this interpretation it is related to the emittance ε of the beam.

$$\varepsilon \equiv R\pi \frac{p_{0\perp}}{p_{0z}} \quad \text{rad-m} \tag{7.65}$$

where R is the radius of the electron beam. Usually the emittance of the beam is known from the design of the accelerator . Therefore for a quick estimate of the momentum spread one can determine $p_{0\perp}$ from the numerical value of ε . But for a rigorous analysis one has to consider the distribution functions in the x and y directions.

Assuming a gaussian beam with σ_E , σ_x , $\sigma_{x'}$, σ_y , $\sigma_{y'}$ rms standard deviations ($x' \equiv dx/dz$, $y' \equiv dy/dz$). The distribution function is given by

$$f(E,x,x',y,y') = \frac{e^{-\frac{E^2}{2\sigma_E^2}} e^{-\frac{x^2}{2\sigma_x^2}} e^{-\frac{y^2}{2\sigma_y^2}} e^{-\frac{x'^2}{2\sigma_{x'}^2}} e^{-\frac{y'^2}{2\sigma_{y'}^2}}}{\sqrt{2\pi}\,\sigma_E \sqrt{2\pi}\,\sigma_x \sqrt{2\pi}\,\sigma_y \sqrt{2\pi}\,\sigma_{x'} \sqrt{2\pi}\,\sigma_{y'}} \tag{7.66}$$

now the total spread of the emission line will be [12]

$$\left(\frac{\delta\omega}{\omega}\right)_{TOT} = \left(\frac{\delta\omega}{\omega}\right)_E + \left(\frac{\delta\omega}{\omega}\right)_x + \left(\frac{\delta\omega}{\omega}\right)_y \tag{7.67}$$

where

$$\left(\frac{\delta\omega}{\omega}\right)_E = 2\left(\frac{\delta E}{E}\right) \tag{7.68}$$

$$\left(\frac{\delta\omega}{\omega}\right)_x + \left(\frac{\delta\omega}{\omega}\right)_y = \sum_{u=x,y} - \frac{2\gamma^2}{1+K^2}\left\{\frac{1}{2}u'^2 + \left(\frac{K\pi}{\gamma\lambda_w}\right)^2 u^2\right\} \tag{7.69}$$

the rms width is defined as

$$\left(\frac{\Delta\omega}{\omega}\right)_i = \left(< \left(\frac{\delta\omega}{\omega}\right)^2 > - < \frac{\delta\omega}{\omega} >^2 \right)^{1/2} \tag{7.70}$$

where < > means the average over the input electron distribution (7.66). After a straight forward though lengthy algebra we find

$$\left(\frac{\Delta\omega}{\omega}\right)_{TOT} = \left\{ \left(\frac{\Delta\omega}{\omega}\right)_0^2 + \left(\frac{\Delta\omega}{\omega}\right)_E^2 + \left(\frac{\Delta\omega}{\omega}\right)_u^2 \right\}^{1/2} \tag{7.71}$$

and it turns out that

$$\left(\frac{\Delta\omega}{\omega}\right)_E = 2\sigma_E \tag{7.72}$$

$$\left(\frac{\Delta\omega}{\omega}\right)_u = \frac{2\gamma^2}{1+K^2}\left[\frac{\sigma_u'^2}{2} + 2\left(\frac{K\pi}{\gamma\lambda_w}\right)^2\sigma_u^4\right]^{1/2} \tag{7.73}$$

in terms of the emittance ε

$$\left(\frac{\Delta\omega}{\omega}\right)_u = \frac{2\gamma^2}{1+K^2}\left[\frac{1}{2\sigma_u^2}\left(\frac{\varepsilon}{2\pi}\right)^4 + 2\left(\frac{K\pi}{\gamma\lambda_w}\right)^4\sigma_u^4\right]^{1/2} \tag{7.74}$$

The essential quantities are the ratios of these rms spreads to the homogeneously broadened emission width

$$\mu_E \equiv \left(\frac{\Delta\omega}{\omega}\right)_E \Big/ \left(\frac{\Delta\omega}{\omega}\right)_0 = 2\sigma_E\frac{L_0}{\lambda} \tag{7.75}$$

$$\mu_{x,y} \equiv \left(\frac{\Delta\omega}{\omega}\right)_u \Big/ \left(\frac{\Delta\omega}{\omega}\right)_0 = \frac{\sqrt{2}\,K}{1+K^2}\frac{\gamma\varepsilon L_w}{\lambda_w^2} = R\pi\frac{p_{0\perp}}{p_{0z}}\frac{\gamma L_w}{\lambda_w^2}\frac{\sqrt{2}\,K}{1+K^2} \tag{7.76}$$

Now we are ready to incorporate these inhomogeneous broadening factors into our formulas. Since $(\Delta\omega/\omega)_0$ is given by λ/L_0 these factors can be related to the "effective interaction length". Using (7.71) we obtain

$$\left(\frac{\Delta\omega}{\omega}\right)_{TOT} = \left(\frac{\Delta\omega}{\omega}\right)_0 [1+\mu_E^2 + \mu_x^2 + \mu_y^2\ ]^{1/2} = \frac{\lambda}{L_{eff}} \tag{7.77}$$

therefore

$$L_{eff} = \frac{L_0}{[1 + \mu_E^2 + \mu_x^2 + \mu_y^2\ ]^{1/2}} \tag{7.78}$$

when we combine the inhomogeneous broadening effect with the saturation effect we obtain

$$L_{n+1} = \frac{L_0}{[1+ \frac{2N\lambda b_0 N_p(n)}{c\omega_0}\ ][1 + \mu_E^2 + \mu_x^2 + \mu_y^2\ ]^{1/2}} \tag{7.79}$$

As can be seen from (7.76), $\mu_{x,y}$ are fixed as long as ϵ is constant. In an accelerator, ϵ is strictly constant since it is defined as the phase-space area of the electron beam in the transverse coordinate and Liouville theorem states that the phase-space area of a Hamiltonian system is invariant. μ_E is not constant though. It changes as a result of the introduction of additional energy spread in the FEL interaction. This growth of μ_E is the other reason FEL saturates, the first reason being the saturation mechanism due to the increase in the photon number as we discussed earlier. In fact these two mechanisms of saturation are not totally independent.

From (7.24) one can derive that

$$< \frac{\Delta\gamma}{\gamma} > = < \frac{\Delta E}{E} > = \frac{1}{2}\left(\frac{\Delta\omega}{\omega}\right)_E \tag{7.80}$$

by definition $< \frac{\Delta E}{E} > = \sigma_E$

therefore σ_E given by (7.75) will be proportional to the change in the spontaneous emission linewidth. In other words, μ_E can be written as

$$\mu_E = (L_0/L)\ \mu_{E_0} \tag{7.82}$$

Along with the growth of μ_E , the electron pulselength should also increase as $\Delta' = \Delta\ (L_0/L)$. This is how we include the effects of dynamic energy spread of the FEL interaction in our model. We have calculated these effects numerically for the Stanford oscillator and plotted the growth curve in Figure 35. THe saturation level is lower than the one shown in Figure 32 where we had neglected the inhomogeneous broadening effects.

Equation (7.79) also sheds light on the sensitive dependence of FEL gain on the beam emittance. μ_x and μ_y are proportional to emittance ε . Given the restrictions on γ , λ_w and L_0 (these are the parameters that cannot be changed easily) ε of the accelerator has to be carefully designed as to make $\mu_{x,y} < 1$. If $\mu_{x,y} > 1$ then when squared one obtains even a larger number and the "effective interaction length" L can be severely reduced. Under these conditions the gain may decrease rapidly and FEL can never start. To achieve reasonable saturation densities the accelerator must be carefully designed or modified as to make μ_x and μ_y minimum. This is especially crucial in high-frequency low-gain FEL oscillators.

e) Quantum Mechanical Effects

We have discussed the quantum theory of the FEL operating in the CW regime in great detail in previous chapters. In this chapter we shall only discuss the quantum mechanical effects which are relevant to the

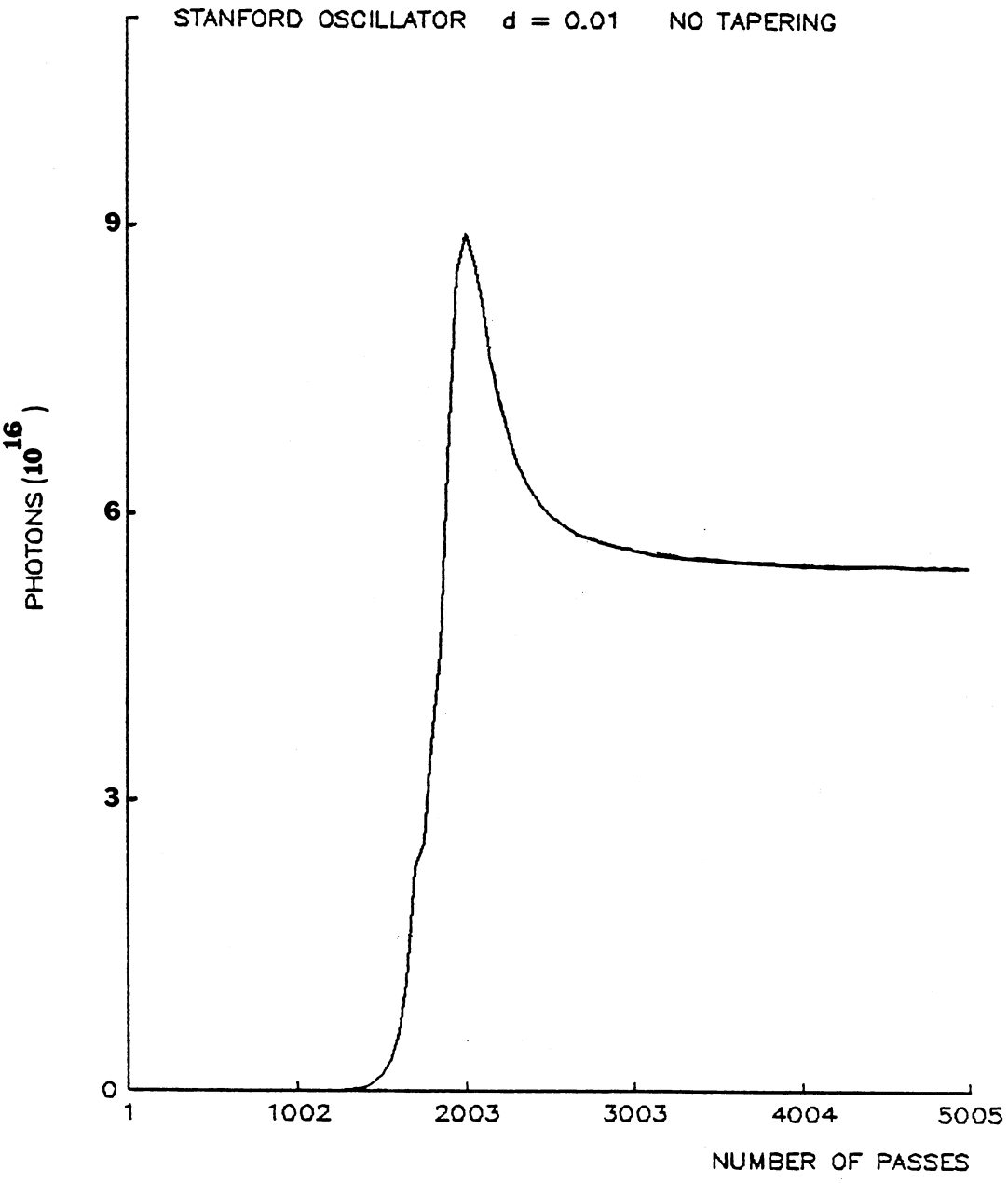

Figure 35. Power growth, inhomogeneous broadening effects have been included.

pulsed-operation.

There are two ways that quantum mechanics can modify the pulsed operation calculations. First, the quantum mechanical corrections to the electron dynamics will indirectly affect the "effective interaction length" through corrections to μ_x , μ_y and μ_E . Secondly, the photon statistics, namely, the photon-number fluctuations during the early start-up phase of the FEL oscillator, will affect every expression that contains N_p . Let us first examine the quantum mechanical line-broadening effect.

In Chapter IV we derived the quantum mechanical correction to the transverse momentum. Even though this correction is small for the Stanford Oscillator we examine its consequences here with an application to high-frequency, E > 1 GeV, FELs in mind. Quantum mechanically broadened relative-linewidth is given by (Eq.(5.48))

$$\left(\frac{\Delta\omega}{\omega}\right) = \frac{\lambda_w}{2L_w}\left\{1 + \frac{2\gamma}{\Delta E}\left(\frac{(m_0c^2)(\hbar ck_w)}{K}\right)^{1/2}\right\} \tag{7.83}$$

this allows us to define a broadening-ratio parameter μ_{QM}

$$\mu_{QM} = \frac{2\gamma}{\Delta E}\left(\frac{(m_0c^2)(\hbar ck_w)}{K}\right)^{1/2} \tag{7.84}$$

therefore (7.79) will be further modified

$$L_{n+1} = \frac{L_0}{\left[1+\frac{2N\lambda b_0(n)N_p(n)}{c\omega_0}\right]\left[1+\mu_E^2+\mu_x^2+\mu_y^2+\mu_{QM}^2\right]^{1/2}} \tag{7.85}$$

in addition to this external modification of the form of the equation, there are inherent changes in μ_x and μ_y due to quantum mechanics. From (7.76) we know that $\mu_{x,y}$ are proportional to $p_{0\perp}$. Here $p_{0\perp}$ refers to the average value of the transverse momentum for the electrons in an

electron beam, not to the initial value of transverse momentum of an individual electron. If we take $p_{1,2x}$ as the average value of quantum mechanical correction to the average transverse momentum then ε in (7.76) should be replaced by

$$\varepsilon = R\pi \frac{(cp_{0\perp}+cp_{1,2x})}{p_{0z}} = R\pi \frac{p_{0\perp}}{p_{0z}} \left(1+ \frac{p_{1,2x}}{p_{0\perp}}\right) \tag{7.86}$$

If ε is such that $\mu_{x,y} << 1$, the effect of $p_{1,2x}$ will be very small even when $\frac{p_{1,2x}}{p_{0\perp}}$ ratio is appreciable because $\mu_x^2+\mu_y^2$ has no effect on L. But if $\mu_{x,y} \cong 1$, such as the case in SXRC FEL, then $\frac{p_{1,2x}}{p_{0\perp}}$ becomes very important. For the SXRC FEL we have the following numerical values

$$\mu_{x,y} = 1.1589773 \text{ (classical)} \quad , \quad \frac{p_{1,2x}}{p_{0\perp}} = 0.133173$$

therefore

$$\mu_{x,y_{QM}} = 1.313321784 \quad , \quad \mu^2_{x,y_{QM}} = 1.7248141$$

which along with $\mu^2_{QM} = 3.0276 \times 10^{-4}$

brings a 4.8% decrease in L. Since gain is proportional to $(L^2-\alpha_2 L+\alpha_3)$ this 4.8% change in L translates into approximately 9.366% decrease in gain. This is a surprising and interesting result since one does not expect quantum mechanical effects to cause drastic changes such as 9.366% decrease in gain. But as we mentioned earlier this result is unique to high energy, x-ray FELs. Quantum mechanical line-broadening and emittance degradation effects can be neglected for the FELs operating in the visible and infrared or microwave regions.

The other aspect of quantum mechanical corrections, namely the photon statistics, is equally important in all types of FELs short or long wavelength, and these effects have macroscopic consequences. This

is due to the extreme sensitivity of gain to photon number fluctuations in the early start-up phase.

There is no solid theory of how much the photon number fluctuates in the FEL. As mentioned by the active researchers in this area [8], [13], [14] there are only conjectures about fluctuations. One such conjecture based on approximate Dirac electron calculations [8] claims that the relative size of the intensity fluctuations in the steady-state (saturation) might be given by

$$\frac{\sqrt{\langle \Delta^2 N_p \rangle}}{\langle N_p \rangle} \sim \frac{1}{\sqrt{N_e}} \tag{7.87}$$

where N_e is the number of electrons in the bunch.
But there is no solid theory, not even a conjecture, as to the magnitude of intensity fluctuations in the early start-up phase. As mentioned by Colson [6] every numerical simulation has to model this behaviour and unfortunately the number of passes to saturation n_T is model dependent. On the other hand, since we know n_T for the Stanford oscillator experimentally ($n_T \cong 1800$), this number can serve as a testing gauge for different models. One tries different models with different photon number fluctuation conjectures and examines which one produces $n_T \cong 1800$

We have already developed a model which we would like to call "the optical model of the FEL". Now we will modify all the expressions containing N_p in order to include the photon fluctuations. We shall assume a dependence of

$$N_{p_{rms}} = N_p \left(1 + \frac{\Delta_{rms}}{N_p}\right) \tag{7.88}$$

for the rms value of N_p . Δ_{rms} is the rms value of the photon number fluctuation. As can be seen from (7.88) the relative importance of

Δ_{rms} will decrease as N_p increases. For the particular case of Stanford oscillator we chose Δ_{rms} = 500000 photons. We arrive at this number by extrapolating (7.87) for the steady-state to the early start-up phase. We substitude (7.88) in the expression for "b", (7.36) and in the expression for "effective interaction length" L, (7.85). This way the gain G and the pulse length L_p will be affected. Gain is further reduced by the uncertainty in λ_0 due to these fluctuations. Gain is inversely proportional to λ_0 as shown in (7.32) and the uncertainty relation for the pulse energy states that

$$\Delta (\hbar\omega_0 N_p)\, \Delta(L/c) > \hbar/2 \tag{7.89}$$

since $\Delta L/c$ is not affected by photon number fluctuations, we conclude

$$\Delta\lambda_0 = \lambda_0(1+RMS) \tag{7.90}$$

where

$$RMS \equiv \Delta_{rms} / N_p \tag{7.91}$$

We implemented this conjecture in our simulation and obtained the curves in Figures 36 and 37.

Figure 36 shows our conjecture with Δ_{rms} = 500000 photons. In Figure 37 we changed Δ_{rms} to 10^6 photons to see how sensitive it was to the change in Δ_{rms}. The number of passes to the saturation n_T in Figure 36 is 1920 which is very close to the experimental value of n_T= 1800 (n_T is defined as the number of passes at which the FEL reaches the saturation density, there may or may not be an overshoot but the first n that corresponds to this photon density defines n_T).

Before we conclude this section, we would like to comment on the effect of quantum mechanics on the optical pulse length. When N_p is small, $(\delta L_p)_{n+1}$ is negative since $b_n < a_n$ in this early stage. This

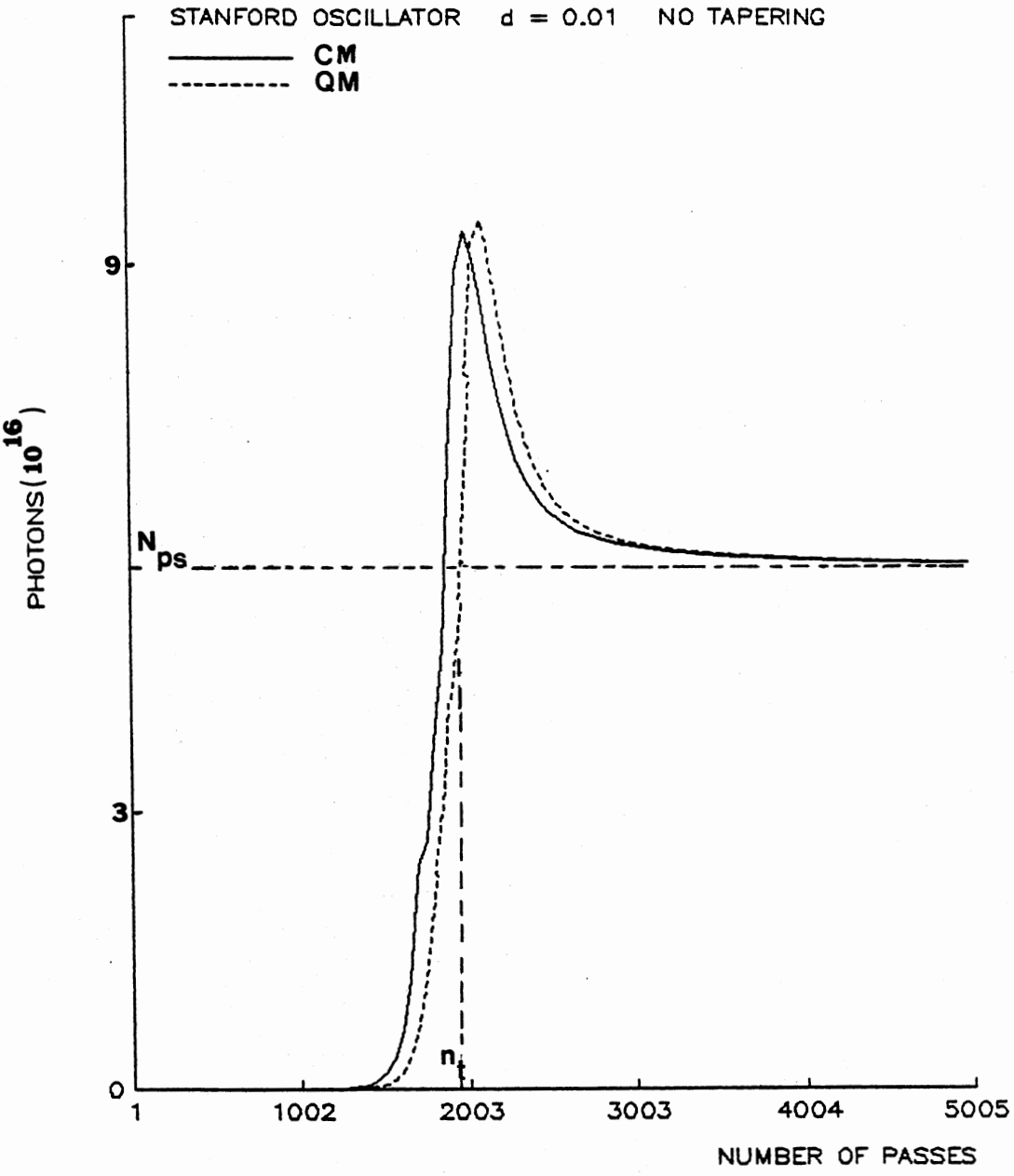

Figure 36. Power growth, all the experimental details including the quantum mechanical effects have been taken into account. $n_t = 1920, N_{ps} = 5.61 \times 10^{16}$, $\Delta_{rms} = 5 \times 10^{5}$

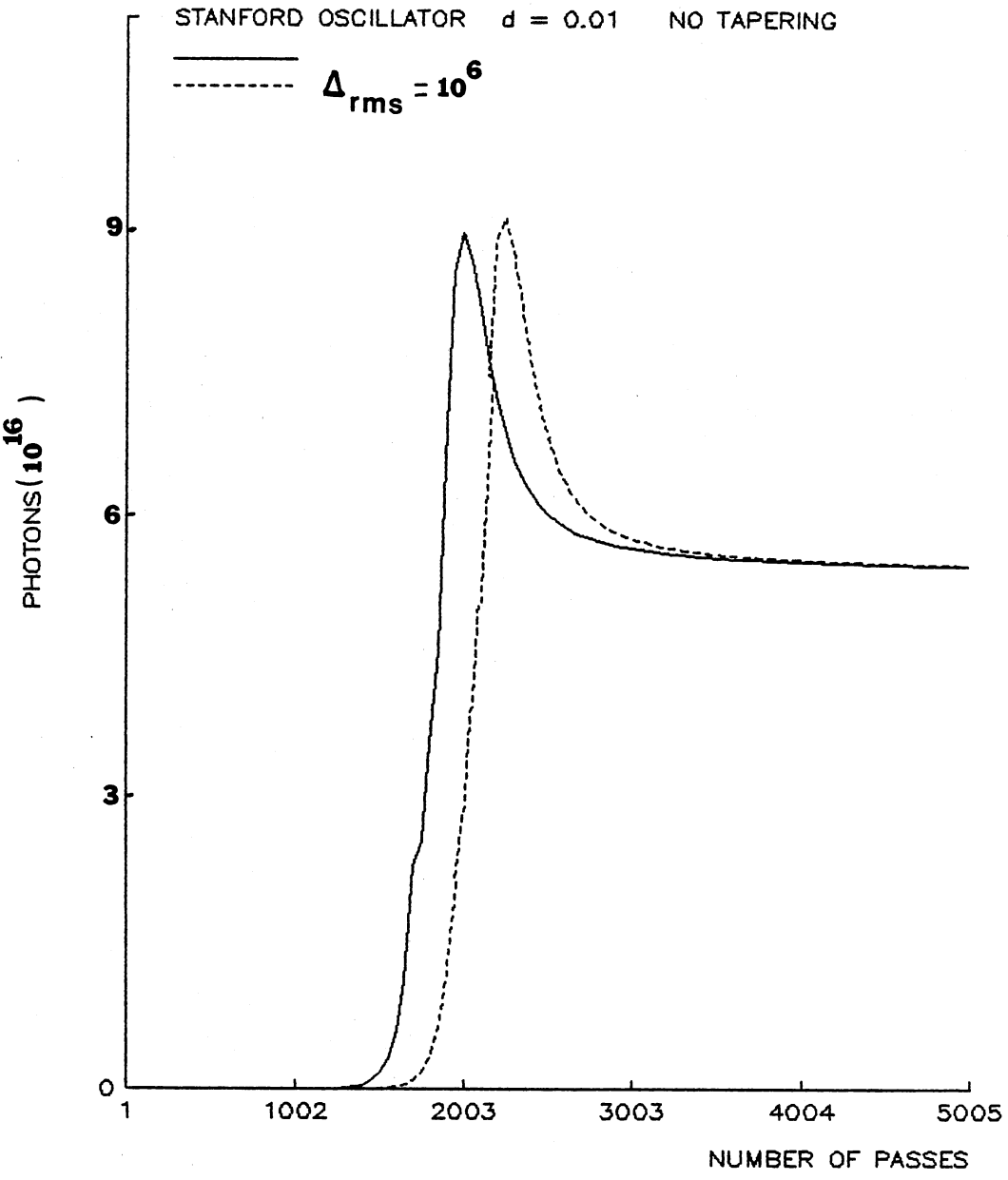

Figure 37. Power growth with $\Delta_{rms} = 10^6$

can be seen from (7.57). Therefore, in the early start-up phase the optical pulselength is slightly broadened instead of shortened. This analytical result is compatible and in complete agreement with the qualitative description of optical pulses in terms of photons as folllows.

Consider a chirped optical pulse whose instantaneous frequency varies with time in the form $\omega_i(t) = \omega_0 + 2bt$, as we have in this chapter. Instead of thinking of this as a single pulse with carrier frequency ω_0 , let us assume this pulse is made up of a number of subpulses, each with a slightly different carrier frequency. Each individual pulse will have zero chirp but since there are different subpulses with different carrier frequencies the overall pulse will exhibit a chirping. Since the individual subpulses have no chirping they will not be compressed in passage through a medium. This picture is equivalent to an optical pulse consisting of photons.

f) Tapering Effects

In order to discuss the effects of tapering on power evolution, optical and electron pulse length we need to go back to (7.34). $(d\omega_0'/dt)$ is now given by

$$\frac{d\omega_0'}{dt} = \frac{2c}{[1+K^2+K_{0\perp}^2+2\gamma_0 K_0+\gamma_0 K_0(\gamma_0/K\mp 1)]} \frac{d}{dt}(k_w\gamma^2) \qquad (7.92)$$

since k_w is no longer a constant but is a function of z-coordinate (hence of time). Here we shall assume a linear-tapering since it is the most commonly employed tapering in experiments including the Original Stanford Oscillator.

$$k_w(z) = k_{w0} + b_t z \qquad (7.93)$$

where b_t is the slope of this tapering. Assuming electrons to be highly relativistic, we can take z = ct then

$$\frac{d}{dt}(k_w\gamma^2) = b_t c\gamma^2 + (k_{w0}+b_t z)2\gamma_0\frac{d\gamma}{dt}$$

$$= b_t c\gamma_0^2 + 2k_{w0}\gamma_0\frac{d\gamma}{dt} \qquad (7.94)$$

then by substituting this in (7.34) and carrying out the algebra we identify

$$b = -16\pi^4\frac{\alpha_0}{\alpha}\frac{K^2F}{(1+K^2)}\frac{r_0(1-\alpha_1)(L^2-\alpha_2 L+\alpha_3)}{\lambda_0^2\lambda_{w0}\Sigma}\frac{Icr_0N_p}{e} + \frac{c^2b_t\gamma^2}{(1+K^2)} \qquad (7.95)$$

The $|b|$ term in (7.49) should thus be replaced by the negative of (7.95). The effective interaction length including all the effects will look like

$$L_{n+1} = \frac{L_0}{\left\{1+\frac{2N\lambda\,(b_0N_p-c^2\gamma^2b_t/\,[1+K^2])}{c\omega_0}\right\}\left\{1+\mu_E^2+\mu_x^2+\mu_y^2+\mu_{QM}^2\right\}^{1/2}} \qquad (7.96)$$

Eq. (7.96) constitutes the core of our so called "the optical model of the FEL". This expression inherently contains all of the FEL dynamics. Only the desynchronism and optical pulse propogation features need to be treated seperately.

In addition to the change in L due to tapering there is also a change in gain G since it is proportional to $k_z(z)$. The change of G with tapering was discussed in detail in reference [10]. For the case of linear tapering we derive

$$G \rightarrow G\left[\frac{k_{w0}+b_tL_w/2}{k_{w0}}\right] \qquad (7.97)$$

We carried out a numerical calculation to investigate the effects of

tapering on power evolution using (7.96) and (7.97). The results are summarized in Figures 38 and 39. As can be guessed from analytical expressions, the Stanford FEL (if k_w is tapered with a 3% slope) reaches saturation at a higher photon density compared to $N_{ps} = 5.618775 \times 10^{16}$ of Figure 36 .

We therefore conclude that the main effect of tapering is not only to increase gain but also to raise the saturation level of the FEL.

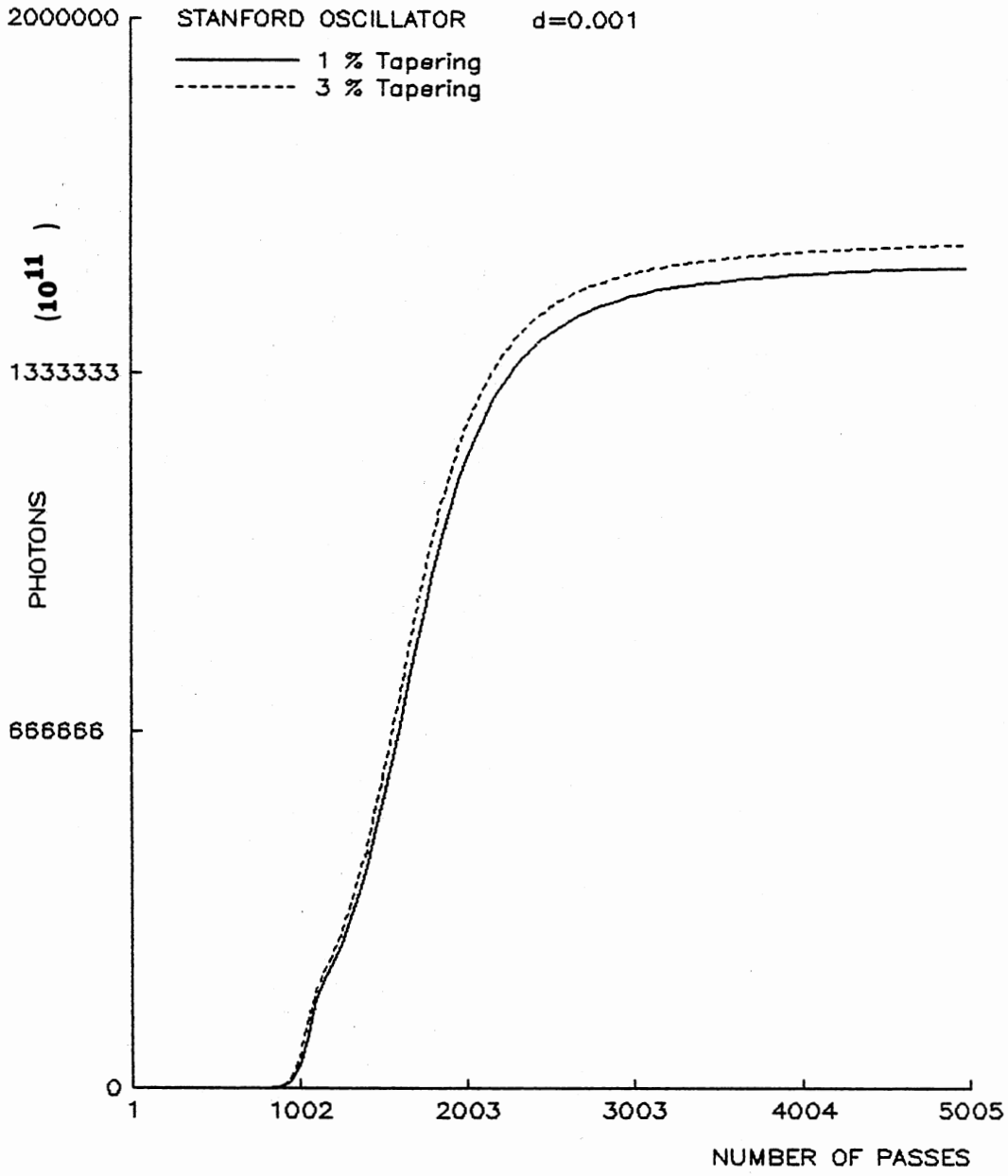

Figure 38. Effect of tapering on power growth

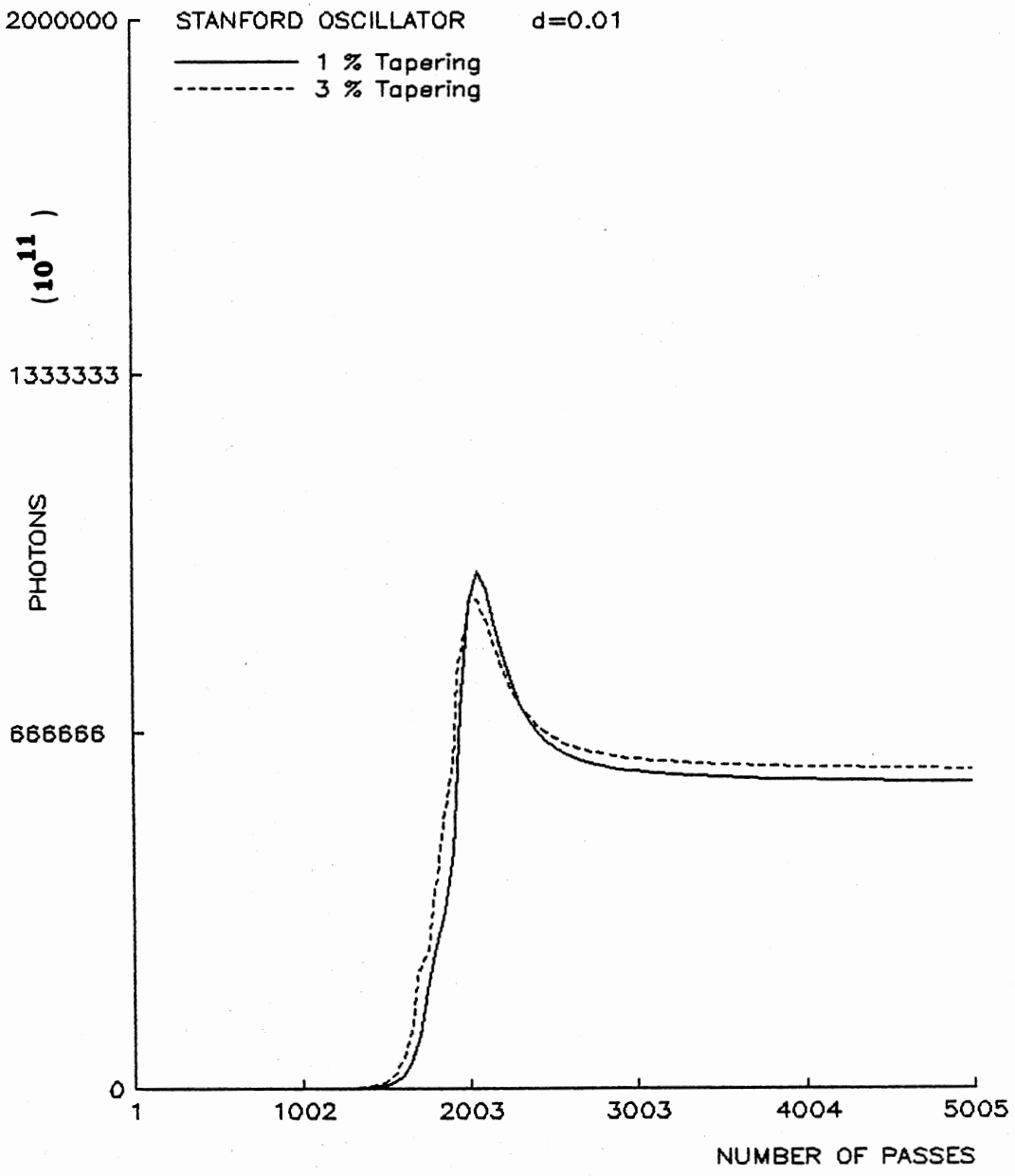

Figure 39. Effect of tapering on power growth

REFERENCES

[1] L.R. Elias and G. Ramian, Phys.Quant.Elec., Vol 9, p:577 (1982).

[2] F. A. Hopf et al, in Phys.Quant.Elec. Vol 7, p:31 (1980). eds: S.F. Jacobs, H.S. Pilloff, M. Sargent (Addison-Wesley).

[3] G. Dattoli et al, IEEE J.Quant.Elec. QE-17, 1371 (1981).

[4] W.B. Colson, Phys.Lett. 64A, 190 (1977).

[5] W.B. Colson and S.K. Ride, Phys.Lett. 76A, 379 (1980).

[6] W.B. Colson, Phys.QuantElec. Vol 7, p:457.

[7] P. Sprangle, C.M. Tang and I. Bernstein, Phys.Rev A, 28, 2300 (1984).

[8] J. Gea-Banacloche, Phys.Rev.A, 31, 1607 (1985).

[9] A.E. Siegman, "Lasers", University Science Books, Mill Valley, Ca. (1986).

[10] S. Saritepe and N.V.V.J. Swamy, Phys.Lett. A113, 69 (1985).

[11] T.C. Marshall, "Free Electron Lasers", p:36 , MacMillan (1985)

[12] G. Dattoli and A. Renieri, in "Laser Handbook Vol 4", page 1. eds: M. L. Stitch and M. Bass (North Holland, New York) (1985).

[13] W. Becker et al, Proc.SPIE Vol 582, p:326 (1985).

[14] W. Becker and M.S. Zubairy, Phys. Rev. A25, 2200 (1982).

CHAPTER VIII

OPTICAL PROPERTIES OF THE FEL RADIATION

Introduction

We have already discussed in previous chapters, some of the optical properties of the FEL radiation. From matrix element calculations in Chapter V we know that the FEL radiation is circularly polarized, the sense of polarization being dependent on the sense of winding of the helical wiggler. We also know the mathematical form of the lineshape of the spontaneous emission but we have not yet discussed the final laser line shape which is much sharper than that of the spontaneous emission and it's properties depend on cavity design but not on electron dynamics. In real FEL systems, diffraction effects play a very important role but since research in this area is currently incomplete we shall not discuss diffraction effects in this chapter, we shall rather concentrate on the photon statistics of the FEL radiation.

Spontaneous Emission

As we mentioned in the lst chapter, spontaneous emission from electrons moving in a wiggler is a synchrotron radiation. As such the angular distribution of the spontaneous radiation can be calculated from classical electrodynamics (Jackson [1]) . Such an analysis specific to electron dynamics in a helical wiggler was given by Kincaid [2]. Figures 40 and 41 describe the results of this calculation. As can be

seen from figure 41, in a strong wiggler most of the radiation is emitted in an off-axis direction and this is not desirable. Therefore in most FEL set-ups K is kept around 0.7 so that the radiation cone is centered on the axis and is very narrow for relativistic electrons.

The expression for the angular distribution of radiated power is [2]

$$\frac{dW}{d\Omega} = \frac{8Ne^2\omega_0\gamma^4}{c(1+K^2+\theta^2\gamma^2)^3} \sum_{n=1}^{\infty} n^2 \left[J_n'^2(x_n)+\left(\frac{\gamma\theta}{K} - \frac{n}{x_n}\right)^2 J_n^2(x_n)\right] \qquad (8.1)$$

where $x_n \equiv \frac{2Kn\gamma\theta}{(1+K^2+\gamma^2\theta^2)}$, $\omega_0 \equiv 2\pi\beta c/\lambda_w \cong ck_w$

and $J(x_n)$ is the Bessel function. All the other parameters are same as defined in previous chapters.

Coherence

From a classical point of wiew, coherence in a radiation can be understood in terms of a phase distribution which is well correlated over large transverse and longitudinal distances. We can define a "coherence-length" measured in the direction of propagation

$$l_c = \frac{\lambda^2}{\Delta\lambda} \qquad (8.2)$$

where λ is the wavelength of the emitted radiation and $\Delta\lambda$ is the bandwidth. Eq.(8.2) defines the "longitudinal coherence". One can also define a "transverse coherence" as the radiation satisfying the following condition.

$$d\,\theta = \frac{2\lambda}{\pi} \qquad (8.3)$$

where d is the $1/e^2$ diameter at the waist of the radiation beam and θ is the $1/e^2$ divergence-half-angle (the radiation beam is assumed to

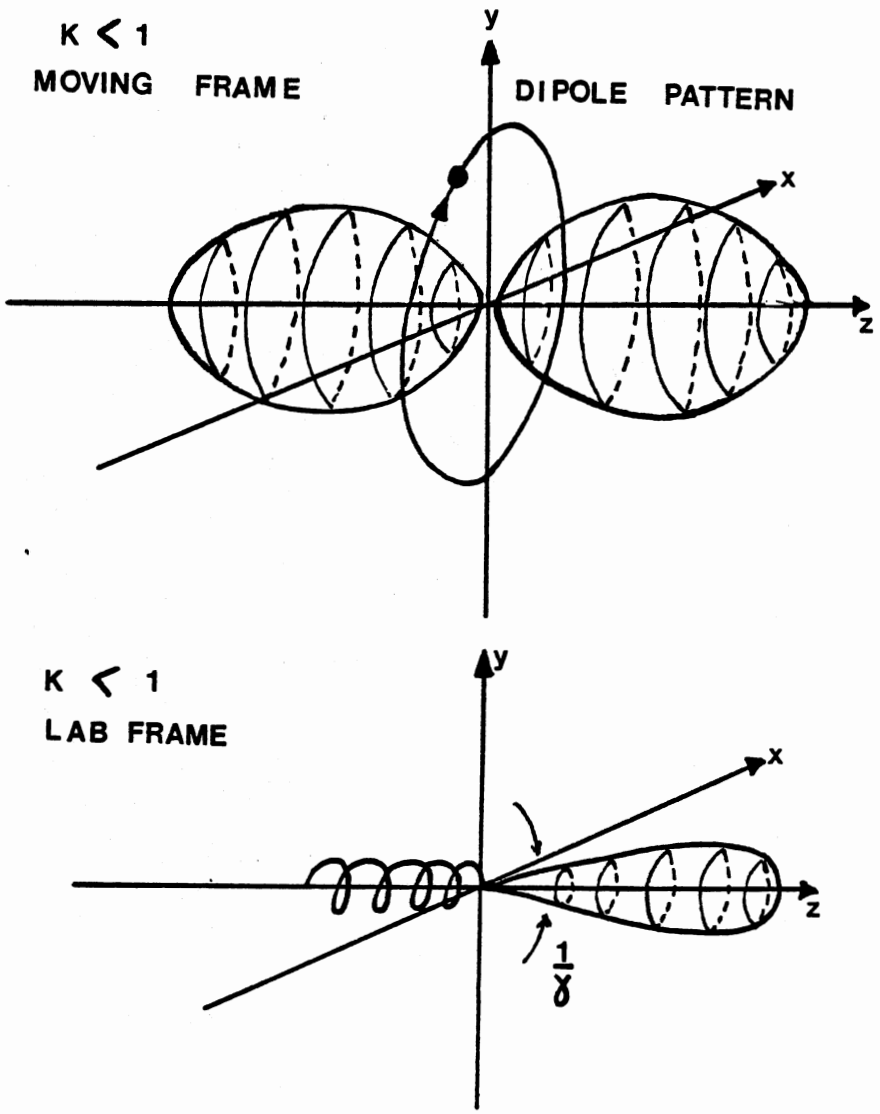

Figure 40. Radiation pattern produced in a weak wiggler field

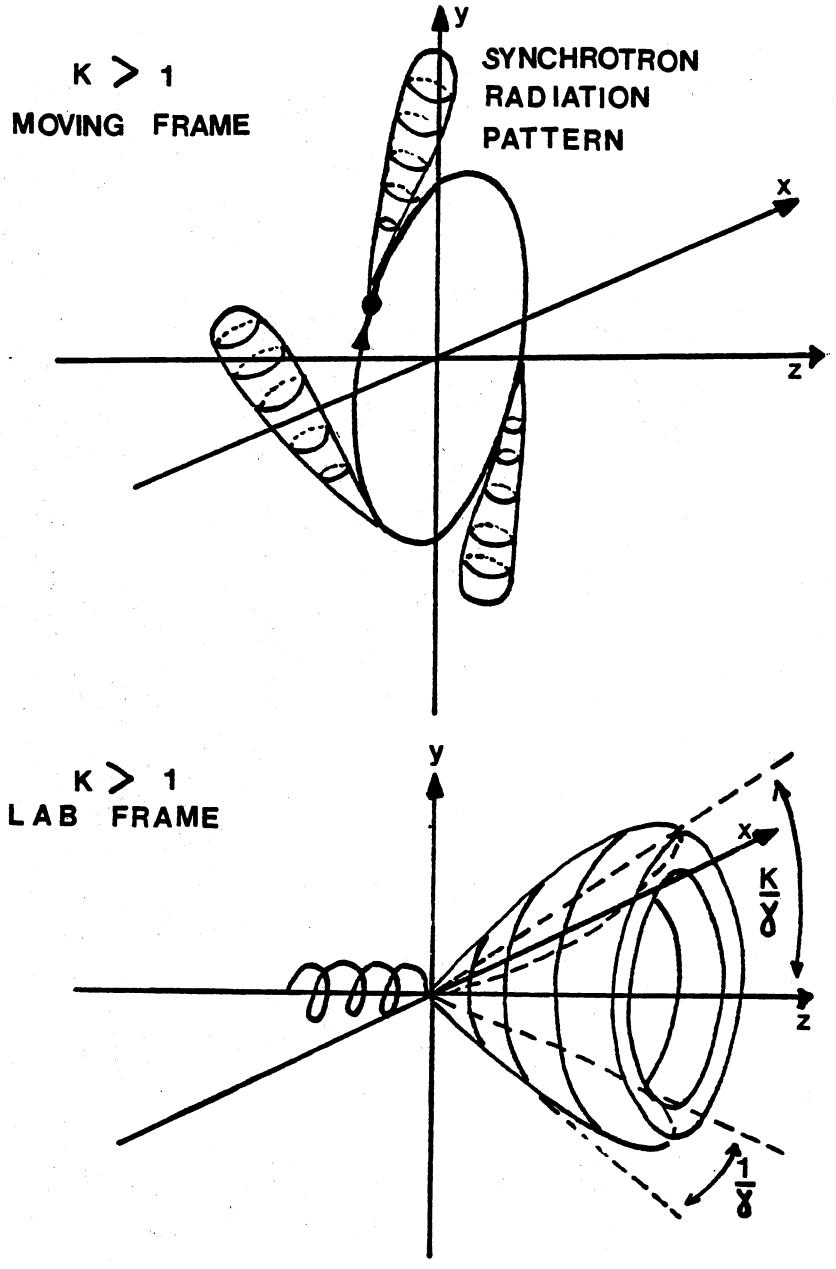

Figure 41. Radiation pattern produced in a strong wiggler

have a Gaussian transverse intensity distribution). Such a radiation beam is said to be "diffraction-limited" and it has near perfect phase front and can be focused to the smallest possible spot-size. Another name for such a condition in radiation is "full-spatial coherence". Ruby laser when its optical cavity is designed to allow only one axial and one transverse (TEM_{00}) mode generates ligth near perfect full-spatial coherence. We cannot claim the same thing for FEL radiation. As we shall see shortly, FEL radiation exibits very good "temporal coherence" in that it's linewidth is reasonably narrow , in other words the coherence length l_c is quite long ($\sim N\lambda$) but the "spatial coherence" is poor. This can be improved by using wider or broader electron beams but then electron dynamics spoils the spatial coherence since it is not easy to design a wiggler in which the field amplitude is uniform over the transverse plane. In the short wavelength (x-ray, vuv) FELs there are no mirrors therefore no mode control resulting in a radiation beam which is only "partially coherent". In passing we would like to point out that even an atomic laser generating x-ray or vuv wavelengths would also radiate partially coherent light because in this region of the electromagnetic spectrum coherence is limited by the quantum nature of light. As the wavelength decreases, individuality of photons dominate the pysical processes and coherence by definition is limited.

Fortunately there are various filtering mechanisms available to improve the coherence of a "partially coherent light". One such mechanism would be to send this "partially coherent" light through a dispersive element such as crystal monochromator or grating of high resolving power to narrow the linewidth (at a cost of losing some of the

flux) and then through a lens-pinhole spatial filter in which higher order spatial frequencies (noise) are removed. This mechanism is illustrated in Figure 42.

Before we move on to photon statistics of the FEL radiation we need to explain the line-narrowing that occurs as the optical power inside the FEL cavity grows. Figure 43 shows the line-narrowing in the original Stanford Oscillator. This is basically a classical process and easy to explain. Since the peak of the gain curve occurs at a lower frequency than the peak of the spontaneous emission line-shape curve in an FEL this lower frequency will be amplified instead of the central frequency. The photons with other frequencies will be lost due to losses in the cavity and as a result the final lineshape curve will be one order of magnitude narrower than the spontaneous emission curve and centered on a lower frequency (higher wavelength). Recall that the gain-peak frequency shifts towards lower frequencies continously as the radiation intensity grows so the final frequency that the FEl settles on depends on the saturation level of the FEL radiation. As we discussed in Chapter VII the final frequency will be given by

$$\omega_{final} = \omega_0' - 2.6\ (c/L) \tag{8.4}$$

where ω_0' is the central frequency of spontaneous emission and L is the final effective interaction length. The final FEL linewidth is given by [3]

$$(\Delta\omega)_{FEL} = 0.27\pi \frac{[R + S(\hbar\omega/4\pi)(e^{\hbar\omega/kT} - 1)^{-1}]\frac{c}{L_c}}{P} (\Delta\omega)_{cavity} \tag{8.5}$$

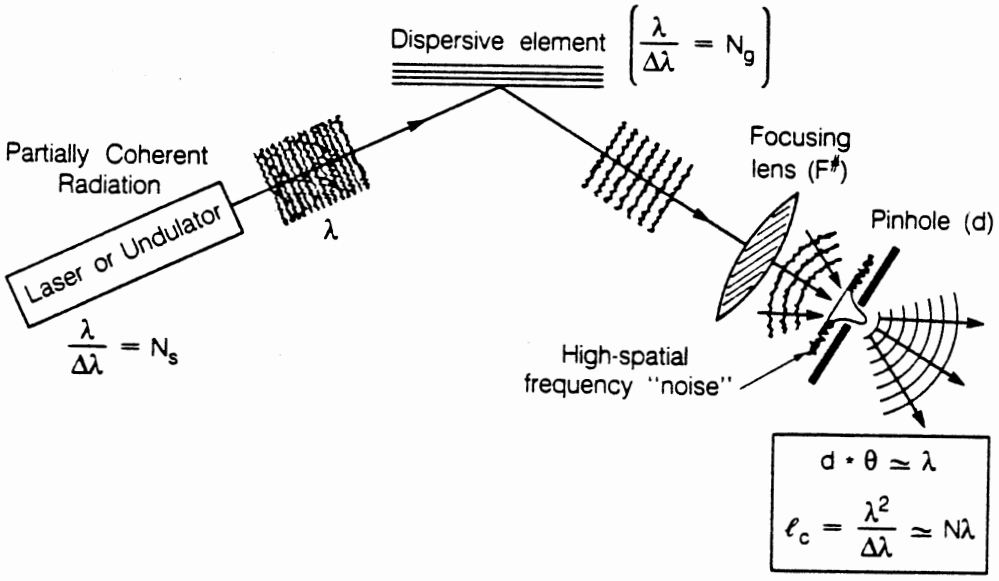

Figure 42. Filtering of partially coherent light

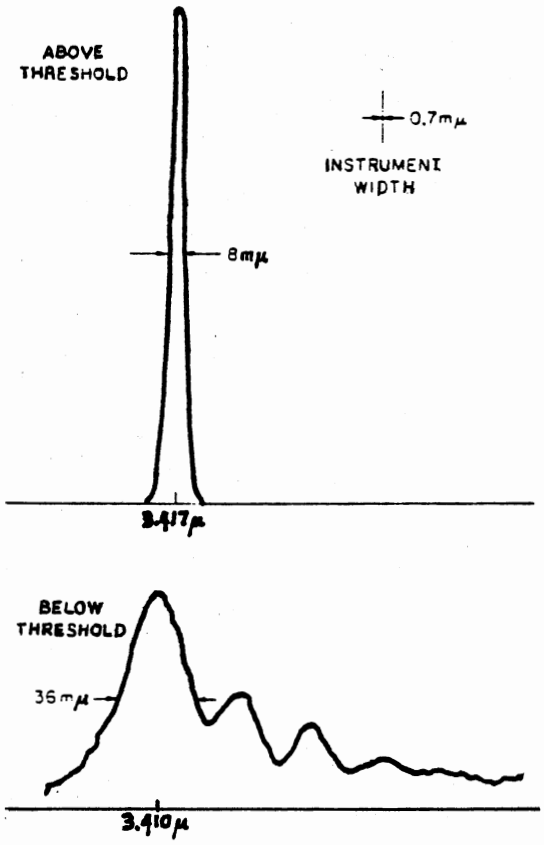

Figure 43. FEL line-narrowing

$$\text{where} \quad R \equiv \frac{1}{8\pi} I_0 e \frac{L_w^2}{A} \frac{K^2}{\gamma^2} \quad , \quad S \equiv \pi \frac{I_0 e}{m_0 c^2} \frac{L_w^3}{A\lambda_w} \frac{K^2}{\gamma^3} \tag{8.6}$$

Here L_c is the cavity length, I_0 is the peak beam-current, A is the effective cross-sectional area of the light beam, P is the total power in the oscillator. Compare this to the Schawlow-Townes formula for atomic lasers [4]

$$(\Delta\omega)_{\substack{\text{atomic} \\ \text{lasers}}} = 2\pi\hbar\omega \frac{(\Delta\omega)^2_{\text{cavity}}}{P} \frac{N_2}{\Delta N} \tag{8.7}$$

where N_2 is the upper level population and $\Delta N = N_2 - N_1$ is the population inversion at lasing threshold. For visible atomic lasers $(\Delta\omega/\omega)$ can be as low as 10^{-6} but $(\Delta\omega/\omega)_{FEL}$ given by (8.5) is usually in the order of 10^{-3}. A single mode, CW FEL would produce a relative linewidth of $10^{-5}$and a high average power compared to atomic lasers. The possibility of such an FEL was demonstrated by Elias [5] and is currently under development. As for the pulsed-FELs the intrinsic linewidth is determined by the electron pulse shape and length and may never exceed 10^{-3}(relative linewidth) therefore pulsed-FELs will not exhibit high degree of coherence. As a final note we would like to add that the FEL linewidth given by (8.5) is called the intrinsic linewidth and in reality may never be realized due to various inhomogeneous broadening processes.

Coherence From A Quantum Mechanical Point Of View

The intrinsic linewidth that was derived classically in reference [3] can also be derived quantum mechanically [6] [7]. The quantum mechanical expression for the intrinsic linewidth will be

$$\left(\frac{\Delta\omega}{\omega}\right)_{FEL_{QM}} = \frac{1}{2}\left(\frac{\omega}{Q}\right)^2 \frac{1}{P}\frac{2(\Delta E)}{\pi} \tag{8.8}$$

Here Q is the Q-factor of the cavity and ΔE is the energy acceptance of the FEL resonance.

$$\Delta E = \frac{1}{4N}\gamma m_0 c^2 \tag{8.9}$$

The most important fundemental difference between FELs and the atomic lasers is that in the FEL, light is not emitted by transitions between discrete energy levels but rather by transitions from one continuum level to another continuum level. We have also seen that FEL light is also different from atomic laser light in that FEL linewidth is much larger and therefore the 1st order coherence (spatial and temporal) properties poorer than that of atomic lasers. It is well known that a monochromatic (filtered) light from a thermal source, even it be made identical to a laser light as far as temporal coherence is concerned, would still differ in its "2nd order coherence" properties; in particular it's photon statistics would be different. In order to assess the uniqueness of the FEL radiation we therefore need to examine the photon statistics of the FEL radiation.

The probability of finding n photons in the radiation field (ie, the probability of the system being in state $|n\rangle$) is given by

$$P_n = \frac{\bar{n}^n}{(1+\bar{n})^{n+1}} \tag{8.10}$$

for a thermal source, and by

$$P_n = \frac{e^{-\bar{n}}\,\bar{n}^n}{n!} \tag{8.11}$$

for a laser well above the threshold. Equation (8.11) is commonly called the Poisson distribution. The difference between a laser light

and a thermal light can be best demonstrated by the expressions for intensity fluctuations. If one defines

$$\Delta n = [\langle n^2 \rangle - \langle n \rangle^2]^{1/2} \tag{8.12}$$

as the intensity fluctuation then one can obtain

$$\Delta n_{thermal} = \left(\frac{1}{n^2} + \bar{n}^2 \right)^{1/2} \tag{8.13}$$

$$\Delta n_{laser} = \sqrt{\bar{n}} \tag{8.14}$$

The derivation of the photon number distribution and the intensity fluctuation for a real FEL (emittance, diffraction, etc. effects included) from a fully quantum mechanical and complete theory still remains to be done at the moment but there are few calculations based on a hypothetical, CW, single-mode FEL.

The first expectation [8] was that the FEL light would exhibit a Glauber coherent state [9]. The Glauber coherent state is defined as the state $|\alpha >$ that gives a probability of finding n photons in the cavity, $P_n = |\langle n|\alpha >|^2$, with $\bar{n} = |\alpha|^2$, which reduces to the expression given in (8.11) (Poisson distribution) when $\bar{n}$ is large. It was shown later [10] [11] however that an electron in an FEL radiates a coherent state only if the quantum recoil is neglected but then the gain is identically zero. A semiclassical analysis [11] concludes that the FEL light exhibits a bunched photon statistics namely $\Delta n > \sqrt{\bar{n}}$ therefore the intensity fluctuations are larger compared to that of atomic lasers. The quantitative expression for Δn for an FEL operating in the steady-state (saturation) was derived [12] based on 1-D approximate solutions of Dirac equation for the motion of electrons. It

is as follows

$$\Delta n = \frac{1}{2q} \left\{ \frac{N_e(\langle\mu^2\rangle - \langle\mu\rangle^2)/2}{1+\frac{N_e}{2q}\frac{d}{dn}(\langle\mu\rangle-\mu_0)} \right\}^{1/2} \tag{8.15}$$

where $$q \equiv \frac{\hbar c k_w}{\gamma_0 m_0 c^2} \tag{8.16}$$

and μ is defined as

$$\gamma\, m_0 c^2 = \gamma_0 m_0 c^2 \left(1+\frac{\gamma_0^2 \mu}{k}\right)$$

here ω and k are the angular frequency and wavenumber of the laser light, N_e is the number of electrons and $\mu_0 = 2.6$

As a conclusion we can say that FEL radiates a state that has larger intensity fluctuations than the coherent state ($\Delta n > \sqrt{\bar{n}}$) and does not approach a coherent state as the laser is brought higher and higher above threshold, unlike the conventional laser.

REFERENCES

[1] J.D. Jackson, "Classical Electrodynamics", p:671, Wiley (1975).

[2] B.M. Kincaid, J.App.Phys. 48, 2684 (1977).

[3] A. Gover et al, Phys.Rev A35, 164 (1987).

[4] A.L. Schawlow and C.H. Townes, Phys.Rev, 112, 1490 (1958).

[5] L.R. Elias et al, Phys.Rev.Lett., 57, 424 (1986).

[6] W. Becker et al, Phys.Rev, A33, 2174 (1986).

[7] M. Orszag, Phys.Rev. A36, 189 (1987).

[8] R. Bonifacio, Opt.Comm. 32, 440 (1980).

[9] R.J. Glauber, Phys.Rev. 84, 395 (1951).

[10] G. Dattoli et al, Opt.Comm. 34, 240 (1980).

[11] W. Becker and M.S. Zubairy, Phys.Rev A25, 2200 (1982).

[12] J. Gea-Banacloche, Phys.Rev. A33, 1448 (1986).

CHAPTER IX

SUMMARY AND CONCLUSIONS

We have developed a 2-Dimensional Quantum theory of the Free Electron Laser based on the solutions of Dirac equation for the motion of an electron moving in various wiggler geometries. In other words we examined the inclusion of transverse momentum effects right from the beginning . The research presented in this thesis can be divided into three parts. First the derivations of 2-D solutions for the Dirac equation in three different wiggler geometries, uniform wiggler, tapered wiggler and the combined field of a wiggler and an axial guide field.

The second thrust area of this thesis was the calculation of matrix elements, transition rates, frequencies and gain using the Dirac solutions and the perturbation theory. We have shown that a Dirac theory of the FEL predicts interesting effects that cannot be explained by the classical theory.

Third part is the development of an optical model for the FEL interaction. This model incorporates most of the FEL electron dynamics into a parameter called the "effective interaction length". Then the physics of the FEL interaction is reduced to a pulse propagation problem. Using the already developed techniques of pulse propagation theory we were able to follow the evolution and growth of the optical pulse in an FEL and be able to explain "Laser Lethargy" and other short pulse effects and predict the rise-time of the FEL oscillator correctly.

The utility of this model is that the nonlinear problem of intensity growth and saturation is handled numerically without having to tackle a troublesome nonlinear differential equation . Numerical algorithm involves only iterative computations.

Now we would like to summarize our results chapter by chapter.

In Chapter I, we gave a general introduction to Free Electron Lasers and presented the simplest classical gain calculation for later discussion.

In Chapter II, we demonstrated the importance of the accelerator characteristics on the performance of the FEL. We have shown that the requirements for an FEL interaction, i.e., high current density and small energy spread in the electron beam are conflicting when one considers the properties of storage-ring accelerators. Therefore one has to optimize or redesign the storage-ring accelerators for an FEL operation. We have also reported in this chapter the development of a classical FEL theory based on the analogy between electron dynamics in an rf-cavity and the ponderomotive potential.

In Chapter III we have presented the preliminaries of the quantum theory of the FEL and laid out a plan for the formulation of a Dirac theory of the FEL. We have mentioned some of the calculational difficulties and examined the validity of using lst order perturbation theory even though the FEL interaction is dominated by higher-order processes.

In Chapter IV we presented our derivation of the 2-D solutions of the Dirac equation for a uniform helical wiggler and also for a tapered wiggler. The solutions can be written in terms of the closed form expressions containing Mathieu functions of fractional order. This

derivation revealed that there is a nonnegligable quantum mechanical correction $p_{1,2x}$ to the classical transverse momentum (ea/c) . This correction is proportional to γ and therefore becomes more important for short-wavelength (x-ray, vuv) FELs which use electron energies with $\gamma > 10^3$. We also demonstrated that these 2-D solutions are consistent with previously derived 1-D Dirac solutions and the free-particle Dirac-spinors.

In Chapter V, we have calculated the matrix elements, transition rates, frequencies and gain for a uniform wiggler FEL using the 2-D Dirac solutions derived in Chapter IV. Our conclusions are as follows:

a) Dirac theory predicts four different frequencies whereas the classical theory claims one single frequency for the on-axis emission in helical-wiggler-FELs.

b) Emitted radiation is circularly polarized.

c) Expressions for these four frequencies contain terms of quantum mechanical origin in their denominators. The quantum recoil term is proportional to γ and thus smaller than $p_{1,2x}$- effect which is proportional to γ^2 in the same denominator.

d) 2-D Dirac theory of the FEL predicts that the so-called "first-harmonic" which is the frequency generated by down-spin electrons making a transition to another momentum state and flipping to up-spin, is more prominent than it was predicted by 1-D Dirac theory. Therefore a spin-polarization mechanism is possible for SCL type accelerators by utilizing various helical wiggler magnetic field geometries.

e) Due to quantum mechanical transverse momentum effects the width of the spontaneous emission lineshape is broadened and the centers of $\uparrow\uparrow$ and $\downarrow\downarrow$ lineshapes are seperated slightly.

f) Due to the same transverse-momentum effects, gain is decreased. The gain depreciation can be as high as 10% in x-ray FELs (such as the SXRC FEL).

g) In general, the quantum mechanical transverse momentum effects are γ times larger than the quantum recoil effects.

In Chapter VI, we derived the 2-D solutions of the Dirac equation for an electron moving in the combined helical wiggler and an axial guide field. The solutions are consistent with 2-D solutions of wiggler without an axial field. The presence of the axial field makes the solutions basically unstable and we were able to predict the instability region, first discovered by using classical theory, correctly. We then applied these solutions to calculate gain and frequencies as we did in Chapter V. Some of our conclusions are as follows:

a) The axial field makes the difference between the longitudinal momenta of up-spin and down-spin electrons greater hence the increase in frequency of the "harmonic".

b) Even though the "harmonic" frequency is up-shifted the rate for the emission of this frequency is lower. This implies that the spin-polarization of the electron beam is preserved.

c) The effects of an axial guide field on gain is positive. Quantum theory confirms clearly that the gain is enhanced by the application of an axial guide field on the helical wiggler.

d) The fundamental frequency is down-shifted in the presence of an axial guide field.

In Chapter VII, we have analysed the pulsed operation of the FEL. Our purpose was to explain the "laser Lethargy" effect and the quantum intensity fluctuations in the early stages of FEL start-up. This effort

led us to the development of an optical model for the FEL interaction which combines classical and quantum effects in the "effective interaction length" concept. We developed a numerical algorithm based on this optical model and demonstrated the effect of Laser Lethargy for the short-pulse FELs. The basic idea in this calculation was to show that a uniform-wiggler FEL generates a chirped optical pulse and the gain mechanism compresses it which is possible because of the chirp. This way we showed that the "Laser Lethargy" in short-pulse FELs is basically a pulse-compression phenomenon.

Then we investigated the growth of the optical signal from spontaneous emission to saturation. We wrote a computer code which is simpler than the other codes employed up to now to investigate this nonlinear process. Our model and the algorithm based on it correctly predicts the rise-time of the FEL oscillator. In this chapter we have paid special attention to saturation effects. Towards the end of the chapter we incorporated inhomogeneous broadening, quantum mechanical effects and the tapering effects into our model.

In Chapter VIII we summarized the optical properties of the FEL radiation. We paid special attention to its coherence properties both 1st degree and 2nd degree and are led to conclude that the FEL radiation exhibits a good temporal coherence and a poor spatial coherence. We also reported that the FEL radiation never reaches the "Glauber coherence" even when the radiation intensity is high.

APPENDIXES

APPENDIX A

DIRAC ELECTRON IN AN ELECTROMAGNETIC PLANE WAVE

Introduction

The solution of the Dirac equation for the motion of an electron moving in the field of a plane electromagnetic wave was first derived by Volkov in 1935 [1]. Since then this solution found many applications. The results of this thesis can be extended to the strong-signal regime of the FEL by using the solution of the Dirac equation which includes the radiation field ab initio in the Dirac Hamiltonian. The exact solution of this problem is very difficult. There is however a way of solving the problem approximately. To a moving electron the wiggler field appears to be a plane electromagnetic wave (akin to Weissacker-Williams approximation) therefore one can take the superimposed field of wiggler and the strong-signal as a single wave and use the Volkov solution to calculate gain, frequencies etc.

The Volkov form of the solution is however a formal one with complicated operators in the denominator. Swamy [2] rederived this in a form which is suitable for matrix element calculations of the FEL theory. Here we present the solutions given by Swamy.

Solution

The vector potential for ae electromagnetic wave is given by

$$\vec{A} = \vec{A}_0 \, e^{i\phi} \, \hat{x} \equiv A_x \, \hat{x} \tag{A.1}$$

where $\phi \equiv kz-\omega t$ is the phase of the plane wave.

Dirac equation can be written as

$$(\underset{\sim}{H} - E) \Psi = 0 \tag{A.2}$$

where

$$H = c\rho_1 \sigma_x (\underset{\sim}{p}_x - eA_x) + c\rho_1\sigma_y \underset{\sim}{p}_y + c\rho_1\sigma_z \underset{\sim}{p}_z + \rho_3 m_0 c^2$$

we assumed $\underset{\sim}{p}_y = 0$ just like we did throughout the thesis.

In 4x4 form the Dirac equation will look like

$$\begin{bmatrix} m_0c^2 - i\hbar\frac{\partial}{\partial t} & 0 & c\underset{\sim}{p}_z & c\underset{\sim}{p}_x - eA_0e^{i\phi} \\ 0 & m_0c^2 - i\hbar\frac{\partial}{\partial t} & c\underset{\sim}{p}_x - eA_0e^{i\phi} & -c\underset{\sim}{p}_z \\ c\underset{\sim}{p}_z & c\underset{\sim}{p}_x - eA_0e^{i\phi} & -m_0c^2 - i\hbar\frac{\partial}{\partial t} & 0 \\ c\underset{\sim}{p}_x - eA_0e^{i\phi} & -\underset{\sim}{p}_z & 0 & -m_0c^2 - i\hbar\frac{\partial}{\partial t} \end{bmatrix} \begin{bmatrix} \phi_1 \\ \phi_2 \\ \phi_3 \\ \phi_4 \end{bmatrix} e^{i/\hbar\, \phi_5} \tag{A.3}$$

the solution is given as (unnormalized)

$$\begin{aligned} \phi_1 &= (-cp_z + cp_0 + m_0c^2)q_1 + (cp_x - eA_x)q_2 \\ \phi_2 &= (-cp_x + eA_x)q_1 + (-cp_z + cp_0 + m_0c^2)q_2 \\ \phi_3 &= (cp_z - cp_0 + m_0c^2)q_1 + (cp_x - eA_x)q_2 \\ \phi_4 &= (cp_x - eA_x)q_1 + (-cp_z + cp_0 - m_0c^2)q_2 \end{aligned} \tag{A.4}$$

$$\phi_5 = (p_x x + p_z z - p_0 ct + d_1 e^{i\phi} + d_2 e^{2i\phi}) \tag{A.5}$$

for the up-spin electron we have

$$q_1 \equiv \frac{E - cp_z + m_0c^2}{2(E-cp_z)(E+m_0c^2)} \tag{A.6}$$

$$q_2 \equiv \frac{cp_x}{2(E-cp_z)(E+m_0c^2)} \tag{A.7}$$

for the down-spin electron $q_1 \rightarrow q_2$ and $q_2 \rightarrow q_1$.

Here p_x , p_z , p_0 are c-numbers and

$$(cp_0)^2 \equiv E^2 = (cp_x)^2 + (cp_z)^2 + m_0^2c^4 \tag{A.8}$$

$$i\omega\, d_1 \equiv \frac{eA_0p_x}{p_z - p_0} \tag{A.9}$$

$$i\omega\, d_2 \equiv \frac{(eA_0)^2}{4c(p_0-p_z)} \tag{A.10}$$

Note that when $A_x \rightarrow 0 \Rightarrow d_1, d_2 \rightarrow 0$, above solutions reduce to the well known free particle spinors.

REFERENCES

[1] D.M. Volkov , Comptes Rendus de l'Acad. des Sciences, U.S.S.R. March 21, pp:605-610 (1935)

[2] N.V.V.J. Swamy , private communication

APPENDIX B

COMPUTER CODE FOR THE OPTICAL MODEL OF FEL

The following computer code is written in GW-BASIC language. It generates data files to be plotted later. The function graphing software used in this thesis was TG written by Dr.M. Oner of Oklahoma State University. The following computer code calculates the number of photons as a function of number of passes. It also calculates the optical pulse length as the FEL intensity rises and reaches saturation. This computer code is an implementation of the algorithm developed in Chapter VII where we discussed the pulsed operation of FELs and developed a model for the pulsed-FEL mechanism based on the concept of "Effective Interaction Length".

```
100  IDM=101
110  DIM NV(IDM),NPV(IDM),PL(IDM)
120  FLAG=1
130  LCA=0                        :'CAVITY LENGTH DETUNING
                                          (DESYNCHRONISM)
140  LO = .001                    :'THE INITIAL PULSE LENGTH
                                          (METERS )
150  LD = .0000033                :'THE LASER WAVELENGTH
                                          (METERS)
160  K  = .71                     :'WIGGLER STRENGTH PARAMETER
                                          (UNITLESS)
170  F  = .075                    :'THE FILLING FACTOR
180  S  = .00000019634954#        :'ELECTRON BEAM CROSS-SECTION
                                          ( M SQUARE )
190  IP = 1.3                     :'PEAK CURRENT   (AMPERES)
200  RO = 2.82E-15                :'CLASSICAL ELECTRON RADIUS
                                          (METERS)
210  A  = 137                     :'FINE STRUCTURE CONSTANT
220  AO = .0131574685#            :'ALPHA ZERO
230  C  = 3E+08                   :'SPEED OF LIGHT(METERS PER SECOND)
240  'NP                          :'NUMBER OF PHOTONS IN THE
                                           OPTICAL PULSE
```

```
250  EC = 1.602E-19              :'ELECTRON CHARGE  (COULOMBS)
260  LDW= .033                   :'WIGGLER WAVELENGTH (METERS)
270  LW = 5.3                    :'WIGGLER LENGTH  (METERS)
280  NN = 160                    :'NUMBER OF MAGNET ELEMENTS IN
                                          THE WIGGLER
290  PI = 3.141592654#           :'PI
300  P4 = 97.40909103#           :'PI TO THE POWER OF 4
310  AN = 1.2476646D+23          :'PULSE PARAMETER A
320  KA = 2.6826823D-29          :'PULSE PARAMETER K SUB ALPHA
330  GAMMA=69                    :'RELATIVISTIC FACTOR
340  Q11=.02837                  :'LOSS FACTOR
350  EMIT = 3.642426E-07         :'EMITTANCE OF THE ELECTRON BEAM
355  GE=.0005
360  L=LO
370  AN1=AN       : AN0 = AN
390  LOO=LO
410  SCALE=1
420  NUM=1
430       IF FLAG=1 THEN INPUT "ENTER (DYS=0)
                          OUTPUT FILENAME",FIL$
440       IF FLAG=1 THEN OPEN
                    FIL$ FOR OUTPUT AS #NUM
450       LCA=0    :GOSUB 5000
460       IF FLAG=1 THEN GOSUB 10000
470       CLOSE #NUM
480  NUM=2
490       IF FLAG=1 THEN INPUT "ENTER (DYS NONZERO)
                          OUTPUT FILENAME",FIL$
500       IF FLAG=1 THEN OPEN FIL$ FOR OUTPUT AS #NUM
510       LCA=5E-09    : GOSUB 5000
520       IF FLAG=1 THEN GOSUB 10000
530       LCA=.0000005     : GOSUB 5000
540       IF FLAG=1 THEN GOSUB 10000
550       LCA=.000005      : GOSUB 5000
560       IF FLAG=1 THEN GOSUB 10000
570       IF FLAG=1 THEN CLOSE #NUM
580   NUM=1
590        IF FLAG=1 THEN INPUT "ENTER (INHOMO)
                           OUTPUT FILENAME",FIL$
600        IF FLAG=1 THEN OPEN FIL$ FOR OUTPUT AS #NUM
610        LCA=.000005 : GOSUB 5000
620        IF FLAG=1 THEN GOSUB 10000
630        FL=1  :NUM=1  :LCA=.000005
640        GOSUB 5000
650        IF FLAG=1 THEN GOSUB 10000
660        IF FLAG=1 THEN CLOSE #NUM
670  NUM=1
680       IF FLAG=1 THEN INPUT "ENTER (TAPER1)
                          OUTPUT FILENAME",FIL$
690       IF FLAG=1 THEN OPEN FIL$ FOR OUTPUT AS #NUM
700       FL=1 :LCA=.000005  :BT=.36
710       GOSUB 5000
720       IF FLAG=1 THEN GOSUB 10000
```

```
730       FL=1  :LCA=.000005  :BT=1.078
740       GOSUB 5000
750       IF FLAG=1 THEN GOSUB 10000
760       IF FLAG=1 THEN CLOSE #NUM
770   NUM=2
780       IF FLAG=1 THEN INPUT "ENTER (TAPER2)
                               OUTPUT FILENAME",FIL$
790       IF FLAG=1 THEN OPEN FIL$ FOR OUTPUT AS #NUM
800       FL=1  :LCA=5E-09  :BT=.36
810       GOSUB 5000
820       IF FLAG=1 THEN GOSUB 10000
830       FL=1  :LCA=5E-09  :BT=1.078
840       GOSUB 5000
850       IF FLAG=1 THEN GOSUB 10000
860       IF FLAG=1 THEN CLOSE #NUM
870       END
880   '
890   '
900   '
910   '
920   '
930   '
5000   'THIS SUBROUTINE CALCULATES THE EVOLUTION OF THE FEL
5010   'PHOTON NUMBER AND THE OPTICAL PULSE LENGTH
5030   DN=20616.75
5035   NP=20000  :LO=.001  :LOO=LO  :L=LO
5040   A1=.4147222*LD/LOO
5050   A2=.8294*LD
5060   A3=.1719*LD*LD
5070   DD=A*(1+K*K)*(1+K*K)*EC*LD*LD*LDW*S
5080   WO=2*PI*C/LD
5085   MUXY=(SQR(2)*K/(1+K*K))*(GAMMA*EMIT*LW/(LDW*LDW))
5086   MUE=2*GE*LOO/LD
5087   TAPER=C*C*GAMMA*GAMMA*BT/(1+K*K)
5088   TR=((BT*LW)/2+(2*PI/LDW))/(2*PI/LDW)
5090   SLIP=2*NN*LD/LOO
5100   DYS=4*LCA/LOO
5110   IST=5
5120   II=0
5130   Q11=.02837
5132   AN = 1.2476646D+23
5135   KA = 2.6826823D-29
5137   AN1=AN       : AN0 = AN
5140   RMS=0   : RMSD=0
5150   FOR I=0 TO 5000 STEP IST
5160       N=I+1
5170       BO=(16*P4*AO*K*K*F*IP*C*RO*RO*(1-A1)
                              *(L*L-A2*L+A3))/DD
5180       BN = BO*NP*(1+RMS)
5190       DLP=C*1.1774*(1/SQR(AN0)-1/SQR(AN1))
5200       SHORT=DLP-2*LCA
5210       IF DLP>2*LCA THEN SHORT=2*DLP+2*LCA
5220       IF LCA=0 THEN Q11=Q1
```

```
5230      Q1=Q11+ABS(SHORT)/LOO
5240      AN0=AN
5250      AN=(AN*(1+KA*AN)+KA*BN*BN)/
                ((1+KA*AN)*(1+KA*AN)+KA*BN*KA*BN)
5260      AN1=AN
5270      IF I/50=FIX(I/50) THEN II=II+1
                          :PL(II)=C*1.1774*(1/SQR(AN))
5275      INHOMO = SQR(1+MUE*(LOO/L)*MUE*(LOO/L)+2*MUXY*MUXY)
5280      L=LOO/((1+(2*NN*LD*(BO*NP*(1+RMS)-TAPER))/(C*WO))
                                                    *INHOMO)
5290      G=(2*PI*PI*K*K*F*LW*(L*L-A2*L+A3)*IP*RO*AO)/
                                  (GAMMA*(1+K*K)*LD*S*EC*C)
5300      G=G*SCALE*TR /(1+RMS)
5310      NP= NP+DN*IST+(G-Q1)*NP*IST
5320      IF NP<0 THEN NP=0
5330      IF FL=1 THEN RMS=500000!/NP
5350      IF I/50=FIX(I/50) THEN NPV(II)=NP
5360      IF I/50=FIX(I/50) THEN NV(II)=N
5370      DN=DN*(1-DLP  /LOO)
5380      PRINT N,NP, G-Q1,RMS ,L
5390      KA=(2*2.0603*G*L*L/(C*C*4*NN*NN))*
                                  (1+(SLIP+2*DYS)*.5)
5400  NEXT
5410  RETURN
5420  '
5430  '
10000     'THIS SUBROUTINE CREATES THE
                       OUTPUT DATAFILE
10020     PRINT #NUM,"THEORETICAL CURVE OBTAINED
                                    FROM OUR MODEL"
10025     PRINT #NUM,"......"
10030     PRINT #NUM,"#OFPASSES  #OFPHOTONS PULSELENGTH"
10040     PRINT #NUM,".                .              M"
10050     FOR II=1 TO IDM
10060     PRINT #NUM,NV(II);NPV(II);PL(II)
10070     NEXT
10080     RETURN
```

VITA

Selcuk Saritepe

Candidate for the Degree of

Doctor of Philosophy

Thesis: QUANTUM MECHANICAL ASPECTS OF FREE ELECTRON LASERS

Major Field: Physics

Biographical:

Personal Data: Born in Kandilli, Zonguldak, Turkey, January 25, 1960, the son of Hasan and Yuksel Saritepe. Married to Nilufer Anlar on August 3, 1982.

Education: Graduated from Isik High School, Istanbul, Turkey, in June, 1977; received Bachelor of Science degree in Physics and Electrical Engineering from Bogazici University in June, 1981; received Master of Science degree from Oklahoma State University in December, 1985; completed requirements for the Doctor of Philosophy degree at Oklahoma State University in July, 1988.

Professional Experience: Undergraduate Teaching Assistant, Department of Physics, Bogazici University, September, 1979, to June, 1981; Teaching Assistant, Department of Physics, Oklahoma State University, January, 1982, to August, 1987; Lecturer, Oklahoma State University, Department of Physics, August, 1987, to January,1988, and from June, 1988, to July, 1988.